

AFRL-VA-WP-TR-1999-3011

**PIEZOCERAMIC ACTUATOR ACTIVE
VIBRATION SUPPRESSION SYSTEM
B-1B FLIGHT DEMONSTRATION PROGRAM**



**ERIC T. FALANGAS
CHARLES R. LARSON
JOSEPH S. ROSENTHAL
MELVIN WEISS
DEMETRIOUS G. ZEFERIS**

**BOEING NORTH AMERICAN, INC.
2600 WESTMINSTER BLVD.
P.O. BOX 3644
SEAL BEACH, CALIFORNIA 90740-7644**

JANUARY 1998

FINAL REPORT FOR 09/01/1997 – 11/01/1997

APPROVED FOR PUBLIC RELEASE; DISTRIBUTION UNLIMITED

19990715 040


**AIR VEHICLES DIRECTORATE
AIR FORCE RESEARCH LABORATORY
AIR FORCE MATERIEL COMMAND
WRIGHT-PATTERSON AIR FORCE BASE OH 45433-7542**

NOTICE

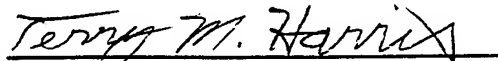
USING GOVERNMENT DRAWINGS, SPECIFICATIONS, OR OTHER DATA INCLUDED IN THIS DOCUMENT FOR ANY PURPOSE OTHER THAN GOVERNMENT PROCUREMENT DOES NOT IN ANY WAY OBLIGATE THE US GOVERNMENT. THE FACT THAT THE GOVERNMENT FORMULATED OR SUPPLIED THE DRAWINGS, SPECIFICATIONS, OR OTHER DATA DOES NOT LICENSE THE HOLDER OR ANY OTHER PERSON OR CORPORATION; OR CONVEY ANY RIGHTS OR PERMISSION TO MANUFACTURE, USE, OR SELL ANY PATENTED INVENTION THAT MAY RELATE TO THEM.

THIS REPORT IS RELEASABLE TO THE NATIONAL TECHNICAL INFORMATION SERVICE (NTIS). AT NTIS, IT WILL BE AVAILABLE TO THE GENERAL PUBLIC, INCLUDING FOREIGN NATIONS.

THIS TECHNICAL REPORT HAS BEEN REVIEWED AND IS APPROVED FOR PUBLICATION.



DOUGLAS A. HENDERSON
Aerospace Engineer
Structural Dynamics Branch



TERRY M. HARRIS, Chief
Structural Dynamics Branch
Structures Division



ERICA ROBERTSON, Major, USAF
Deputy Chief, Structures Division
Air Vehicles Directorate

Do not return copies of this report unless contractual obligations or notice on a specific document requires its return.

REPORT DOCUMENTATION PAGE			Form Approved OMB No. 0704-0188	
Public reporting burden for this collection of information is estimated to average 1 hour per response, including the time for reviewing instructions, searching existing data sources, gathering and maintaining the data needed, and completing and reviewing the collection of information. Send comments regarding this burden estimate or any other aspect of this collection of information, including suggestions for reducing this burden, to Washington Headquarters Services, Directorate for Information Operations and Reports, 1215 Jefferson Davis Highway, Suite 1204, Arlington, VA 22202-4302, and to the Office of Management and Budget, Paperwork Reduction Project (0704-0188), Washington, DC 20503.				
1. AGENCY USE ONLY (Leave blank)	2. REPORT DATE JANUARY 1998	3. REPORT TYPE AND DATES COVERED FINAL REPORT FOR 09/01/1997 - 11/01/1997		
4. TITLE AND SUBTITLE PIEZOCERAMIC ACTUATOR ACTIVE VIBRATION SUPPRESSION SYSTEM B-1B FLIGHT DEMONSTRATION PROGRAM		5. FUNDING NUMBERS C F33615-95-D-3217 PE 62201 PR 2401 TA ST WU AP		
6. AUTHOR(S) ERIC T. FALANGAS, CHARLES R. LARSON, JOSEPH S. ROSENTHAL, MELVIN WEISS, DEMETRIOUS G. ZEFERIS				
7. PERFORMING ORGANIZATION NAME(S) AND ADDRESS(ES) BOEING NORTH AMERICAN, INC. 2600 WESTMINSTER BLVD. P.O. BOX 3644 SEAL BEACH, CALIFORNIA 90740-7644		8. PERFORMING ORGANIZATION REPORT NUMBER		
9. SPONSORING/MONITORING AGENCY NAME(S) AND ADDRESS(ES) AIR VEHICLES DIRECTORATE AIR FORCE RESEARCH LABORATORY AIR FORCE MATERIEL COMMAND WRIGHT-PATTERSON AFB, OH 45433-7542 POC: DOUGLAS A. HENDERSON, AFRL/VASS, 937-255-5200 EXT. 407		10. SPONSORING/MONITORING AGENCY REPORT NUMBER AFRL-VA-WP-TR-1999-3011		
11. SUPPLEMENTARY NOTES				
12a. DISTRIBUTION AVAILABILITY STATEMENT APPROVED FOR PUBLIC RELEASE; DISTRIBUTION UNLIMITED			12b. DISTRIBUTION CODE	
13. ABSTRACT (Maximum 200 words) This report describes all of the tasks required to design, develop and install an active vibration suppression system on a B-1B aircraft. Piezoceramic actuators were used to damp the acoustically excited vibrations on a skin panel located at the aft end of the aircraft. The program was accomplished through three phases of effort. First was the development and testing of a laboratory prototype system. Laboratory testing also included tests needed to optimize the actuators to be applied on the aircraft. Second was the design and fabrication of the hardware to be installed on the aircraft. Third was the flight test segment used to demonstrate the performance of the system. During the flight test portion of the program, information on system maintainability and reliability were collected. Performance of the system was determined by acceleration data recorded on the panel during aircraft takeoff and flight. Data with the system operating and non-operating show that excellent performance was obtained in attenuating both the first symmetric and anti-symmetric modes of the panel. Damping of the second anti-symmetric mode was also accomplished, but to a lesser extent.				
14. SUBJECT TERMS			15. NUMBER OF PAGES 72	
			16. PRICE CODE	
17. SECURITY CLASSIFICATION OF REPORT UNCLASSIFIED	18. SECURITY CLASSIFICATION OF THIS PAGE UNCLASSIFIED	19. SECURITY CLASSIFICATION OF ABSTRACT UNCLASSIFIED	20. LIMITATION OF ABSTRACT SAR	

Contents

Section	Page
1.0 INTRODUCTION	1-1
1.1 Background	1-1
1.2 Objectives	1-1
1.3 AVSS Team	1-1
1.4 Challenges	1-2
1.5 Program Overview	1-3
1.6 Demonstration Panel Description	1-4
2.0 AVSS DEVELOPMENT	2-1
2.1 Aircraft Tap Test/FEM Results	2-1
2.2 Selection of PZT Geometric Properties and Adhesive	2-3
2.2.1 Coupon Description and Testing	2-4
2.2.2 Actuator Thickness Selection	2-6
2.2.3 Frequency and Temperature Considerations	2-7
2.2.4 Adhesive Selection	2-8
2.2.5 Actuator Patch Configuration Selection	2-9
2.2.6 Actuator/Adhesive Durability	2-11
2.3 Laboratory Test Configurations	2-11
2.3.1 Flat Panel	2-12
2.3.2 Curved Panel	2-13
2.4 Electronic Hardware	2-14
2.4.1 Power Amplifier Unit	2-14
2.4.2 Control Unit	2-17
2.5 Control System Design	2-18
2.5.1 Generating the Design Plant Model	2-18
2.5.2 Loop Shaping	2-19
2.5.3 Shaping Filters $W_i(s)$	2-20
2.5.4 Control System Analysis	2-22
2.5.5 Software/Hardware Interface	2-23
2.6 Laboratory Tests	2-27
2.6.1 Flat Panel	2-28
2.6.2 Curved Panel	2-29
3.0 FLIGHT DEMONSTRATION	3-1
3.1 Hardware Installation	3-1
3.2 Instrumentation	3-2
3.3 Preflight Aircraft Measurements	3-4
3.3.1 Open-Loop Transfer Functions	3-4
3.3.2 Closed-Loop Gain Adjustment	3-4
3.4 Results	3-8
3.4.1 Life Issues	3-8
3.4.2 Performance During Takeoff (Maximum Engine Noise)	3-8

Section	Page
3.4.3 Performance for In-flight Conditions	3-11
3.4.4 Adjacent Structure/Acoustic Responses	3-17
4.0 SUMMARY AND RECOMMENDATIONS	4-1
4.1 Summary	4-1
4.2 Conclusions.....	4-3
4.3 Recommendations.....	4-3
5.0 REFERENCES	5-1

Illustrations

Figure		Page
1-1	B-1B External Configuration.....	1-5
1-2	Location of AVSS Demonstration Panel on B-1B Aft Equipment Bay.....	1-5
1-3	AVSS Demonstration Panel Configuration.....	1-6
2-1	Predicted Mode Shapes and Frequencies.....	2-2
2-2	Representative Top Test Accelerometer Time History.....	2-3
2-3	Representative Autocorrelation Plot From Tap Test.....	2-4
2-4	Comparison of Tap Test Results With Predicted First Symmetric Mode.....	2-5
2-5	Comparison of Tap Test Results With Predicted First Anti-symmetric Mode ..	2-5
2-6	AVSS Test Coupon.....	2-6
2-7	Configuration of Conducting and Non-conducting Epoxies.....	2-6
2-8	Typical Strain Gage and Optical Displacement Measurements.....	2-7
2-9	Effect of Coupon Length on the Resonance Frequency.....	2-8
2-10	Coercive Field (E_c) Vs. Temperature.....	2-8
2-11	Displacement Comparison —High Vs. Room Temperature.....	2-9
2-12	Displacement Comparison—Low Vs. Room Temperature.....	2-10
2-13	Comparison of EA 9395 and XEA 9360 Epoxies.....	2-10
2-14	Comparison of Different Mosaic Patch Structures.....	2-11
2-15	Fatigue Test of Coupons With Different Epoxies.....	2-12
2-16	Flat Panel Accelerometer and PZT Locations.....	2-13
2-17	Curved Panel Accelerometer and PZT Locations.....	2-14
2-18	Control Unit and Power Amplifier Unit.....	2-15
2-19	Layout of Symmetric Amplifiers.....	2-15
2-20	Layout of Anti-symmetric Amplifiers.....	2-16
2-21	Schematic of Symmetric and Anti-symmetric Amplifiers.....	2-17
2-22	H_∞ Synthesis Model.....	2-19
2-23	The Loop Shaping Process.....	2-20
2-24	H_∞ Controller Frequency Response.....	2-21
2-25	Nichol's Plot of the Open-Loop System.....	2-21
2-26	Panel Frequency Response With and Without Feedback.....	2-22
2-27	Block Diagram of the Open-Loop Controller.....	2-28
2-28	Closed and Open-Loop Response Flat Panel.....	2-28
2-29	Flat Panel Response for 136 dB Input.....	2-29
2-30	Anti-symmetric Open-Loop Transfer Function.....	2-30
2-31	Symmetric Open-Loop Transfer Function.....	2-31
2-32	Curved Panel Tap Test Response.....	2-32
2-33	Curved panel Anti-Symmetric Response for 141 dB.....	2-32
3-1	Active Vibration Suppression System (SVSS) Block Diagram.....	3-1
3-2	AVSS Control Unit (Left) and Power Supply Mounted in B-1B AEB.....	3-2
3-3	Location of the PZT Patches on the Demonstration Panel.....	3-3
3-4	PZT Patches Located in the B-1B Aft Equipment Bay.....	3-4
3-5	AVSS Instrumentation.....	3-6
3-6	Comparison AVSS Off and On, Initial Control Laws.....	3-12

Figure		Page
3-7	Comparison of AVSS Off and On, Revised Control Laws	3-13
3-8	Comparison of AVSS off and On, Gain Change	3-14
3-9	Antisymmetric Panel Response During Flight With AVSS "Off" and "On"	3-15
3-10	Symmetric Panel Response During Flight With AVSS "Off" and "On"	3-16

Tables

Table		Page
1-1	AVSS Program Breakdown	1-3
3-1	PZT Patch Actuator Attachment Procedures for B-1B.....	3-5
3-2	History of AVSS on TDS Aircraft	3-7
3-3	Anti-symmetric Response Summary	3-10
3-4	Symmetric Response Summary	3-11
4-1	AVSS Attenuation Summary	4-2

1.0 Introduction

1.1 BACKGROUND

Piezoceramic actuators (PZTs) have been used extensively in a laboratory or ground test environment but not, until this program, have they been used on an operational combat aircraft. Because data from prior flight applications were not available, the use of PZTs has not been accepted by the program managers as a viable way to solve vibration, noise, or sonic fatigue requirements on developing or operational systems. On operational aircraft they could be utilized to solve existing field problems or help in life extension programs for systems or structure subjected to oscillatory stresses due to vibration or acoustical fatigue. The program discussed in this report was a unique opportunity to apply PZT actuators to reduce the vibrations of a skin panel on an operational combat aircraft and not incur tremendous flight test related costs. The B-1B Program, at the inception of this effort, was in the midst of adding a segment to its defensive system known as the Towed Decoy System (TDS). Fairings were added to the aft end of the fuselage to house electronic decoys, which can be towed behind the aircraft. A skin panel behind the fairing was chosen to demonstrate the ability of PZT actuators to reduce the acoustically induced skin panel vibrations due to the engine noise during takeoff and the turbulent flow over the fairing at high speed flight conditions. However, it was subsequently determined by an on-aircraft tap test that the candidate panel was heavily damped by RAM (radar absorbing material) on the panel, and, therefore, would not have made a good test bed to demonstrate PZT actuator usage. Fortunately, another panel nearby was available for this demonstration program. Even though it was above, and not behind, the TDS fairing it was still exposed to high acoustic levels from the engines and turbulent flow, in this case, existing in the aircraft empennage region.

1.2 OBJECTIVES

The main objective of the program was to develop, install, and flight test an active vibration suppression system (AVSS) which uses PZT actuators on the TDS B-1B test aircraft and demonstrate its ability to reduce fuselage skin panel vibrations due to high acoustic loads. In accomplishing this demonstration some secondary objectives could also be achieved. These included evaluating the maintainability, reliability, and survivability of the system and collecting information on the resources required to develop, install and maintain such a system. It was hoped that this was only a first step in demonstrating the ability of PZTs to control vibration and noise environments on operational aircraft, and that this would lead to applications on "warm" structures and applications for controlling component motion by vibration isolation or jitter control.

1.3 AVSS Team

At the initiation of this task, the effort was a joint program of Wright Laboratory in Dayton, Ohio and Rockwell International. Three Rockwell divisions were involved: North American Aircraft in Seal Beach and Edwards AFB, California; Space Systems Division in Downey, California and the Rockwell Science Center in Thousand Oaks, California. Subsequently, Rockwell Aerospace and Defense Groups were sold to the Boeing Company. This included the Aircraft and Space Divisions but not the Science

Center which, while it is still part of Rockwell International, receives considerable R&D funding from the former Rockwell Aerospace and Defense, now Boeing North American, business units. This combination of government, Boeing North American and Rockwell Science Center personnel formed a strong multifaceted team with the resources, talent and expertise to perform the required program. The Wright Laboratory personnel, in addition to providing funding, interfaced with the B-1B System Program Office (SPO) in Dayton to get permission to use the TDS aircraft as a test bed on a "piggyback" basis. They also negotiated support from the B-1B Combined Test Force (CTF) at Edwards AFB, California, which was responsible for flight testing of the TDS B-1B aircraft. The BNA North American Aircraft division provided overall program management and finite element modeling support in Seal Beach; the division's B-1B Instrumentation Group at EAFB contributed to the design, fabrication, and installation of the AVSS in the TDS B-1B aircraft. The Rockwell Science Center had developed PZT actuators, which are capable of providing twice the force of comparable commercially supplied PZTs. This team was successful in performing the program even though the flight test schedule was moved up by about 2 months so that the TDS aircraft could be transferred from EAFB to Robins AFB in Georgia for testing at Eglin AFB test range in Florida.

1.4 Challenges

The B-1B AVSS Flight Demonstration Program faced a considerable number of challenges in order to successfully complete the effort. The main challenge was to develop an AVSS that would perform as required and survive the severe service environment existing on the aft end of the B-1B. It was also desired to demonstrate that the system could successfully reduce vibration levels during all phases of the aircraft flight environment including ground and in-flight operations. Also, it was desired to suppress not just the panel primary modes, but to demonstrate that multiple modes of response could be reduced significantly in amplitude. The panel chosen for the demonstration on the aircraft provided a much more difficult challenge than had previously been accomplished in a laboratory environment. It was a relatively thick panel, about 0.080 inches, and fairly sharply curved. The radius of curvature is approximately 38 inches. PZTs would have been more effective in exciting the structure if they could be attached to the outside of the skin panel. However, it was necessary to mount them internally to remove them from the air stream and to facilitate wire connections to the AVSS control boxes. It was also required that relatively low voltages be utilized in order not to endanger the aircraft or maintenance personnel. An adhesive was required which would be able to transfer the motion of the PZTs to the underlying skin panel in the temperature range requirements of the aircraft, which was from -60°F to 185°F. It had to perform this function on a curved surface and survive high cycles of vibration. The whole system required a digital processor that was fast enough (>8000 Hz) to suppress the critical modes, simultaneously. These modes were in the range of 400 to 800 Hz. The computer had to implement the control laws developed for the system by software that could easily be input and changed, if required. Adapting to changing frequencies was also a goal of the effort. It was also necessary to package all of the electronics for the system in available area in the aft equipment bay of the B-1B so that it was as close as possible to the PZTs themselves.

Installation, checkout and testing of the AVSS had to be accomplished on a minimum interference basis with the ongoing TDS flight test program. As stated

before, the shortening of the TDS flight testing at Edwards AFB and the transfer of the aircraft to Georgia exacerbated this challenge.

1.5 Program Overview

The program was divided into three main efforts as shown in Table 1-1.

Essentially, the program plan was to choose a demonstration panel on the aft end of the B-1B aircraft and determine its basic natural frequencies by an on-aircraft tap test. A finite element model of the panel would be developed to produce the dynamic characteristics of the actual panel on the aircraft. A laboratory test panel would be fabricated, which also duplicated the structural dynamics of the on-aircraft

Table 1-1. AVSS Program Breakdown

1.	Laboratory Development and Demonstration
1a.	Verify B-1B Panel Frequencies (A/C test)
1b.	Develop Panel FEM and PZT Modeling
1c.	Develop single/multiple layer patch actuator
1d.	Determine preliminary control laws
1e.	Fabricate test hardware
1f.	Set up test
1g.	Panel demonstration laboratory test
1h.	Finalize patch configuration and control laws
2.	Flight Hardware development
2a.	Define aircraft requirements
2b.	Develop electronic and actuator interfaces
2c.	Design aircraft installation
2d.	Design electronic PZT controller
2e.	Fabricate aircraft installation
2f.	Fabricate electronic PZT controller
2g.	Install aircraft equipment
2h.	Checkout aircraft installation
3.	Flight Test demonstration
3a.	Prepare T-2 Modification package
3b.	Develop Flight test plan
3c.	Coordinate test with AF, CTF, TDS
3d.	Flight test support
3e.	Data reduction
3f.	Data Analysis

panel; and that panel would be used to develop the PZT patch configuration, the method of control, and the electronics to power and control the PZTs on the vehicle. Laboratory tests were also performed to help specify an adhesive for attaching the actuators to the aircraft skin.

The second phase of the program was the development of all of the hardware that needed to be designed, fabricated, and installed in the aircraft to perform the actual panel vibration suppression. This hardware was first envisioned to include a control box that would power and control the system and the PZTs that had to be bonded to the aircraft skin panel. All of the associated wiring had to be installed also. One of the advantages of utilizing the TDS aircraft was the fact that it already had an onboard instrumentation system. Instrumentation specified for the AVSS Program was for two purposes. Accelerometers attached to the PZT patches were used for both feedback control of the system and for recording response of the panel. Other instrumentation included accelerometers, a microphone and a temperature gage mounted near or on the selected skin panel.

The final phase of the program was the actual flight demonstration of the system. This was accomplished in parallel with the TDS flight test program, and the instrumentation outputs were recorded on the same recorder as those required for the TDS. Data obtained were reduced and analyzed and are presented as part of this final report.

A special mention must be made of the exceptional support that was given to the AVSS Program by the B-1B SPO, the TDS program manager at Edwards AFB, Mr. Mario Dorodo, and the B-1B Combined Test Force (CTF) at Edwards under the direction of Lt. Col. James McGinley.

1.6 Demonstration Panel Description

The aft end of the B-1B aircraft is an ideal location for demonstrating the use of PZT actuators to suppress acoustically induced panel vibration and noise attenuation into the interior of the aircraft. That area is exposed to high engine noise levels, in the range of 160 dB, during full afterburner and to turbulent airflow during various other flight conditions. Figure 1-1 shows the aircraft configuration and the relative location of the engines. Figure 1-2 is a picture of the aft end of the aircraft showing the location of the TDS fairing and pointing out the location of the skin panel chosen for the AVSS demonstration.

There is an equipment bay interior to the aircraft in this area which mainly contains components of the aircraft defensive system. The TDS is a recent addition to this defensive system, and its hardware is contained in the fairing and in the interior equipment bay known as the AEB (aft equipment bay). The actual skin panel section is shown in Figure 1-3. It is encompassed by frames on either side and by longerons at the top and bottom. The distance between frame centerlines in the AEB is 10 inches, and the panel is roughly 2 feet along its mean circumference. A radius of curvature of about 38 inches exists in this area. It should be noted that the panel actually has a double curvature as the fuselage diameter is decreasing as the structure proceeds toward the aft end.

The skin is attached to the frames and longerons by fasteners and is part of a bigger skin section, which covers multiple bays of the AEB area. The skin material is 2024-T62 and is chemically milled to go from a thickness of 0.126 inch at the lands

down to 0.100 and then down to 0.077 at the main center section. This part of the aircraft was designed not only to survive the static loads for various flight conditions but also the acoustic noise from the engines. Considerable analysis and testing were done during the B-1B development program to insure an adequate design for the service life of the aircraft. To date, there have been no service problems related to sonic fatigue in the structure associated with the

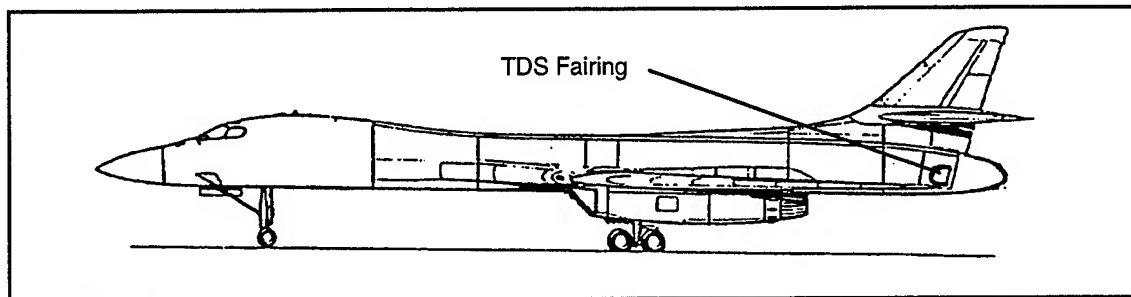


Figure 1-1. B-1B External Configuration

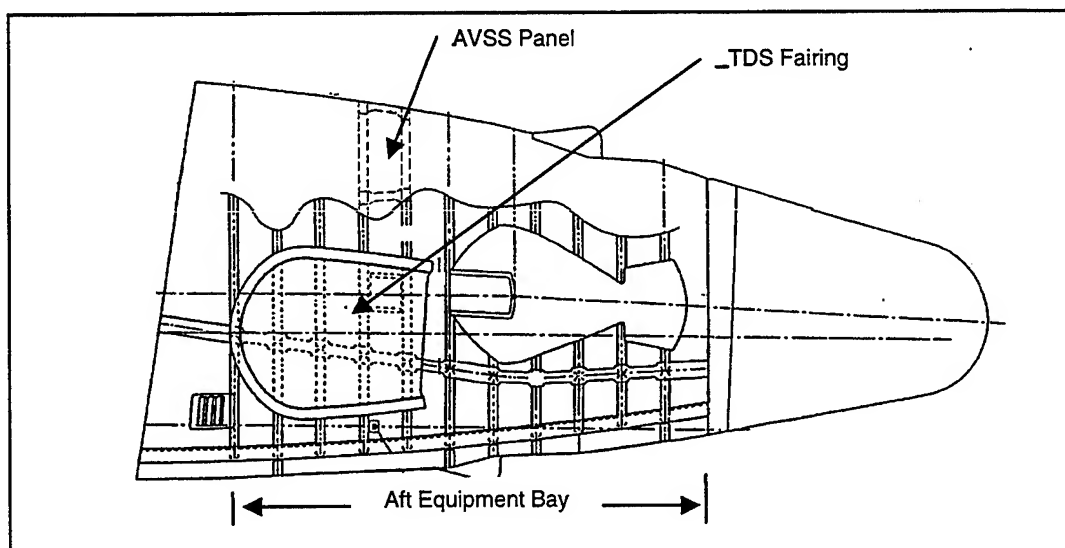


Figure 1-2. Location of AVSS Demonstration Panel on B-1B Aft Equipment Bay

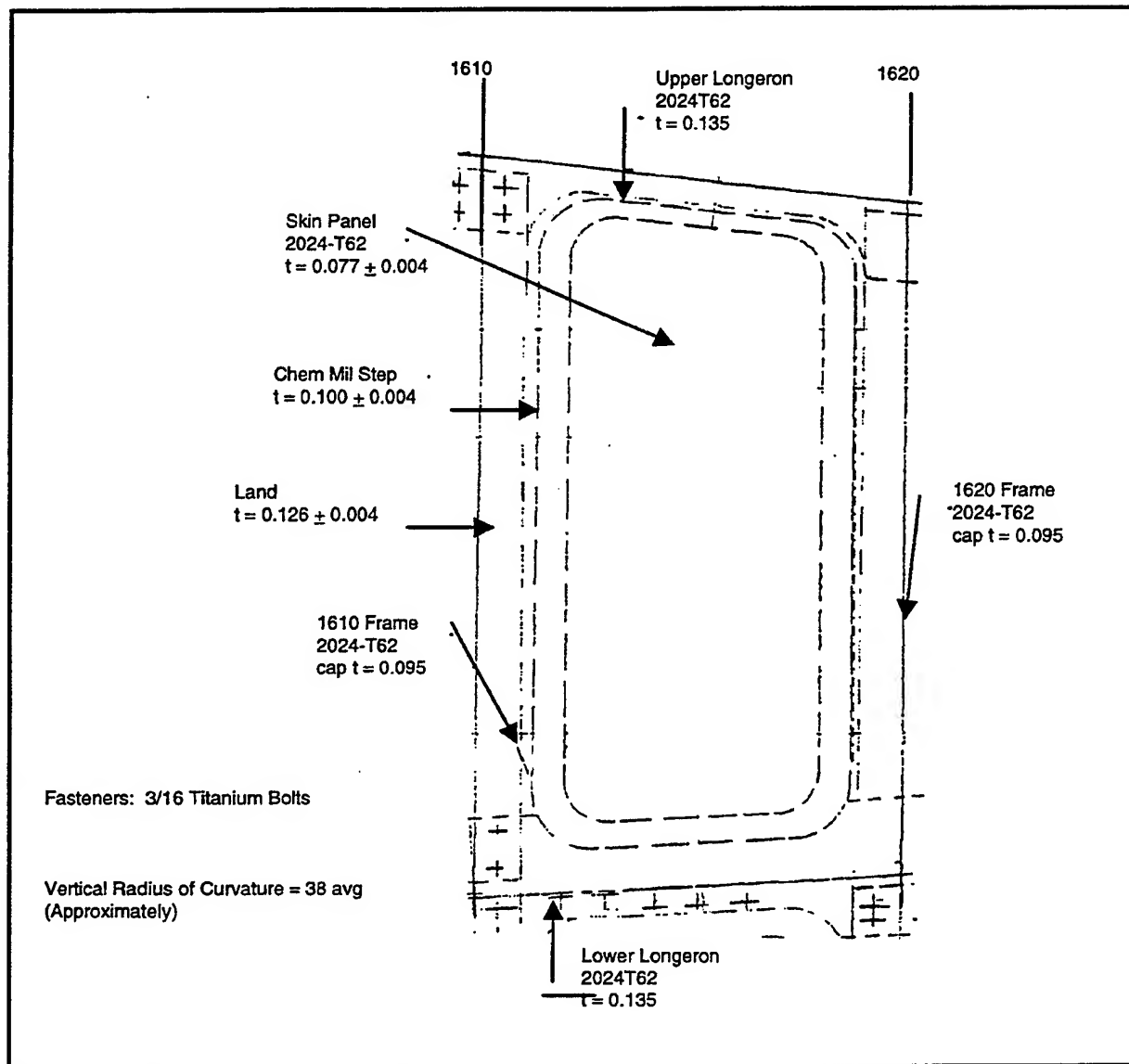


Figure 1-3. AVSS Demonstration Panel Configuration

2.0 AVSS Development

2.1 AIRCRAFT TAPS TEST/FEM RESULTS

A tap test was performed on the actual B-1B skin panel section of the TDS aircraft to obtain natural frequencies, mode shapes, and structural damping. This information was used to validate the structural dynamics finite element model of the panel, to determine the configuration and characteristics of the laboratory test panel built for identifying the optimum PZT layout, and to develop the system control laws.

The structure was excited by tapping it with an instrumented hammer. Accelerometers were used to record the panel responses. Accelerometer signals were fed into a real time analyzer for data analysis during the test and to a tape recorder for subsequent data reduction. In order to know the exact location of the accelerometers and the location of the excitation points, a grid was marked on the skin panel with chalk. Coordinates were given relative to the geometric center of the panel. For ease of measurement distances were all given in vertical arc length or fore and aft distances from the origin.

Before the performance of the test, a finite element model of the panel was developed and the natural modes and frequencies were determined. Shell elements were used to construct the model. The first two modes predicted by the model were a symmetric mode at 603 Hz and an anti-symmetric mode at 610 Hz. Frequencies actually found on the aircraft skin panel were about 100 Hz below those predicted by the model. Boundary conditions for the model were changed such that the outer edges, which had been fixed in both translation and rotation, were only fixed in translation. This had the effect of reducing the frequencies of the predicted modes to 521 and 526 Hz which were in the range of those found on the aircraft. Figure 2-1 shows the first two predicted mode shapes and their corresponding natural frequencies. The accelerometers, because of their mass, influenced the natural frequencies identified during the test. With seven accelerometers on the panel, at all the configurations tested, the test natural frequencies varied from 488 to 504 Hz. With only two accelerometers present the natural frequencies increased to 517 and 528, very close to the predicted values of 521 and 526 Hz. As can be seen from Figure 2-1 mode 1 is a symmetric and mode 2 is an anti-symmetric mode relative to the center of the panel.

The predicted shapes show that the first two modes can be excited individually because the anti-node of one mode is a node for the other mode. Therefore, the panel was excited at the anti-node of the symmetric mode, located at the panel center, and at the anti-nodes of the anti-symmetric mode which are located ± 3.5 inch from the center. Data for all of the tap configurations were recorded on tape. Multiple taps were recorded for each configuration and tap location. In all, 9 records were recorded. Because of the accelerometer mass effects the mode shapes were found to shift on the aircraft relative to those predicted by the model. A typical accelerometer time history pulse can be seen in Figure 2-2. Figure 2-3 is an autocorrelation Power Spectral Density (PSD) plot of the signal from all of the pulses for this particular configuration. The basic frequency is evident in the plot (505 Hz.). Both the time history and the PSD show the damping exhibited by the structure.

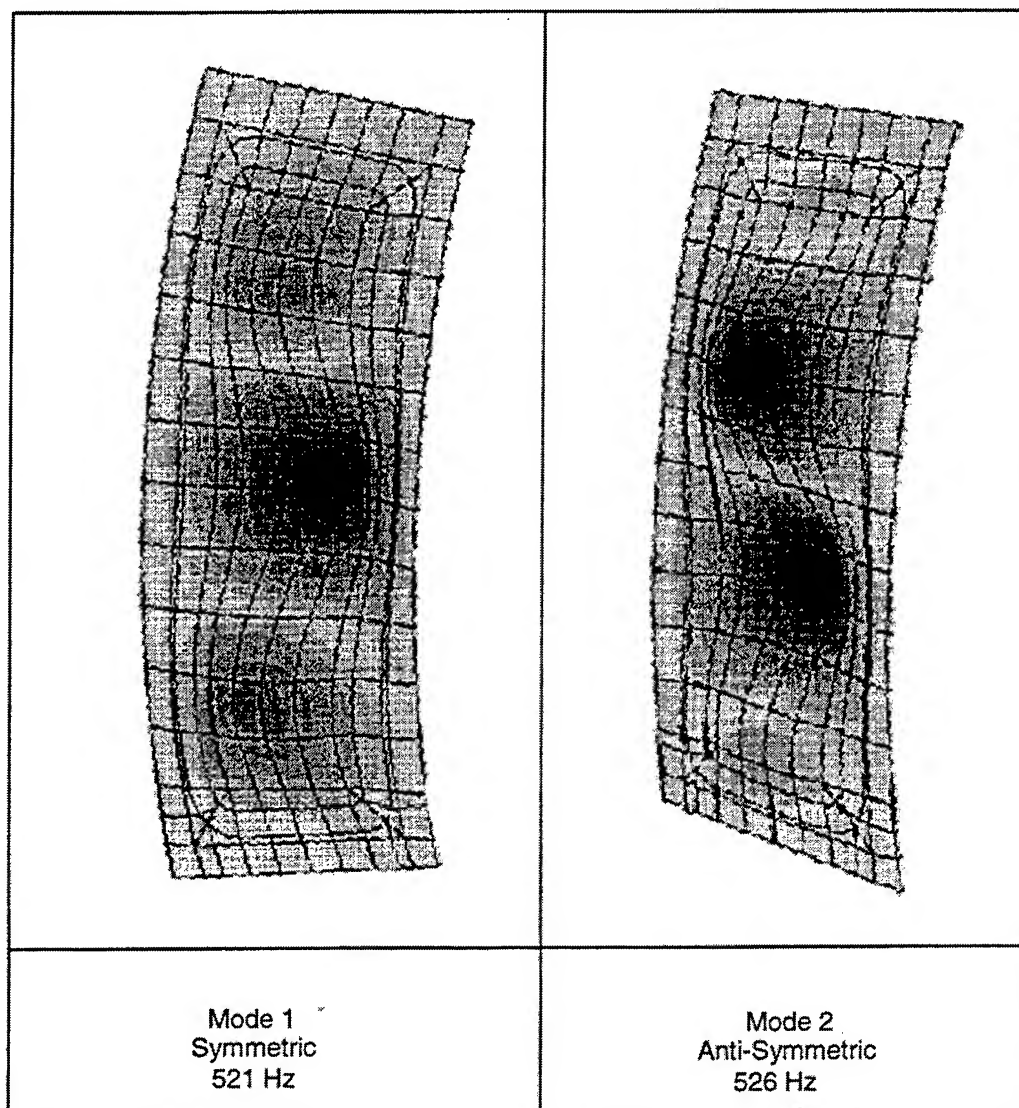


Figure 2-1. Predicted Mode Shapes and Frequencies

Time histories of the data, PSDs, coherence plots and Frequency Response Function (FRF) plots were obtained for each channel recorded when the data were reduced. These results were used to extract mode shape and damping values. Mode shape was determined in two ways, if possible, for each record. The first method utilized the time history plots to determine relative values during the decay and the second used the FRFs generated from all of the pulses on a record. Accelerometer data showed, also, that the widthwise variation of the mode shapes was as expected, i.e., one lobe.

Composite mode shapes were determined by combining data from the separate records. In each case the data were made symmetric or anti-symmetric about the center of the panel depending on the mode under consideration. The symmetric mode was normalized to a deflection of 1.00 at the center of the panel, and the anti-symmetric mode was normalized to a deflection of 1.00 at locations corresponding to

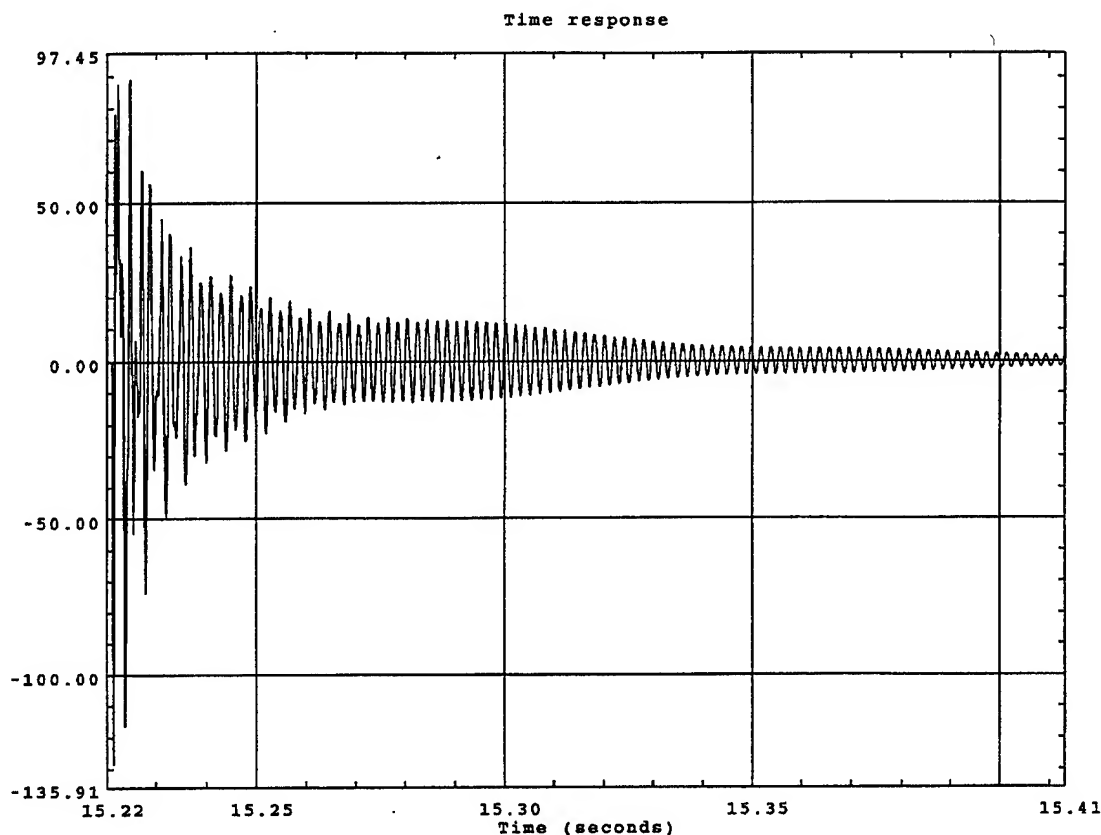


Figure 2-2. Representative Tap Test Accelerometer Time History

shapes. The resulting mode shapes were then used to locate the PZTs on the laboratory test panel for their greatest effectiveness.

Damping was determined in two ways. One was to find the log decrement of the decays exhibited by the time histories. The second was to use the half power method on the PSD plots. Time history decays gave two values for damping: one right after the pulse, and another when the vibration amplitudes had decreased in magnitude and one frequency tended to dominate the record (See Figure 2-2). Damping during the initial decay was approximately 3-4 percent as determined by the log decrement method. The log decrement and the half power methods resulted in damping values ranging from 0.5 percent to 0.7 percent for the later decay on the trace. These results show that the damping is non-linear with the magnitude of the panel vibration. The relatively low damping in the panel made it an excellent test panel for the AVSS Program. It is easily excited by the engine noise during takeoff and climb out, and by the in flight turbulence that exists at the aft end of the B-1B at high subsonic Mach Numbers.

2.2 SELECTION OF PZT GEOMETRIC PROPERTIES AND ADHESIVE

The properties of the PZT patches, size, thickness, the number of PZT layers and the best adhesives for attaching the patches to the B-1B skin were determined by coupon tests. Issues such as size and shape of the actuators, type of epoxy used to bond the actuators to the aircraft skin, performance of the actuator over the temperature range -60 to +185 °F, and determination of the appropriate drive voltage for bipolar operation were investigated.

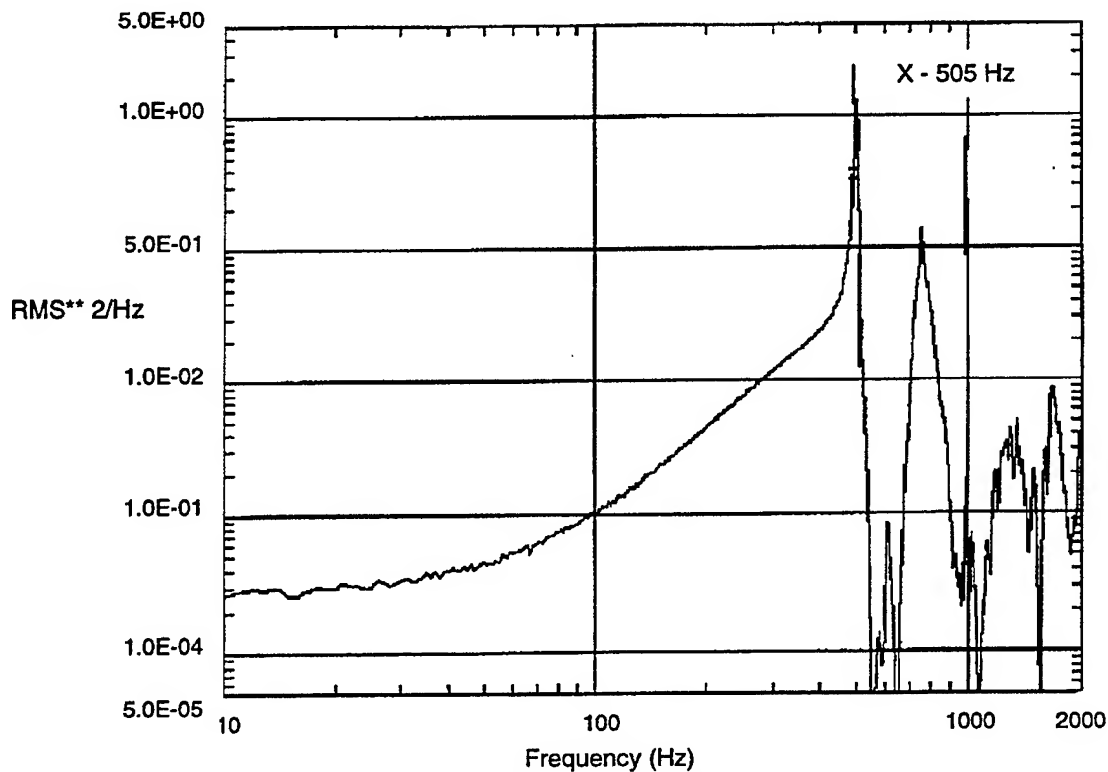


Figure 2-3. Representative Autocorrelation Plot From Tap Test

Piezoelectric materials possess a unique range of properties allowing them to produce very high levels of force, while using very little power. The Rockwell Science Center has developed a patented piezoelectric PLZT (lead and lanthanum + zirconium + titanium) composition which exhibits a piezoelectric constant (d_{33}) > 950 pC/N, strain levels of 0.2 percent, and a well-established fatigue life of over 5×10^8 cycles. The strain level is over twice as large as exhibited by most commercial piezoelectric materials, while the life is 10 times the lifetime quoted by most manufacturers. Because of the superior performance of this new composition, it was selected for use in this study.

Coupon tests were performed to accomplish the following tasks.

1. Determine the optimum thickness, area and shape of the patch actuator.
2. Establish the force output of the actuator as a function of frequency, voltage and temperature.
3. Establish which of the three candidate epoxies had the best overall performance over the -60 to $+185$ °F temperature range.

2.2.1 Coupon Description and Testing

The important PZT parameters were established through a series of experiments on test coupons. The coupons were made from 0.083inch thick, 0.5inch wide 2024-T62 aluminum and varied slightly in length. Figure 2-6 shows a schematic diagram of one test coupon. The piezoelectric patch actuator is bonded to the coupon with one of three different non-conducting epoxies (Hysol EA 9395, Hysol XEA 9360 or Magnolia Plastics 6155). In addition, each coupon has a small dot of conducting epoxy (Eccobond 56C) in the center of the bond to allow the coupon to be used for electrical contact to the back of the patch actuator (Figure 2-7). The test is performed by clamping 0.5 inch of the coupon, applying an electric field to the piezoelectric patch

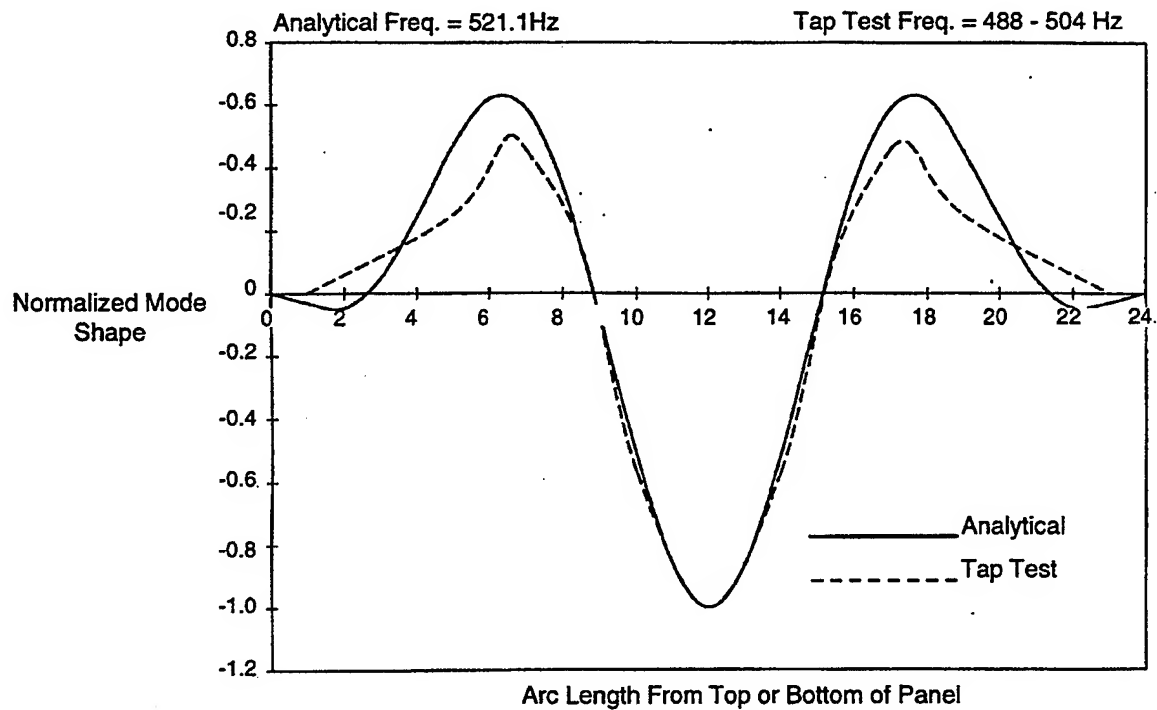


Figure 2-4. Comparison of Tap Test Results With Predicted First Symmetric Mode

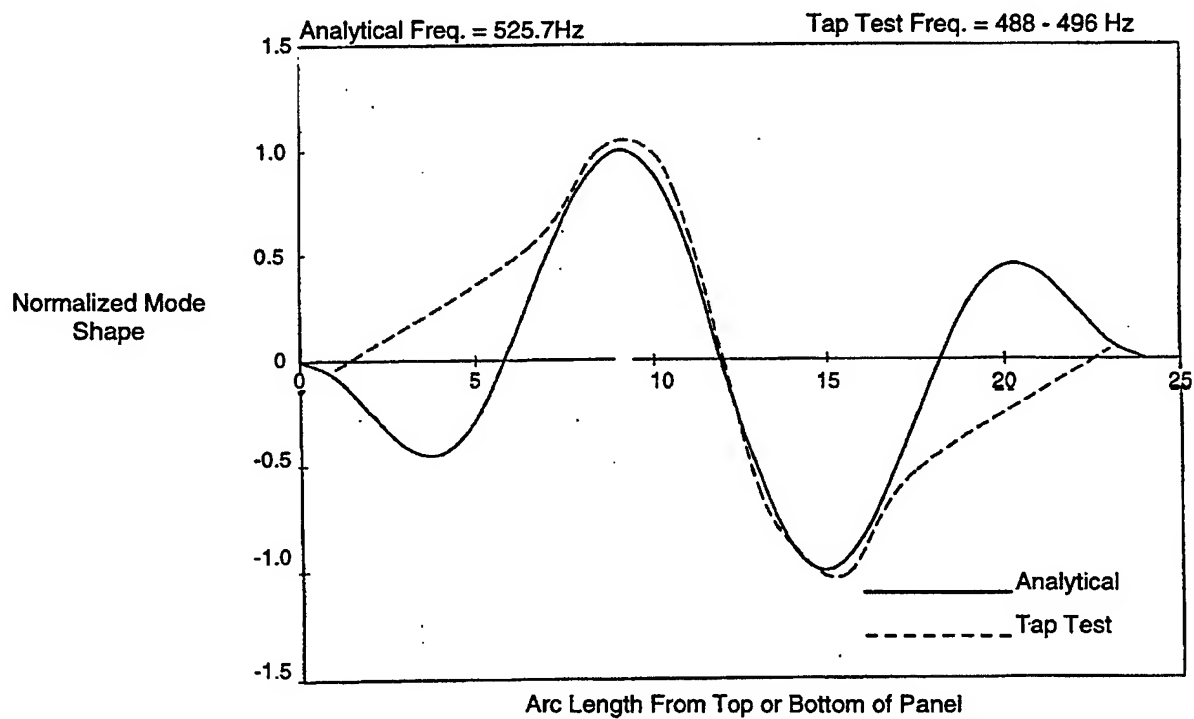


Figure 2-5. Comparison of Tap Test Results With Predicted First Anti-symmetric Mode

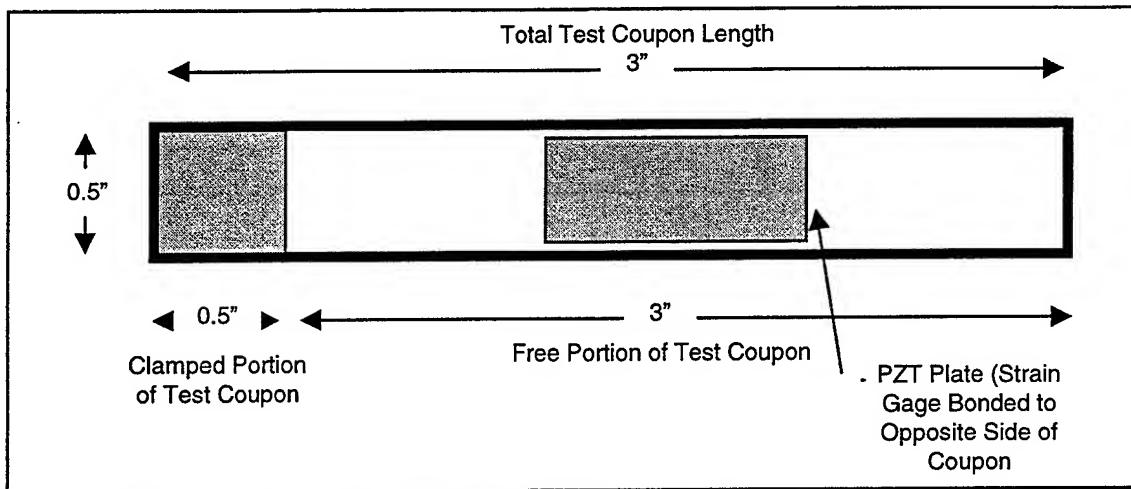


Figure 2-6. AVSS Test Coupon

actuator and measuring the strain generated in the material and/or displacement of the end of the coupon.

The first 12 test coupons were 3.5 inch in total length and had 3.0 inch free to vibrate. The strain was measured through a strain gage mounted on the side opposite the patch actuator. The displacement of the coupon was measured by a MTI 2000 optical displacement meter which works by examining the phase shift of reflected light from the coupon surface. The minimum peak to peak displacement observable with this device is $\pm 1 \mu\text{m}$. A typical strain and displacement versus applied voltage plot is shown in Figure 2-8. Strain and displacement track each other closely, as expected. Tests using both techniques were performed on the first 10 coupons, after which it was decided to drop the strain gage for measurement simplicity.

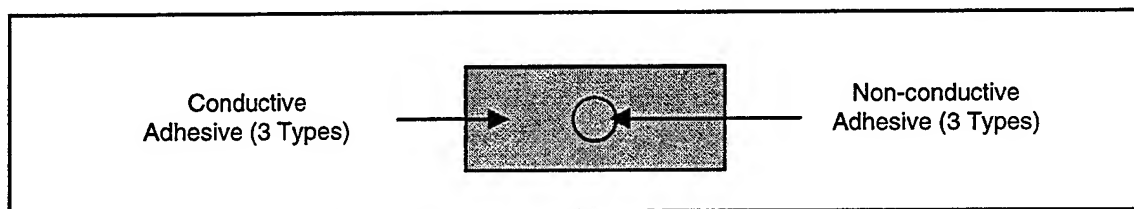


Figure 2-7. Configuration of Conducting and Non-conducting Epoxies

2.2.2 Actuator Thickness Selection

The first nine test coupons were used to examine the coupon performance as a function of actuator thickness and epoxy bond. One patch actuator of each thickness (0.015, 0.030, or 0.060 inch) was bonded to a coupon with one of the three epoxies (9395, 9360 or 6155). This allowed the direct comparison of the performance of each patch thickness in conjunction with each epoxy. The room temperature performances of the three epoxies in this study were comparable. However, distinct differences in performance as a function of actuator thickness, were observed. The thinnest patch (0.015 inch) consistently had the lowest displacement due to its smaller force than the thinnest one, but only slightly more than the 0.030 inch actuator. The added

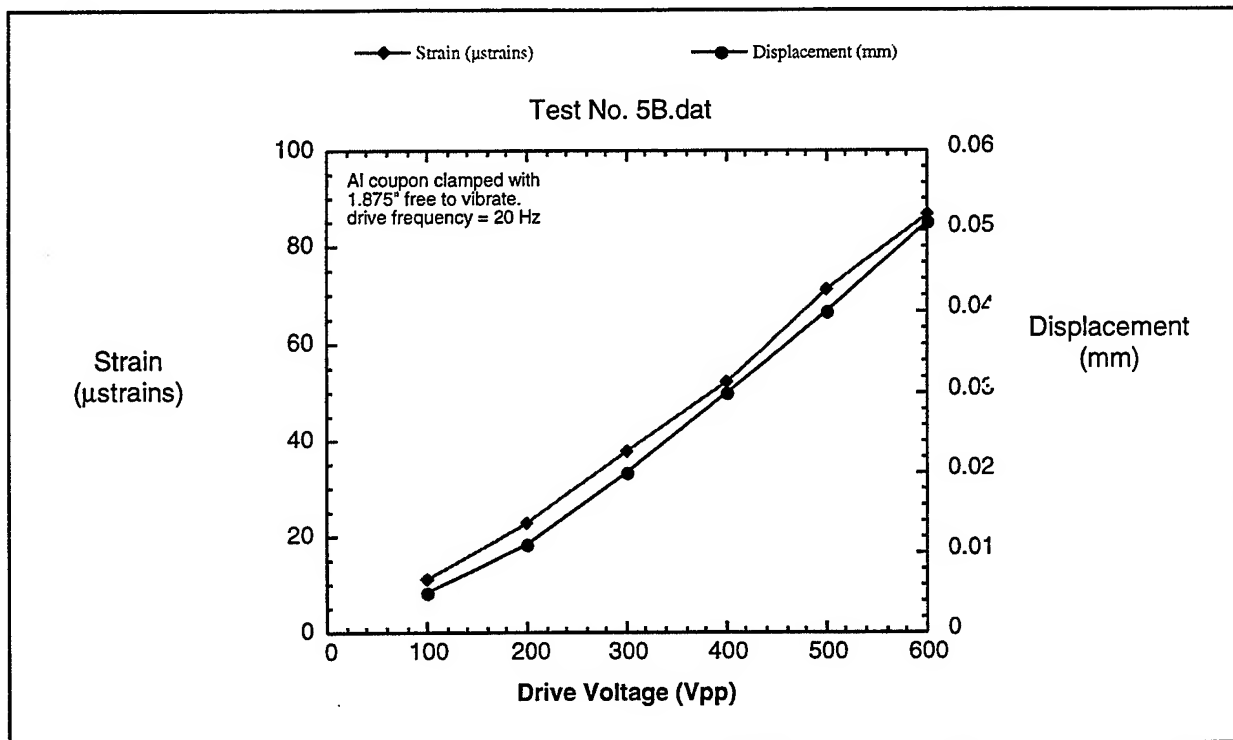


Figure 2-8. Typical Strain Gage and Optical Displacement Measurements

stiffness of the thicker actuator made it less attractive, so the intermediate thickness was deemed the most suitable. Additional experiments were performed comparing the performance of 0.020 inch and 0.030 inch thick actuators and the 0.020 inch consistently exhibited the best results. For this reason, 0.020 inch thick actuators were used in all subsequent studies and on the B-1B test flights.

2.2.3 Frequency and Temperature Considerations

The natural resonance frequency of a vibrating structure is related to its stiffness and length. Figure 2-9 shows the displacement vs. drive frequency of three different length test coupons. As the free length is shortened from 3 to 1.5 inches, the resonance frequency increases from ~220 to ~1000 Hz. Since the resonant frequencies of the B1-B panel were originally thought to be between 600 and 650 Hz, test coupons were made with 1.5 inch free length to allow tests to be performed in that frequency range.

The coercive field (E_C), i.e., the electric field needed to pole a piezoelectric material varies as a function of temperature. This relationship is shown for the Science Center PLZT in Figure 2-10. As the temperature increases and approaches the Curie temperature, the electric field required to pole the material decreases. Since the actuators are operating with a bipolar signal, special consideration has to be given so that the negative portion of the drive voltage is not sufficiently high to switch the polarization of the material. The lower curve in Figure 2-10 shows the allowable electric field for this PLZT composition as function of temperature. As long as the field

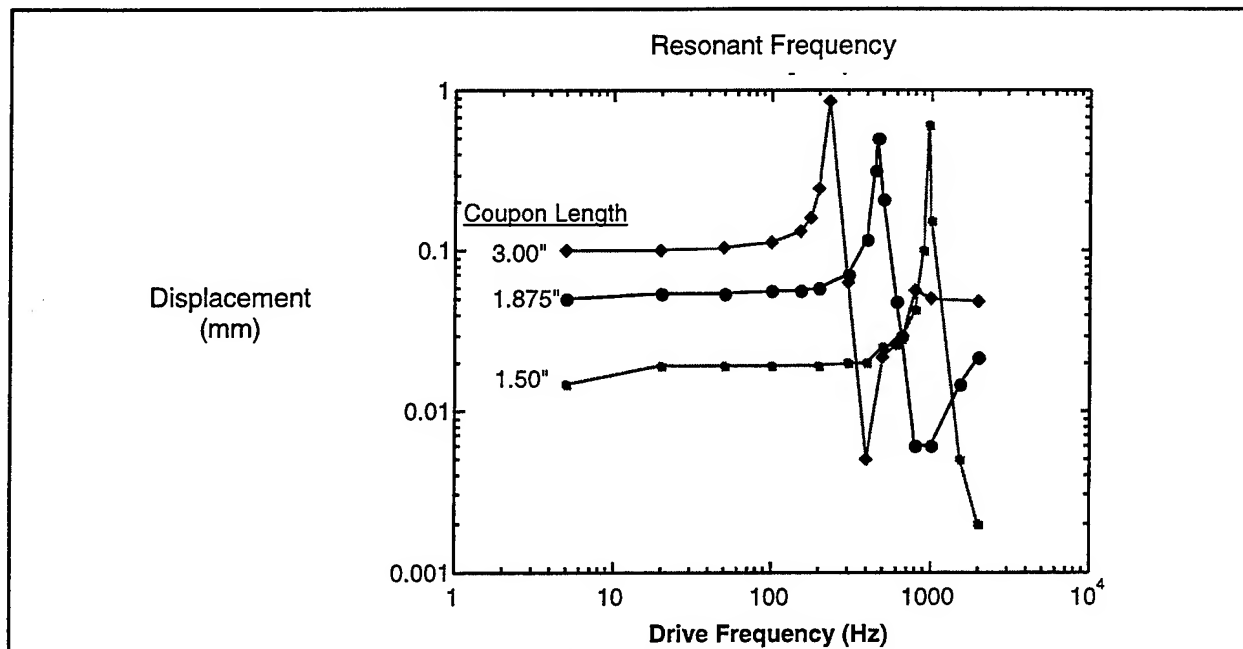


Figure 2-9. Effect of Coupon Length on the Resonant Frequency

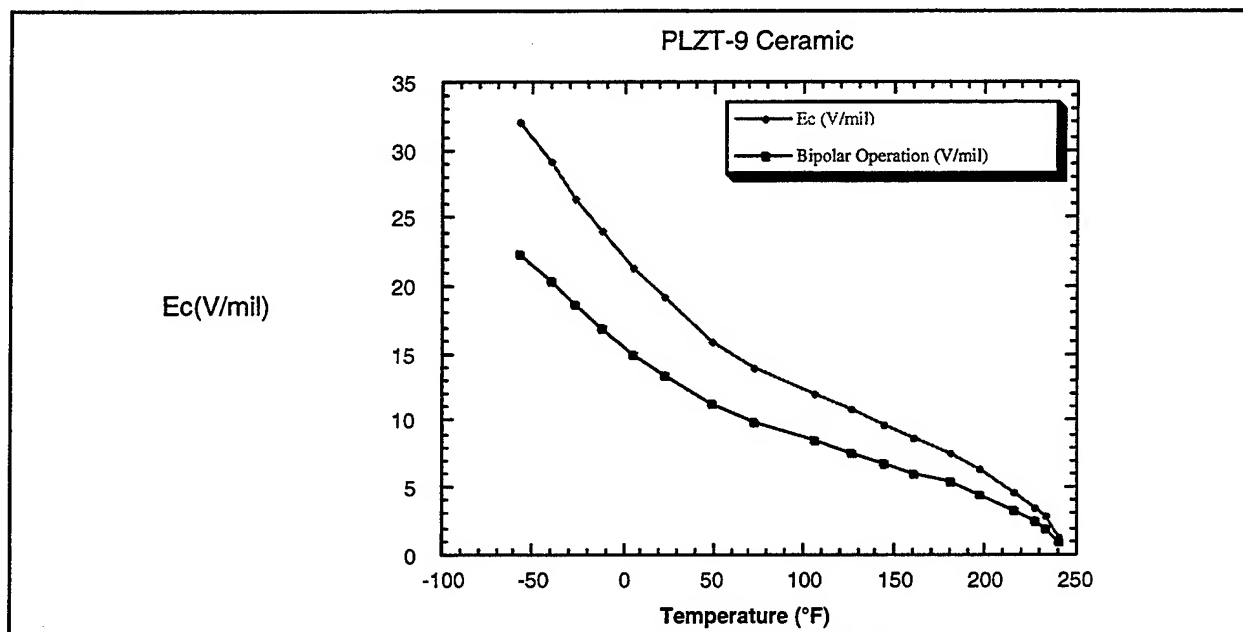


Figure 2-10. Coercive Field (E_c) vs. Temperature

2.2.4 Adhesive Selection

Since the performance of the three epoxies did not vary significantly at room temperature, high (+185 °F) and low (-60 °F) temperature tests were necessary to establish the optimum compound. Figure 2-11 compares the room temperature and high temperature performance of a typical test coupon. Since the piezoelectric performance increases as a function of temperature, the displacement of the coupon

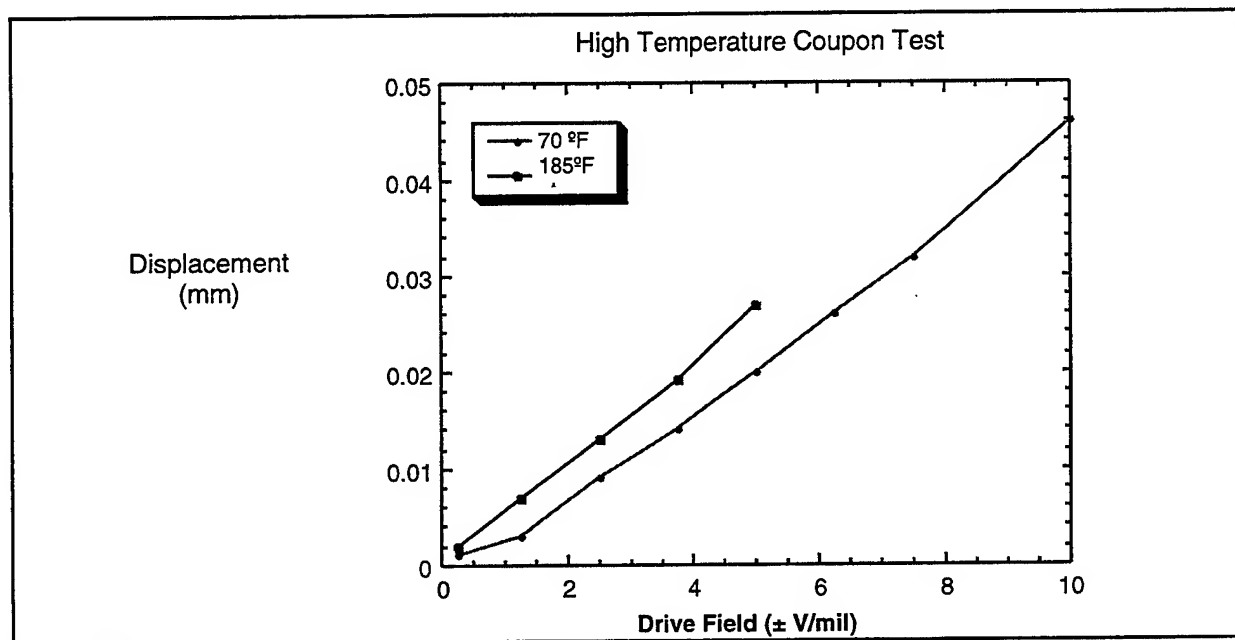


Figure 2-11. Displacement Comparison - High vs. Room Temperature

at 185 °F is higher than at room temperature for a given electric field. However, due to the decrease in E_C at elevated temperatures, the actuator can only be driven at ± 5 V/mil to avoid de-poling. Once again, the performance difference between the two Hysol epoxies (9395 and 9360) was negligible, but the Magnolia Plastics 6155 had significantly reduced performance at this temperature and was deemed unsuitable for this application.

The results of a typical low temperature coupon test are shown in Figure 2-12. Because the piezoelectric performance decreases with temperature, the displacement at -60°F is lower than at room temperature for a given electric field. However, because the E_C is much higher at this temperature, the actuator can be driven at ± 18 V/mil, resulting in higher overall displacement. Once again, the performance difference between the two Hysol epoxies (9395 and 9360) was small, neither showing a significant advantage.

Figure 2-13 shows a summary of the high and low temperature tests performed on actuators bonded with Hysol EA 9395 and XEA 9360. The high temperature performance of the XEA 9360 is slightly better, but the low temperature performance of the EA 9395 is superior. Based on the overall results of all the coupon tests, either epoxy would meet the strength and temperature requirements for this application. The decision was made to use the Hysol EA 9395 on all of the tests at SSD and the B-1B test aircraft, primarily because EA 9395 was a well-established Hysol product, and XEA 9360 was a new experimental compound. However, the actual schedule to fly the AVSS was moved up, and the delivery of the Hysol EA 9395 did not arrive in time, consequently the Hysol 9360 was used for both lab testing and on the aircraft.

2.2.5 Actuator Patch Configuration Selection

Another important issue in this project was the optimization of the size and shape of the patch actuators. Because of the curved surface of the B-1B panel (38

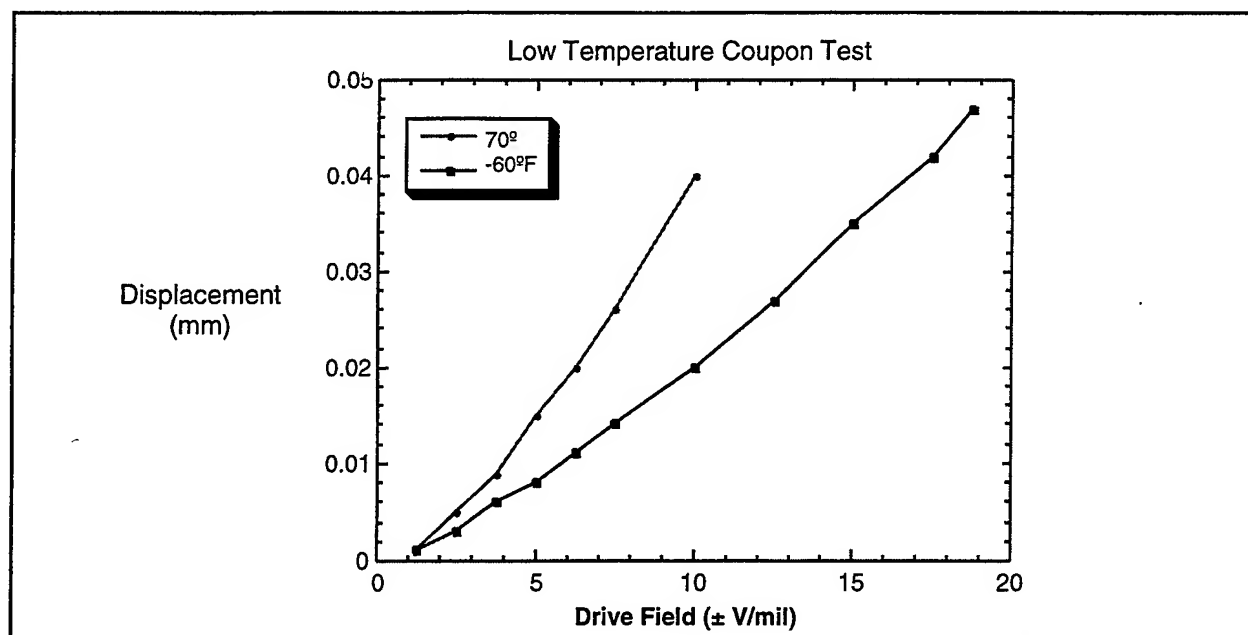


Figure 2-12. Displacement Comparison - Low vs. Room Temperature

inch radius of curvature), flat large area patch actuators would leave significant gaps between the actuator and the aircraft skin. If this gap were filled with epoxy, actuator force would be lost in the much softer epoxy, thus, reducing the performance of the system. To avoid this problem, the use of a mosaic type structure of patch actuators was investigated. For example, instead of using a single 1.0 inch x 1.0 inch actuator, two actuators of 0.5 inch x 1.0 inch area were bonded next to each other. An additional test was performed using three 0.33 inch x 1.0 inch patch actuators. Figure 2-14 compares the performance of each of these devices. Although there is a slight decrease in displacement when using multiple actuators consisting of the same total area as a large single one, it is much preferable to filling large gaps with epoxy. To further minimize the gap behind each actuator, a 38 inch radius of curvature (to

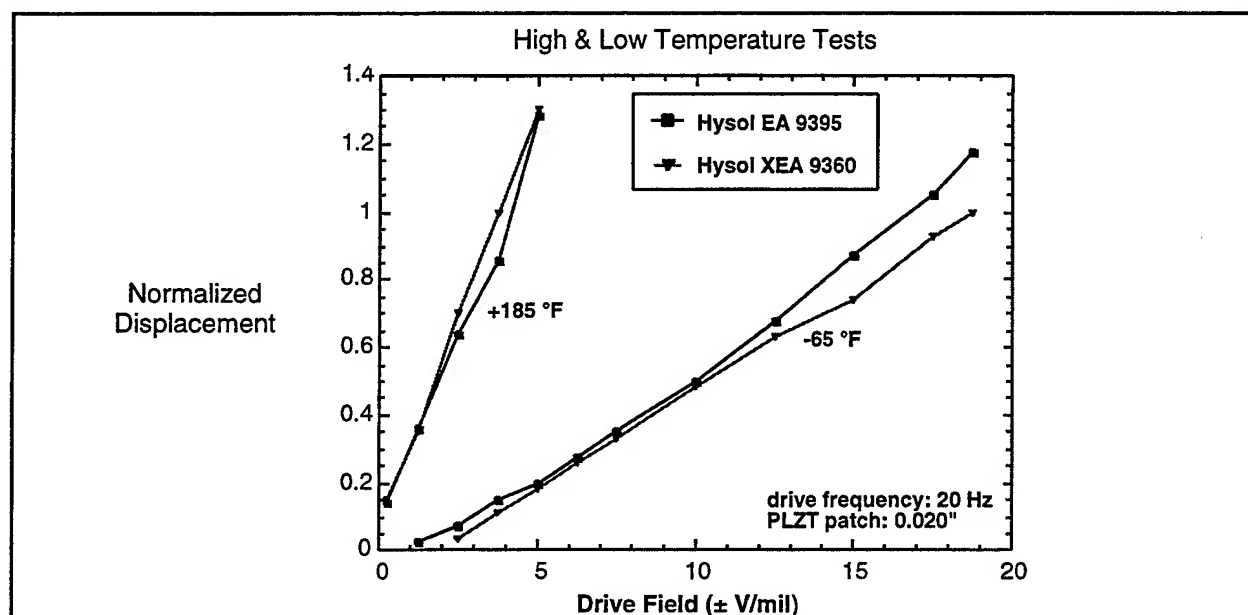


Figure 2-13. Comparison of EA 9395 and XEA 9360 Epoxies

match the B-1B panel) was lapped onto the back of each one. In order to minimize any variation in the force across the actuators, 0.33 inch x 1.0 inch area patch actuators were used on the B-1B test aircraft.

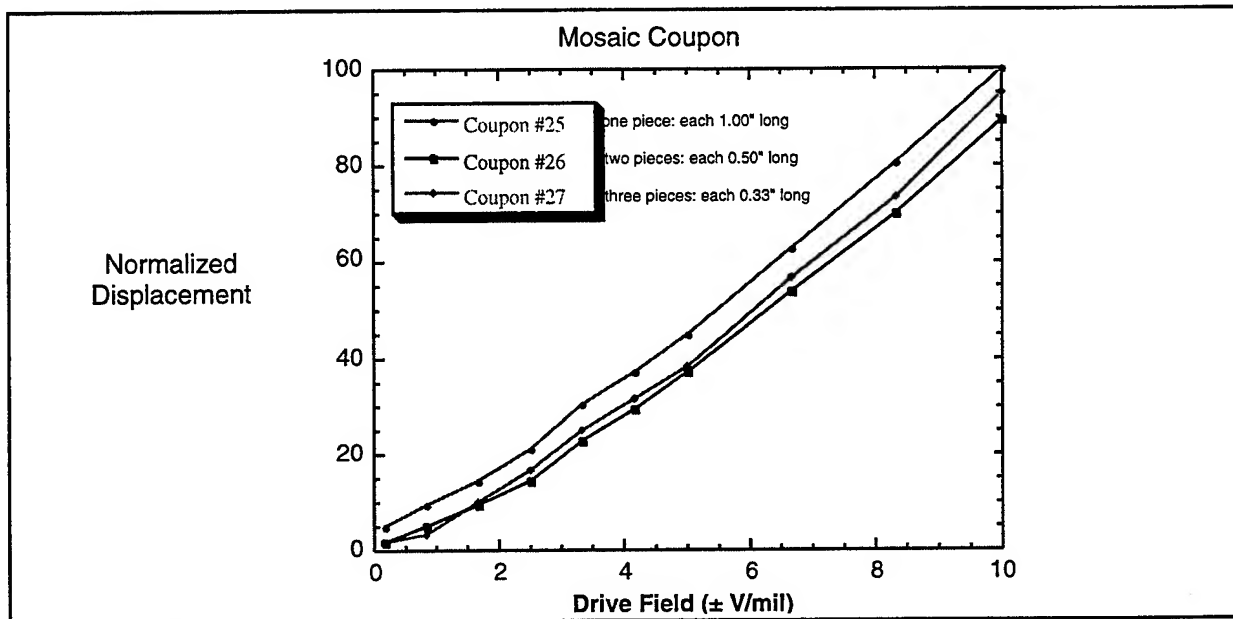


Figure 2-14. Comparison of Different Mosaic Patch Structures

2.2.6 Actuator/Adhesive Durability

The last major issue to be investigated was the expected lifetime of the patch actuator and the epoxy bond. Cracking or fatigue damage to the actuator or delamination of the actuator due to epoxy bond failure would cause problems. To establish the device lifetime, a coupon was driven at near resonant frequency to accelerate the fatigue process, and its performance monitored as a function of time or number of cycles. Figure 2-15 shows the normalized displacement as a function of cycles for actuators bonded with EA 9395 and XEA 9360 epoxy. A decrease in performance was expected as a significant number of cycles were accumulated. However, the displacement of the coupons actually increased with time. After a thorough examination of the coupon, it was determined that the aluminum, not the patch actuator or the epoxy bond, was fatiguing to failure by the stress being put on it by the patch actuator. As the crack in the aluminum coupon continued to grow, the displacement increased because the system became softer. There was no sign of patch actuator fatigue or bond delamination in any of the lifetime studies. For this system, the patch actuator is stronger than the 2024 aluminum.

2.3 LABORATORY TEST CONFIGURATIONS

In order to develop both the PZT patch configuration and the control laws, tests were performed on two laboratory test panels. One was a curved panel which simulated the chosen aircraft test panel. Concern about driving the panel with the PZTs because of its curvature and thickness led to the use of a flat panel first. This was decided upon because previous experience had been with flat panels of thinner

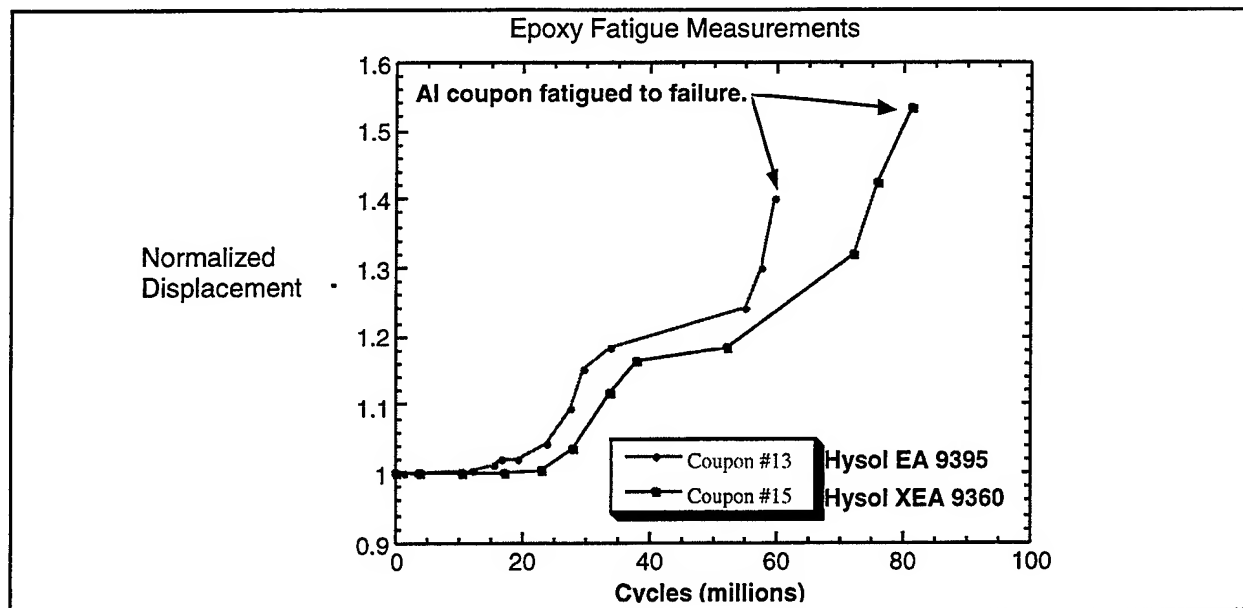


Figure 2-15. Fatigue Test of Coupons with Different Epoxies

gage and their known behavior was fairly well understood. The thickness of the panel would be the new variable in the testing. It was felt that the transformation from the flat plate to the curved panel would then highlight the differences that curvature introduced.

A small reverberation acoustic chamber was available at the Boeing North American facility in Downey, California. It was decided to mount the panels in the wall of this chamber. In this way the panels could be excited by either small shakers to determine their dynamic characteristics or by an acoustic field which simulated Sound Pressure Levels (SPL) the B-1B panel would see on the airplane. This acoustic environment was determined by previous measurements on B-1B aircraft.

2.3.1 Flat Panel

The flat panel was sized to mount to the same fixture used to install the curved panel in the acoustic chamber. It, therefore, represented the projection of the curved panel on a flat surface. Figure 2-16 shows a schematic of the plate and indicates the location of the PZTs and the accelerometers mounted to the plate. Locations of the PZTs were specified by the anti-nodes for the first symmetric and first anti-symmetric modes. The first symmetric mode for a flat plate has the anti-node at the center of the panel. This acoustic environment was determined by previous measurements on B-1B aircraft.

For the panel tested, this first mode was found to have a natural frequency of 237 Hz. Two anti-nodes are located on the panel for the first anti-symmetric mode which in this case had a natural frequency of 266 Hz; they are located approximately 6 inches from the center of the panel in both directions. Originally, 4 PZTs, 1 inch by 1 inch by 0.02 inch thick, were placed at the center of the panel for symmetric mode attenuation. This was later increased to five in order to evaluate the effect of additional PZTs. For the anti-symmetric mode, 2 PZTs were used at the top and three

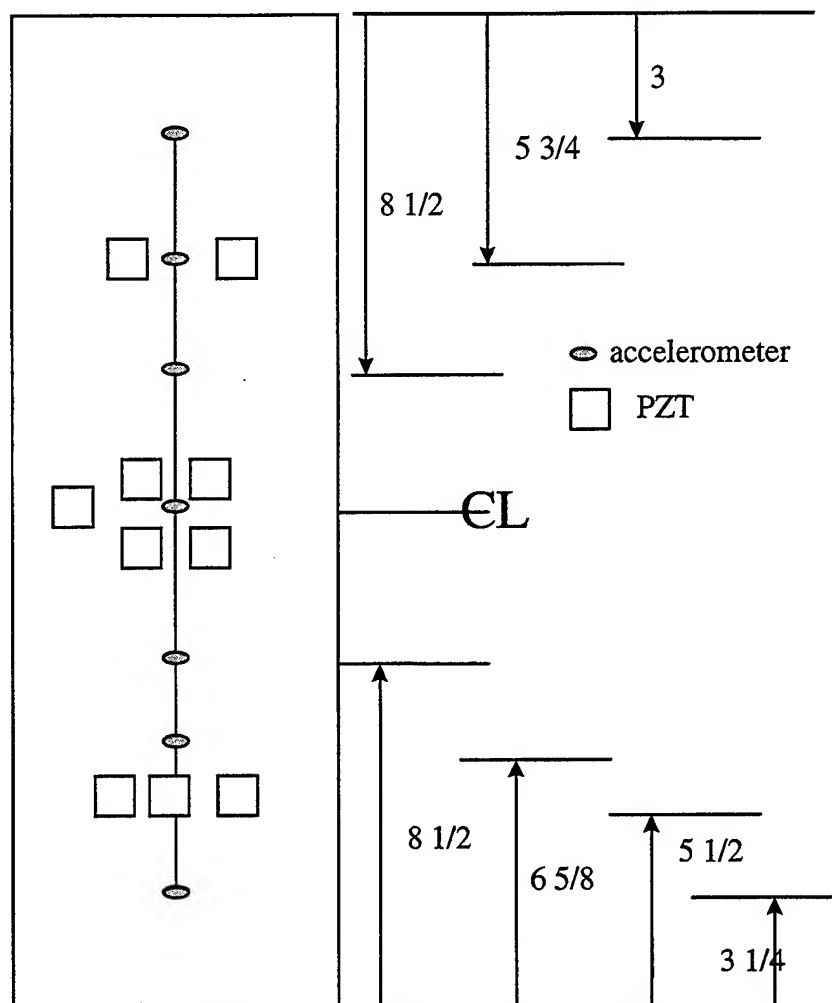


Figure 2-16. Flat Panel Accelerometer and PZT Locations

at the bottom. The difference between the top and bottom had to do with the number of PZTs available for test at that time and not for any technical reason.

2.3.2 Curved Panel

The curved panel had approximately the same width, length, thickness, and radius of curvature (38 inches) as the aircraft panel, but it had no curvature in the widthwise direction, because that was thought to be a secondary effect. Finite element analysis, tap test, and limited modal testing showed that the modal characteristics of the first symmetric and anti-symmetric modes were the same as the panel on the aircraft. However, for the curved laboratory test panel the first symmetric mode frequency was around 437 Hz, rather than the 521 Hz found for the aircraft tap test. This change in frequency was due to the mass effects of the PZTs and the accelerometers mounted on the panel. 437 Hz was very close to the frequency recorded on the airplane (427 Hz) when PZTs and accelerometers were installed on that panel. The first anti-symmetric mode frequency for the laboratory test panel was 420 Hz; on the aircraft it was 527 Hz for the tap test and 427 with PZTs and accelerometers installed. Figure 2-16 shows the configuration of the curved panel and the location of the PZTs and the accelerometers. There were 14 PZTs in the

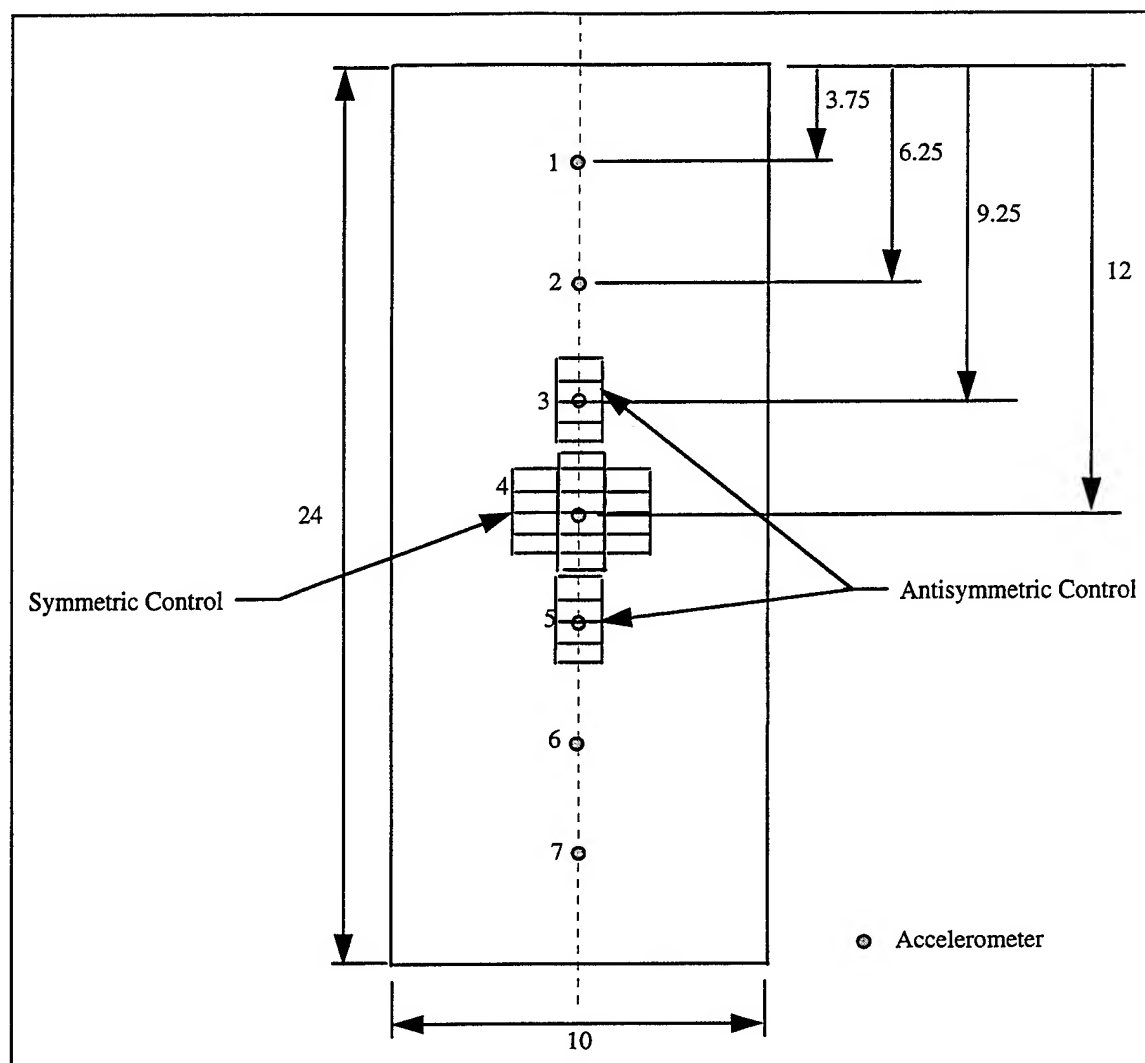


Figure 2-17. Curved Panel Accelerometer and PZT Locations

center of the panel for the symmetric control; they were each 1 inch by 1/3 inch by 0.020 inch thick. Eight PZTs were used for anti-symmetric control, four at the top patch and four at the bottom. Figure 2-17 shows the curved panel mounted in the wall of the acoustic chamber and a small shaker attached for determining natural frequencies and mode shapes.

2.4 ELECTRONIC HARDWARE

The electronic hardware for the AVSS consisted of two units: a power amplifier unit and a control unit. On the aircraft they were supplied with 28 Volt (V) dc. and 110 V ac. On the ground, equipment weight and equipment size are not important factors, but in the aircraft, size and weight are very important. It was desired to use AVSS units that had minimum weight and size in order to fit within the available space with as little impact as possible. The two units are shown in Figure 2-18.

2.4.1 Power Amplifier Unit

Three amplifiers and two analog filters were housed in the amplifier unit, which was specially designed for the B-1B flight demonstration. The amplifiers had a gain of 40 for voltages of 5 Volts and below, and the analog filters were second order low

passes with a bandwidth of 800 Hz. Two Arnold Magnetic +/- 200 V dc 500 milli-Ampere (mA) power supplies were used for the symmetric and anti-symmetric circuits.

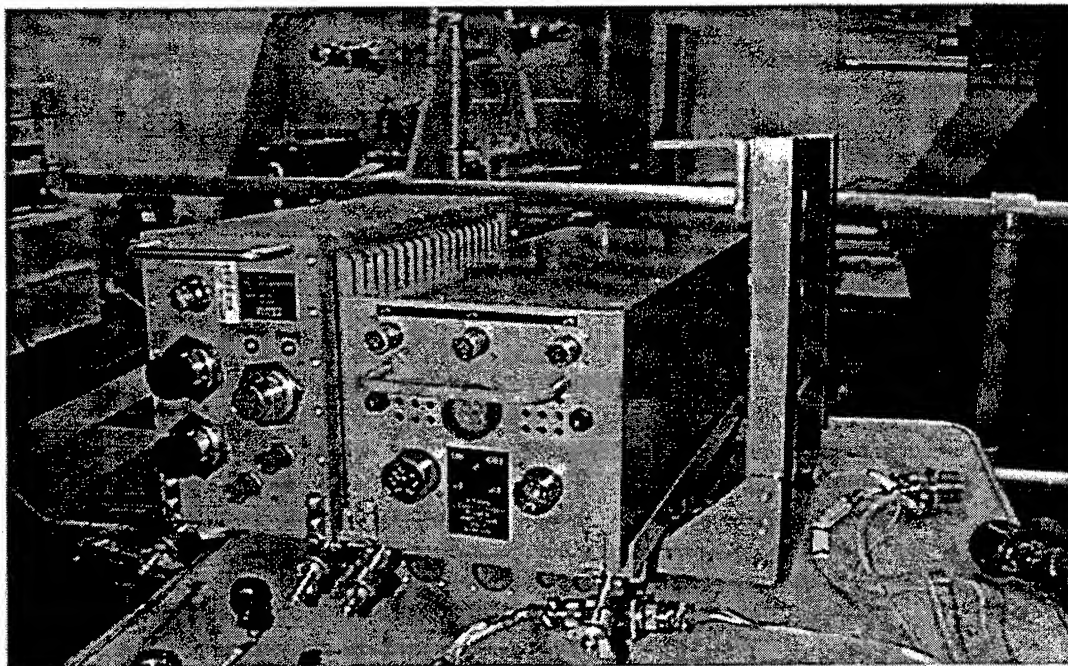


Figure 2-18. Control Unit And Power Amplifier Unit

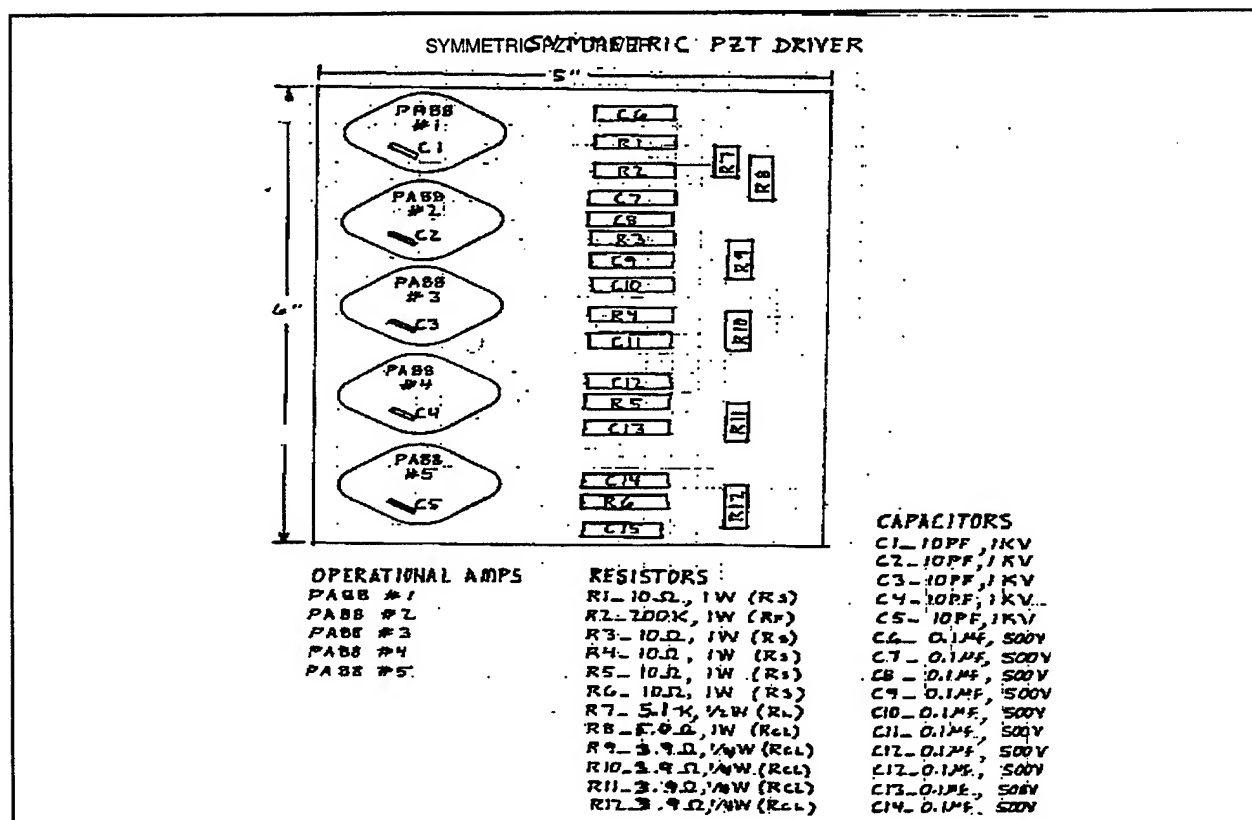


Figure 2-19. Layout of Symmetric Amplifiers

They require an input of 103 to 127 V ac that is 47 to 500 Hz single phase. In addition power conditioning circuitry was developed to supply +/- 15 V dc for the filter networks.

The symmetric amplifier shown in Figure 2-19 was housed on a vector board with an aluminum plate used as a heat sink. Five APEX PA88 amplifiers were designed in parallel in order to provide up to a maximum current of 500 mA. The symmetric amplifier circuit provides amplification of the symmetric control signal to the center PZT patch on the panel.

Two amplifier circuits were used to drive the top and bottom patches for the anti-symmetric control. These two circuits were the same with the exception that the bottom patch driver was 180 degrees out of phase with the top patch driver. Both were mounted on the same vector board. Both anti-symmetric drivers only provide up to 200 mA using two of the APEX 88 amplifiers operating in parallel. Figure 2-20 is the layout of the anti-symmetric amplifiers.

The filter network was housed on a separate vector board and consists of two identical filters as described above. One 747 DIP (Dual Op Amplifier) is used to create the filters. The 28 Volts dc input power was conditioned, using 1N4744 Zener diodes, to create +/- 15 Volts dc for the operational amplifier supplies.

The power amplifier unit schematic is shown in Figure 2-21. All components in the box were potted using RTV silicon based material. The housing also has a duct to receive cooling air from the aircraft. The housing was designed and fabricated at Edwards AFB and supplied to SSD.

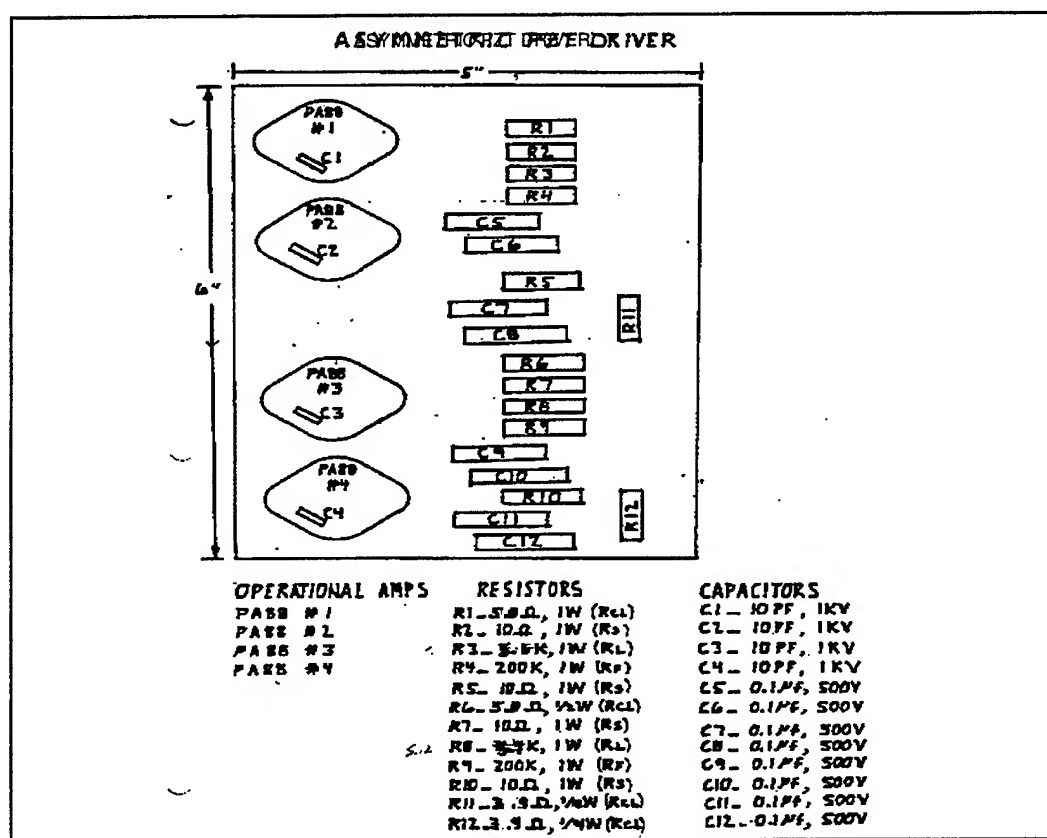


Figure 2-20. Layout of Anti-symmetric Amplifiers

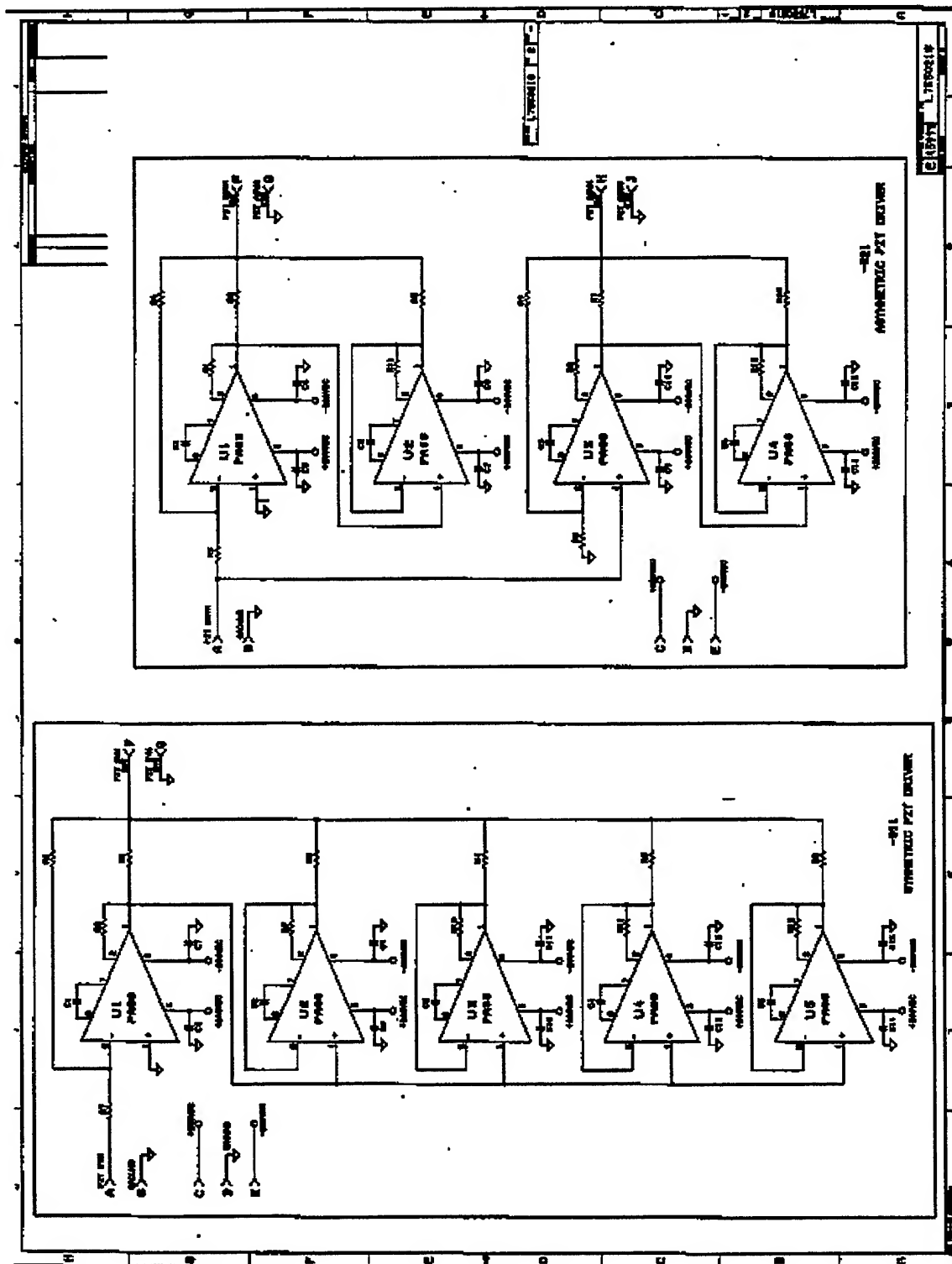


Figure 2-21. Schematic Of Symmetric and Anti-Symmetric Amplifiers

2.4.2 Control Unit

The Control Unit consists of a flight rugged 1/2 ATR chassis with a full military power supply that can house up to five VME boards. Input power required was 28 V dc at 4 A. Three single computer boards were considered because they were thought

to meet the 10,000 Hz sampling rate. The 10,000 Hz rate translates into a 100 microsecond (μ s) time period for converting the three accelerometer analog signals to digital signals, calculating the microprocessor commands for both the symmetric and anti-symmetric controllers, and then converting the digital signals back into analog signals. The three boards considered were: Rigal, Dspace and AITech(Motorola 68040). The Rigal board had been successfully used at the Science Center, the Dspace board could be programmed with Mat-lab and the AITech board had previously been used at SSD. The Rigal board was purchased but was difficult to program. The Dspace board was not tested but its automatic programming was known to be inefficient, and therefore the 100 μ s processing time would be difficult to achieve. It was felt that the safest approach was to use the AITech board since SSD had previous experience in using it. All programming was done in 'C'. The input accelerometer readings (± 2.5 V max.) required three Analog to Digital (A/D) channels, which converted each input to a 12 bit digital number. The outputs of the Control Unit required two channels of Digital to Analog (D/A) conversion, one for symmetric and one for anti-symmetric. A/D and D/A functions were provided by a commercial MATRIX board. This board was modified with a thermal pad, which covered the entire board. The pad was thermally conductive but electrically isolated. An additional aluminum plate was added to provide some level of conduction to the rails of the Control Unit chassis.

2.5 CONTROL SYSTEM DESIGN

2.5.1 *Generating the Design Plant Model*

The H_∞ method was used for control system design. To apply the H_∞ method, a reduced order plant model is needed. The H_∞ model includes the modes that require active control. Additional dominant modes, which happen to be near the modes to be controlled, should also be included in the design model even if they do not require active attenuation. The derived H_∞ controller $K_m(s)$ guarantees to stabilize all modes that have been included in this model, otherwise, some modes, which have not been included, may become unstable when the loop is closed. In the symmetric loop, for example, the design model $G(s)$ (before augmentation) consists of the first four symmetric modes of the aircraft panel at frequencies: 430, 570, 630, and 740 Hz. Even though attenuation is only intended for the first mode, the other three modes are also included in the design model because they are near the cross over frequency. In addition to the flexible modes, the design model contains amplifier low-pass dynamics and computational delays that were included as part of the design plant $G(s)$ using approximations.

The H_∞ control design algorithm uses the H_∞ Synthesis Model (SM), shown in Figure 2-22. It mainly consists of the design model $G(s)$ plus some additional matrices that are design parameters and the designer sets them. The H_∞ synthesis model inputs are: (a) the control input (u_c) which enters the SM via matrix B_2 , (b) the input noise disturbance (w_i) which enters via matrix B_1 , and (c) the output noise disturbance (w_o) which enters via matrix D_{21} . Matrix D_{21} is a design parameter indicating the amount of output noise or the amount of uncertainty corrupting the measurements. The designer can finalize it usually after a few educated guesses. The H_∞ synthesis model outputs are: (a) the sensor measurements (y_m) which is a combination of the state vector via matrix C_2 , (b) the output criteria (z_c) which is a variable that must be minimized by the control system, coming out via matrix C_1 , and (c) the control input

criteria (z_i) which penalizes the controls in the optimization algorithm via matrix D_{12} . Matrices C_1 and D_{12} are design parameters in the optimization algorithm, C_1 is penalizing the modes to be attenuated, and D_{12} is penalizing the controls (u_c). The design parameters can be specified by the designer usually after a few trials.

After the SM has been determined, it is applied to the H_∞ design algorithm (described in Reference 2) which generates the dynamic controller $K_{inf}(s)$ that closes the control loop between the measurements (y_m) and the control inputs (u_c) in Figure 2-22. The H_∞ controller not only stabilizes the dynamic system, but it also minimizes the infinity norm of the closed-loop transfer function between the disturbances (w_i, w_o) and the criteria (z_i, z_o).

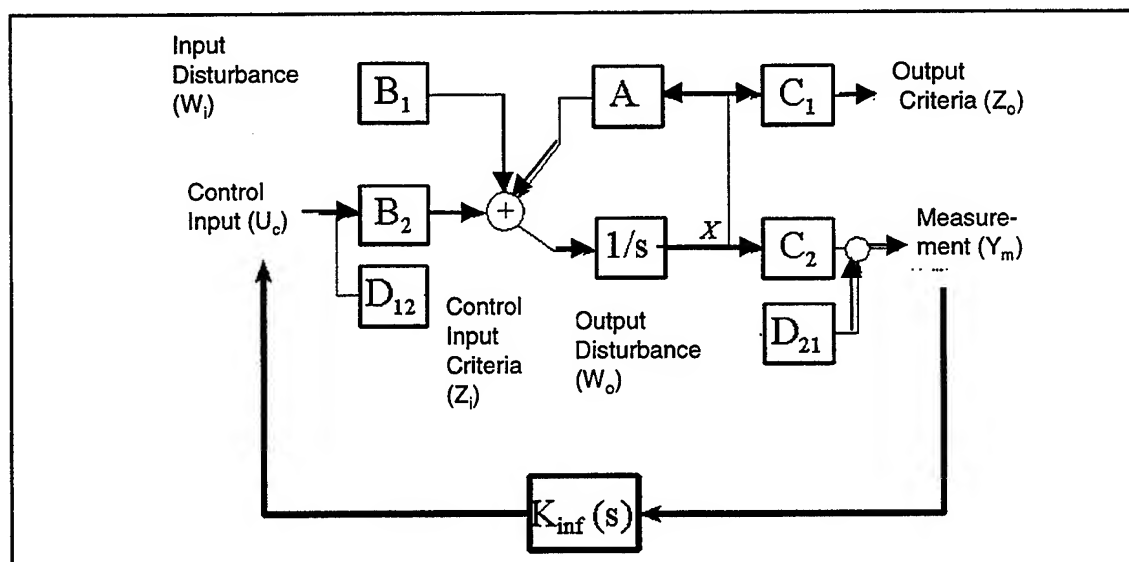


Figure 2-22. H_∞ Synthesis Model

2.5.2 Loop Shaping

Loop shaping on the synthesis model is used to specify closed-loop system objectives in terms of requirements on the open-loop frequency response characteristics. By selecting a controller that has a high open-loop gain at the mode frequencies that require control and a low gain at high and very low frequencies, a good closed-loop performance can be achieved. It will also have robustness against high frequency modes which are not well known. One way of expressing the requirements in the frequency domain is to shape the open-loop characteristics of the design model $G(s)$ by multiplying it with weighting filters, so that the weighted open-loop system exhibits the desired frequency characteristics, see Figure 2-23.

The shaping filters $W_i(s)$ are combined in series with the reduced order design plant model $G(s)$ to form the augmented design plant $G_s(s) = W_i(s) G(s)$, Figure 2-23(b). From the augmented plant an Augmented H_∞ SM similar to Figure 2-22 is formed. The H_∞ algorithm is then applied to the augmented H_∞ SM to obtain an H_∞ controller $K_{inf}(s)$ that stabilizes the augmented plant $G_s(s)$ and it satisfies certain design requirements which are expressed by the shaping filters $W_i(s)$. The final feedback

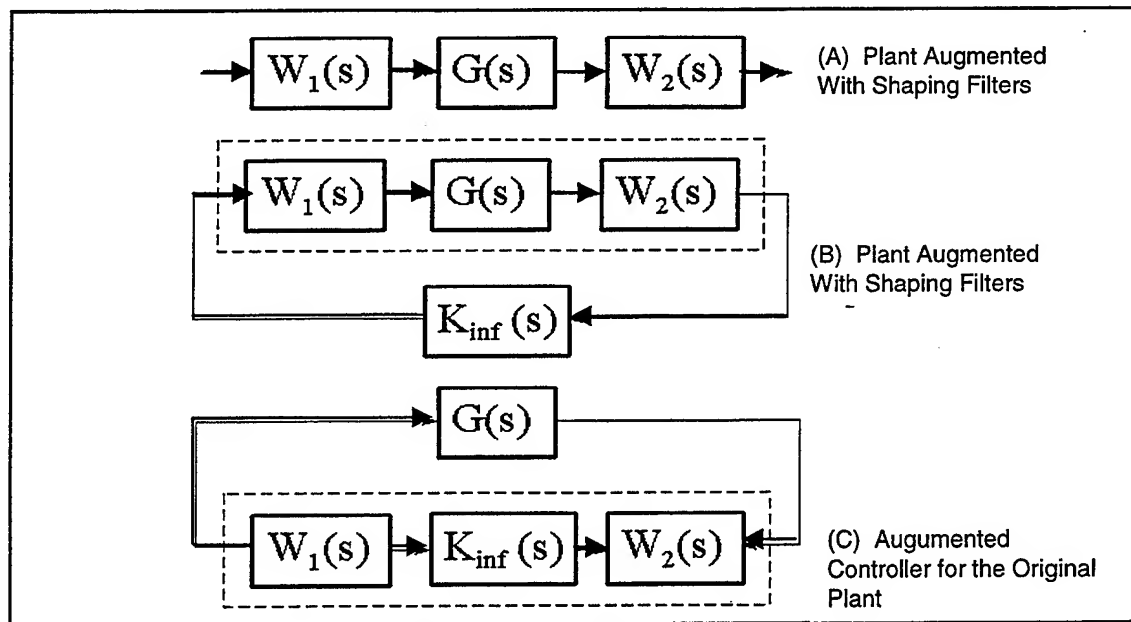


Figure 2-23. The Loop Shaping Process

controller $K_{inf}(s)$ is constructed by combining the controller $K_4(s)$ with the shaping filters $W_1(s)$, so that $K(s) = W_1(s) K_4(s)$, Figure 2-23c.

2.5.3 Shaping Filters $W_i(s)$.

The question now arises, how can the shaping filters for expressing the closed loop system requirements in terms of performance and robustness be chosen. This may require some experimentation in the beginning. The primary requirement for the symmetric loop controller, for example, is to provide active damping for the first symmetric mode which is at 430 Hz. There are some higher frequency modes near or below the cross-over frequency, (at 560, 630, and 740 Hz) that do not require active control. They were, however, included in the design model in order to protect them from instabilities. There is also a cluster of modes at higher frequencies, 1200-1400 Hz. These modes were not included in the design model. They were notched out by one of the shaping filters $W_2(s)$ having a cut-off frequency at 1250 Hz. The other shaping filter $W_1(s)$ is high pass with a cut-off frequency at 200 Hz. The high pass filter is used to: de-emphasize the low frequency measurements in the H_∞ controller optimization (there are no modes below 430 Hz), filter the accelerometer measurements which are usually noisy and unreliable, and prevent the controller from having high gains at low frequencies. High controller gains at low frequencies are undesirable because sometimes accelerometer signals have a small dc bias that could saturate the system. High frequency roll-off is provided by low-pass filtering. A low pass filter, however, was not included in the loop shaping augmentation filters because the amplifier itself, which is part of the plant model, has an analog second order low-pass filter with a cut-off frequency at 800 Hz, and a damping coefficient ($\zeta=0.6$). This low-pass analog filter was included in the design model $G(s)$. The two shaping filters $W_1(s)$ and $W_2(s)$ are now combined with the design plant $G(s)$ to form the augmented synthesis plant $G_s(s)$ as shown in Figure 2-23a.

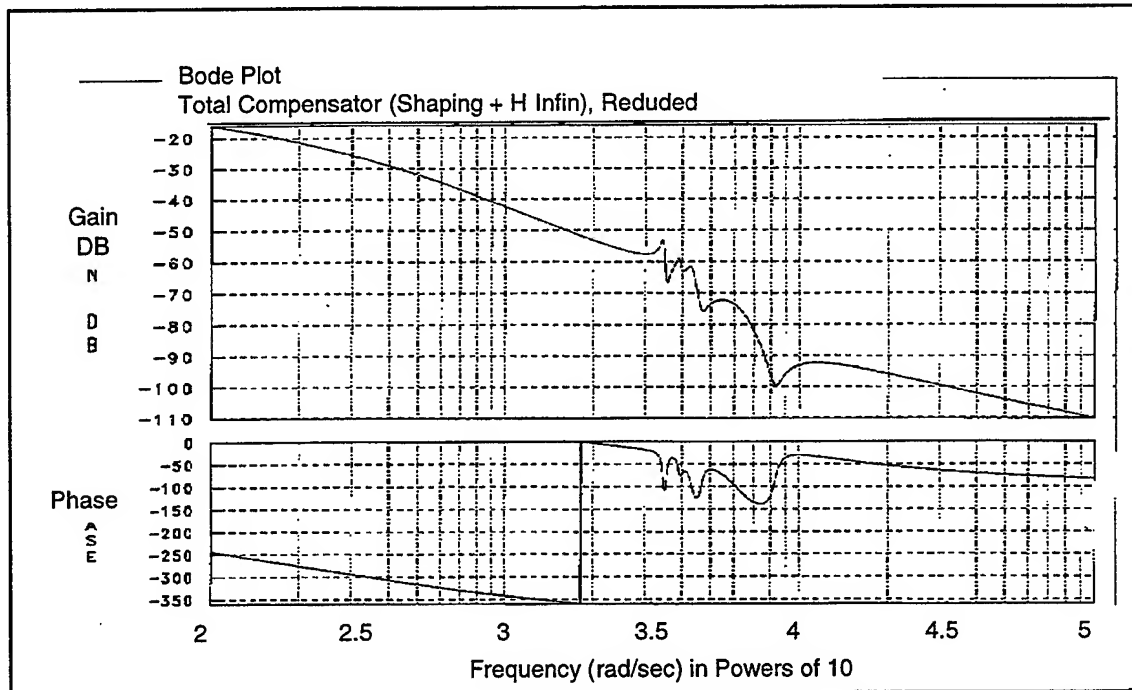


Figure 2-24. H_{∞} Controller Frequency Response

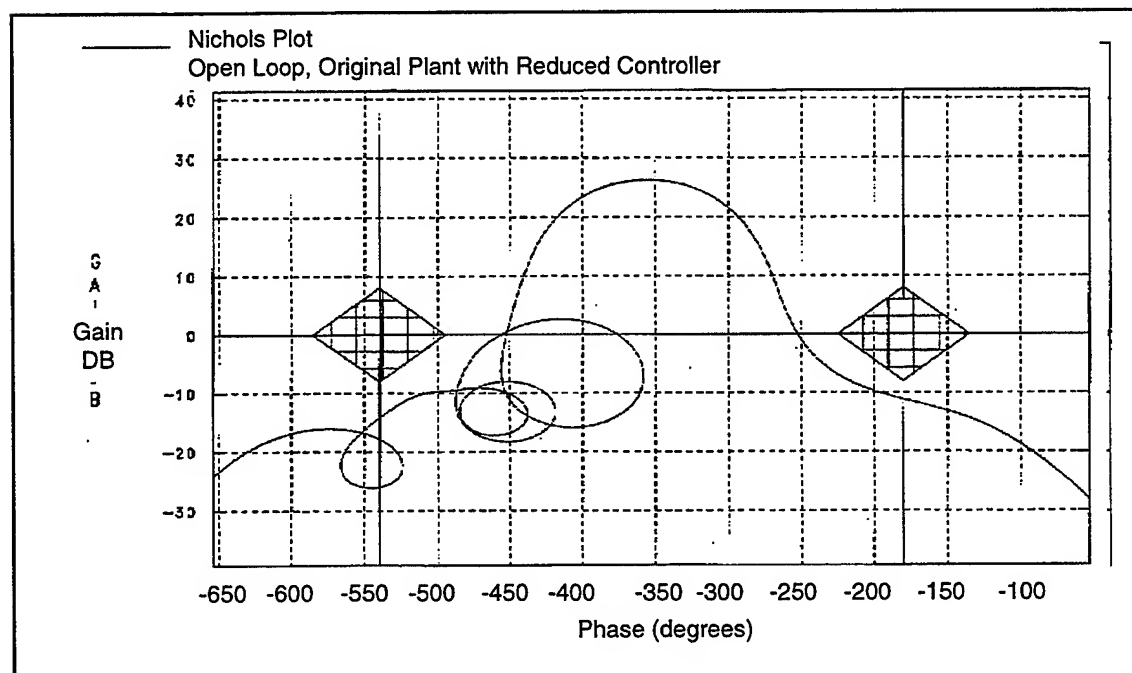


Figure 2-25. Nichol's Plot of the Open Loop System

The augmented (shaped) plant $G_s(s)$ is now presented (in the form of a SM as in Figure 2-22) to the H_∞ optimization algorithm, Reference [2], to produce a controller $H_\infty(s)$. This controller, however, is intended for the shaped plant $G_s(s)$ as shown in Figure 2-23(b). To obtain a controller for the original plant $G(s)$ the shaping filters must be combined with $H_\infty(s)$ to form an augmented controller, as shown in Figure 2-23(c). The approach is similar for both the symmetric and the anti-symmetric loops. The augmented controllers were originally 20th order. They were reduced in size to 12th order by applying the "Internal Balancing Model Reduction" method, Reference [3].

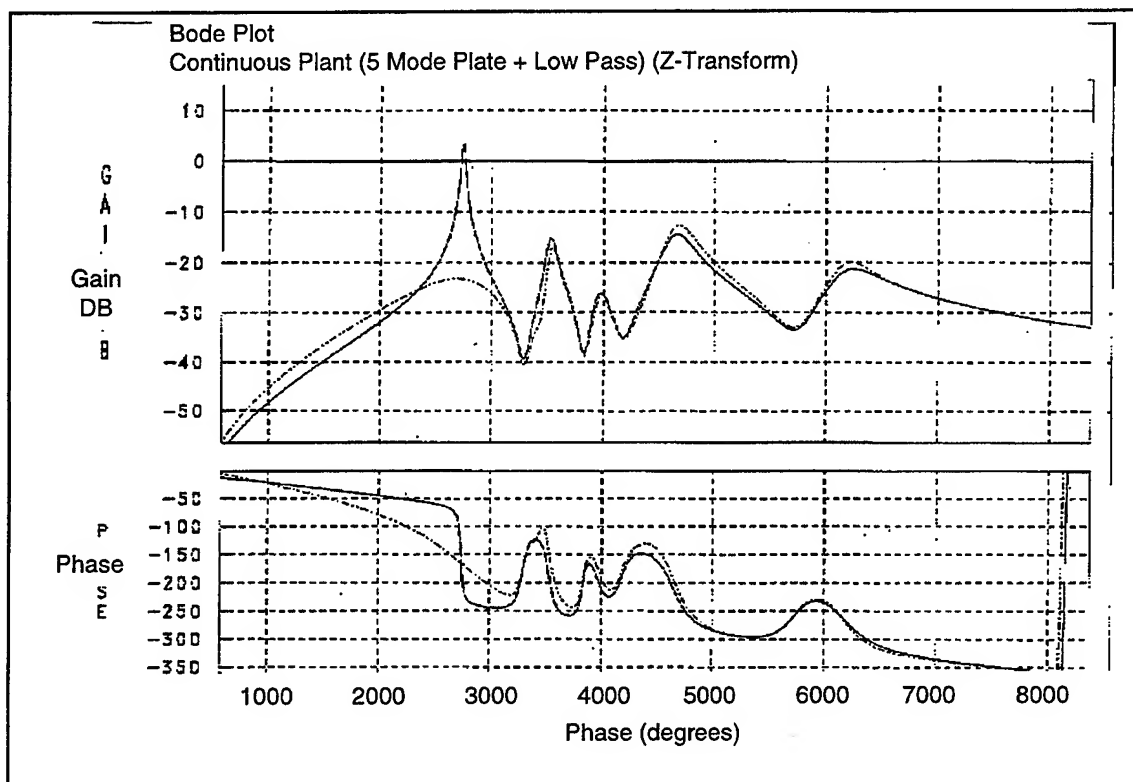


Figure 2-26. Panel Frequency Response With and Without Feedback

2.5.4 Control System Analysis

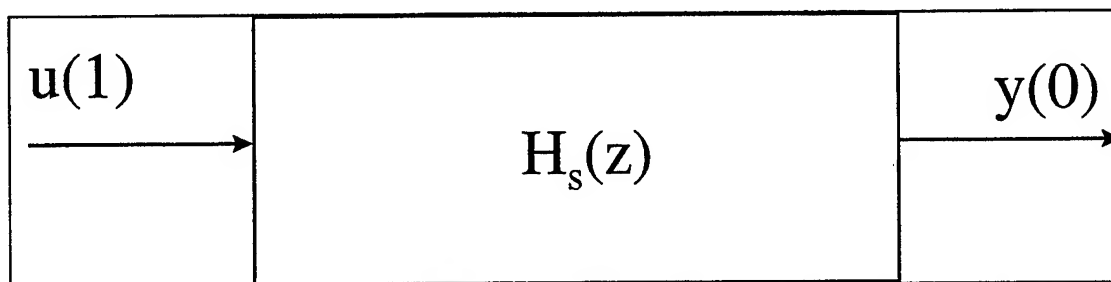
Figure 2-24 shows the frequency response of the total controller, that is, the H_∞ controller combined with the two shaping filters shown in Figure 2-23(c). The controller is combined with the panel and amplifier models in series to generate the open-loop system. Figure 2-25 shows the Nichol's plot of the open-loop system. It has a lot of attenuation at very low and at very high frequencies to provide good stability margin and gain stabilization for the high frequency modes that are to be controlled. The target mode at 430 Hz, however, peaks up with a large amplitude of 25 dB. This high amplitude is needed to provide active control at that frequency. The correct phasing of the resonance which is needed for satisfactory stability and active control is automatically taken care by the H_∞ synthesis. The resonance is exactly between the two diamonds (areas to be avoided for stability). Figure 2-26 shows a frequency response comparison across the panel, with and without controls. The closed-loop system, provides 25 dB of attenuation.

2.5.5 Software/Hardware Interface

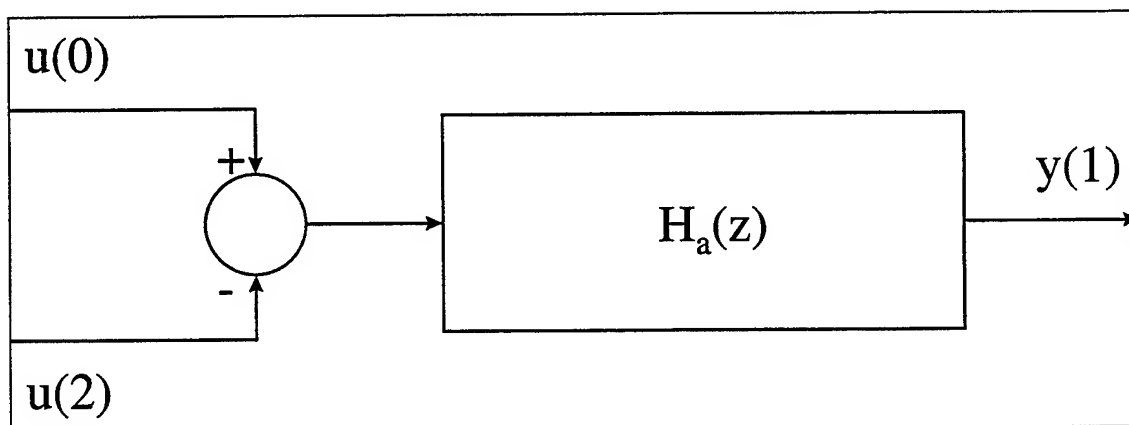
The control system equations are programmed into the AITECH c140 board. The software reads the acceleration signals from the DAADIO board (this board converts the signals from analog to digital) and processes that data through the control system filters. The outputs are the control system commands. The software then writes back to the DAADIO board (the board converts the digital signal back to an analog signal). This process takes 120 μ s. The communication between the DAADIO board and the c140 board is done through the VME. The communication occurs at specific times that are controlled by the VAC timer.

When the board is first powered on, vx Works (software used to operate the board) and the application code (control system equations) are loaded from the flash memory on the AITECH c140 board. It then starts executing the application code. The application code initializes the DAADIO board for VME access (communication between the DAADIO board and the c140 board), sets up the VAC timer (this is a counter on the c140 board) for ticking at a certain rate, and disables all interrupts. It then sits in an infinite loop reading input voltages from the first three A/D channels of the DAADIO card, updating symmetric and anti-symmetric filters, writing voltages to the first two D/A channels of the DAADIO card, and then waiting until the next tick of the timer. The tick time was set to 120 μ s.

Symmetric Filter



Anti-symmetric Filter



The first 3 A/D channels of the DAADIO card are called u(0), u(1), and u(2) and the first two D/A channels y(0) and y(1). u(1) is wired to the symmetric sensor in the center of the plate and y(0) is wired to the symmetric actuator in the center of the plate. Likewise u(0) and u(2) were wired to the anti-symmetric sensors on the plate (top and bottom respectively) and y(1) and its -y(1) were wired to the anti-symmetric actuators on the plate (top and bottom respectively).

The software reads u(0),u(1), and u(2), updates the filters and writes y(0) and y(1) as often as possible but at a uniform rate. Eventually, the reads, updates, and the writes were reduced to occur within a 120 μ s window.

In order to provide a uniform tick for the operations, the VAC timer on the AITECH board was used. This timer consists of a prescaler counter and a count-up timer. By setting the prescaler to 50, each count of the timer becomes 50/25 MHz = 2 μ s where 25 MHz is the CPU clock speed. For a 120 μ s tick, the data register of the VAC timer is set to 65536 - 60 = 65476, where 65536 = 2¹⁶ since the VAC is a 16 bit counter. When the timer is enabled, the counter starts at 65476 increments by 1 every 2 μ s until it eventually reaches 65535 (120 μ s later). It then jumps to 65476 and repeats the process. For purposes of this report, a tick occurs at the jump between 65535 and 65476. Exactly 120 μ s occurs between ticks.

In general, the following formula gives the value that needs to be placed in the data register of the VAC timer as a function of the CPU clock, prescaler value, and therequired tick:

$$\text{VAC_TimerDataValue} = 65536 - \frac{\text{CPU_CLOCK}}{\text{VAC_PrescalerValue}} * \text{TickValue}$$

For example a Tick Value of 120 μ s and a VAC_Prescaler Value of 50 gives a VAC_Timer Data Value of 65536 - 25MHz/50 * 120 μ s = 65476.

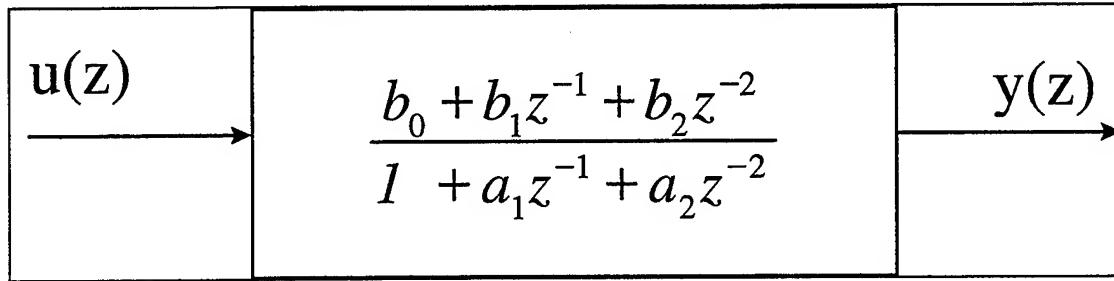
In order to accomplish the three A/D conversions in a minimum amount of time the single_cycle_read feature of the DAADIO card was used. This required a special jumper setting on the DAADIO card and involved pipe lining the three A/D conversions. Substantial savings in read time were achieved this way.

Both the symmetric filter and the anti-symmetric filter were given as a cascade of second order filters, i.e.,

$$H(z) = H_1(z) \cdot H_2(z) \dots H_n(z)$$

where $H_i(z)$ is a second order filter of the form

$$\frac{y(z)}{u(z)} = \frac{b_0 + b_1 z^{-1} + b_2 z^{-2}}{1 + a_1 z^{-1} + a_2 z^{-2}}$$



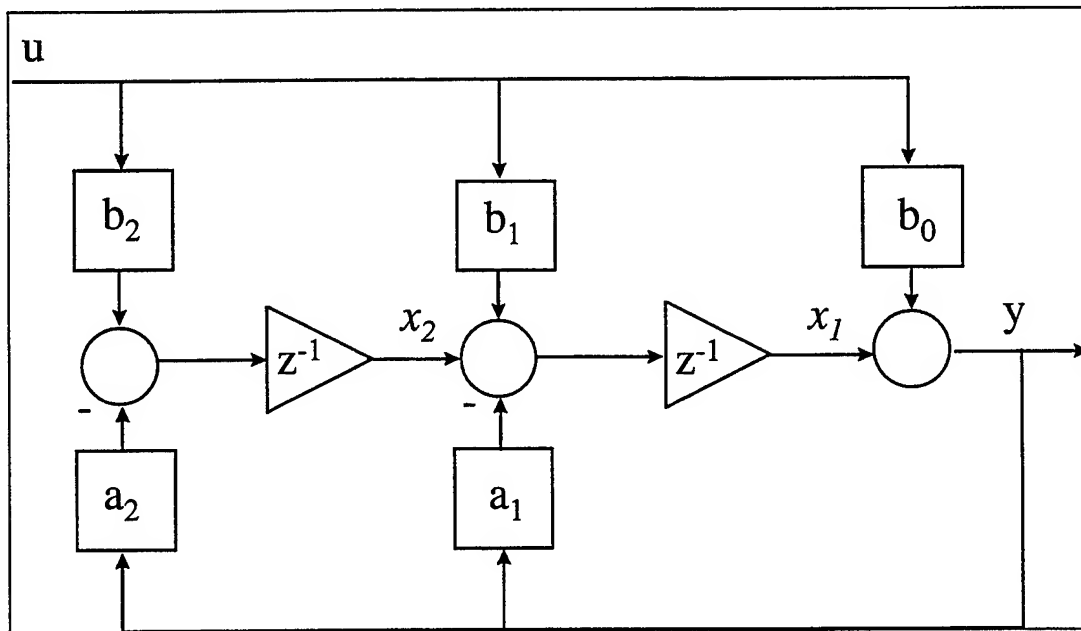
This transfer function is implemented in the second companion canonical form, which is derived as follows:

$$(1 + a_1 z^{-1} + a_2 z^{-2})y(z) = (b_0 + b_1 z^{-1} + b_2 z^{-2})u(z)$$

that can be rewritten as

$$y(z) = b_0 u(z) + z^{-1}(b_1 u(z) - a_1 y(z)) + z^{-2}(b_2 u(z) - a_2 y(z))$$

Using the right to left numbering of state variables, this representation leads to the following structure with two states x_1 and x_2 .



The corresponding difference equations for this structure are:

$$x_1(k+1) = x_2(k) - a_1(x_1(k) + b_0 u(k)) + b_1 u(k)$$

$$x_2(k+1) = -a_2(x_1(k) + b_0 u(k)) + b_2 u(k)$$

$$y(k+1) = x_1(k) + b_0 u(k)$$

which for optimization is better implemented as:

$$\begin{aligned}y(k+1) &= x_1(k) + b_0 u(k) \\x_1(k+1) &= x_2(k) - a_1 y(k+1) + b_1 u(k) \\x_2(k+1) &= -a_2 y(k+1) + b_2 u(k)\end{aligned}$$

As can be seen then each second order filter update requires 5 floating point multiplication and 4 floating point additions. Since both the symmetric and anti-symmetric filters used in this analysis were a cascade of six second order filters, a total of 60 floating point multiplication and 48 floating point additions were required every 120 μ s.

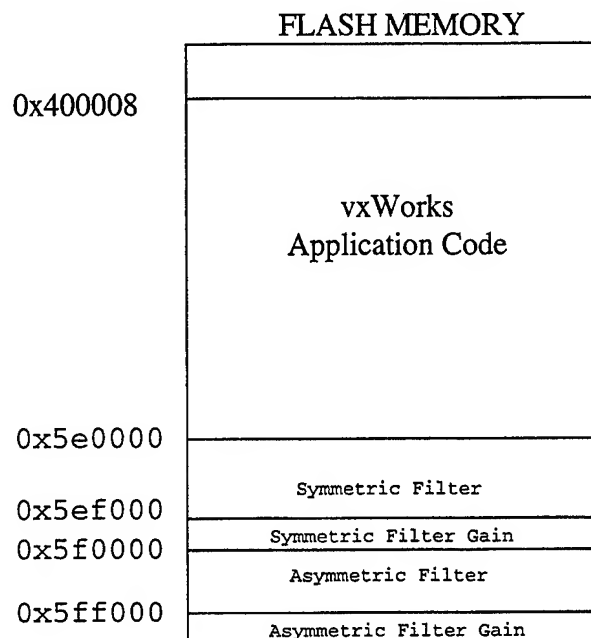
Originally, the filter updates were implemented by calling update Cascade Filter as listed below, which, in turn, called update Filter for as many filters as were cascaded together. This was done to allow flexibility in both the number of filters cascaded and the orders of each of the component filters. Eventually, the number of component filters was reduced to six second order.

It was found that this implementation was costly, it required over 175 μ s to update the two cascades of six second order filters. In order to reduce the time required, the number of filters was fixed to six and the filter coefficients locations were hard coded into the software. This provided time savings by establishing the control system architecture and eliminating the architecture determination in every computation cycle. Time saving was also accomplished during the A/D conversion cycle.

The throughput of multiple A/D conversions on the DAADIO card can be increased by decreasing the number of CPU machine cycles it takes to initiate and complete a conversion. The A/D converter module on the DAADIO card accomplishes this through the use of Single - Cycle Mode. This mode makes it possible to read data from the last A/D conversion and start the next conversion with a single word-wide read cycle. Further savings are achieved by running this mode in pipelined mode, whereby the two tasks of selecting a channel and performing the conversion are done in parallel. The three A/D conversions take approximately 48 μ s, if done individually (without pipelining and single-cycle sampling). With the use of pipelining and single-cycle sampling, this is reduced to 32 μ s.

The filter updating (after modifying the code to hardcode filter locations) takes 58 μ s. The two D/A conversions (voltage writes) take 18 μ s. This gives a total of $32 + 58 + 18 = 108$ μ s. A sampling rate of 120 μ s guarantees that the calculation is complete before the next calculation is started.

Below is a diagram of the physical memory of the flash memory on the AITECH board



The software timing cycle was critical to the success of the active vibration suppression system. The final timing cycle was completed at a frequency of 8333 Hz. This allows the control system to prevent instabilities at frequencies below 1500 Hz. The final timing cycle was achieved by eliminating the architecture determination in every computation cycle and by increasing the throughput of multiple A/D conversions.

2.6 LABORATORY TESTS

The controller for a specific panel is developed using measured open loop transfer functions. The transfer function is between the acceleration output and an input random signal supplied to the PZTs by the amplifier over the frequency range of 0 to 1000 Hz. The poles and zeros are taken from the peaks and valleys of the Bode plot. The controller developed with H_{∞} optimization technique notches out the higher frequency modes while minimizing the phase lag at the lower frequencies. A unity control board was used for the open loop measurement. The board has a unit gain for all frequencies. Normally, the control equations are calculated with the micro-processor in the following manner. The micro-processor first digitizes the analog accelerometer signal. The digital values are used to process the symmetric equations and then the anti-symmetric equations. The processor digital outputs are the commands to the amplifier; however, the digitized signals are converted back to analog before being sent to the amplifier. For the unity controller open loop measurements, no calculations are made and a value of 1 is used as the output. The effective gain of the micro-processor is one, but the computing time adds lag (a phase angle). Therefore, the open-loop transfer function accounts for the computer cycle lag. In Figure 2-27, if the outputs at the right are divided by the random input at the left, the results would be the open loop transfer functions.

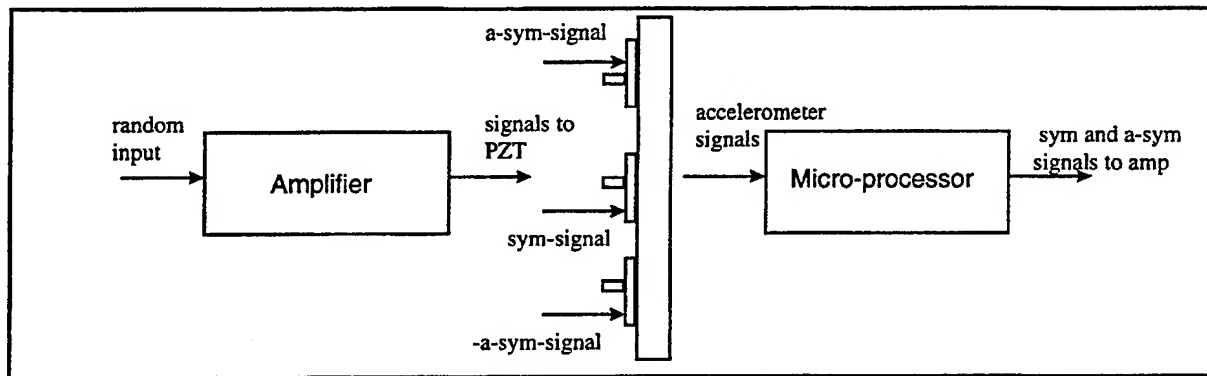


Figure 27. Block Diagram of the Open-loop Controller

2.6.1 Flat Panel

The flat plate tests were performed between January and early April of 1997. The panel was mounted in the door of an acoustic reverberation chamber, and the symmetric modes at 237, 322, and 527 Hz and the anti-symmetric modes at 266 and 407 Hz were measured. The 4 PZT patches in the center of the panel (later changed to five) were able to drive the first symmetric mode up to vibration levels of 30 g's (peak). This g level was important because the PZTs have to provide adequate driving power to damp the vibrations caused by the acoustic driving force. The open-loop transfer functions were measured and used to design a closed-loop controller. Figure 2-28 shows the results of a tap test with and without control. The closed-loop response is 20 dB lower than the open-loop response for the first symmetric mode.

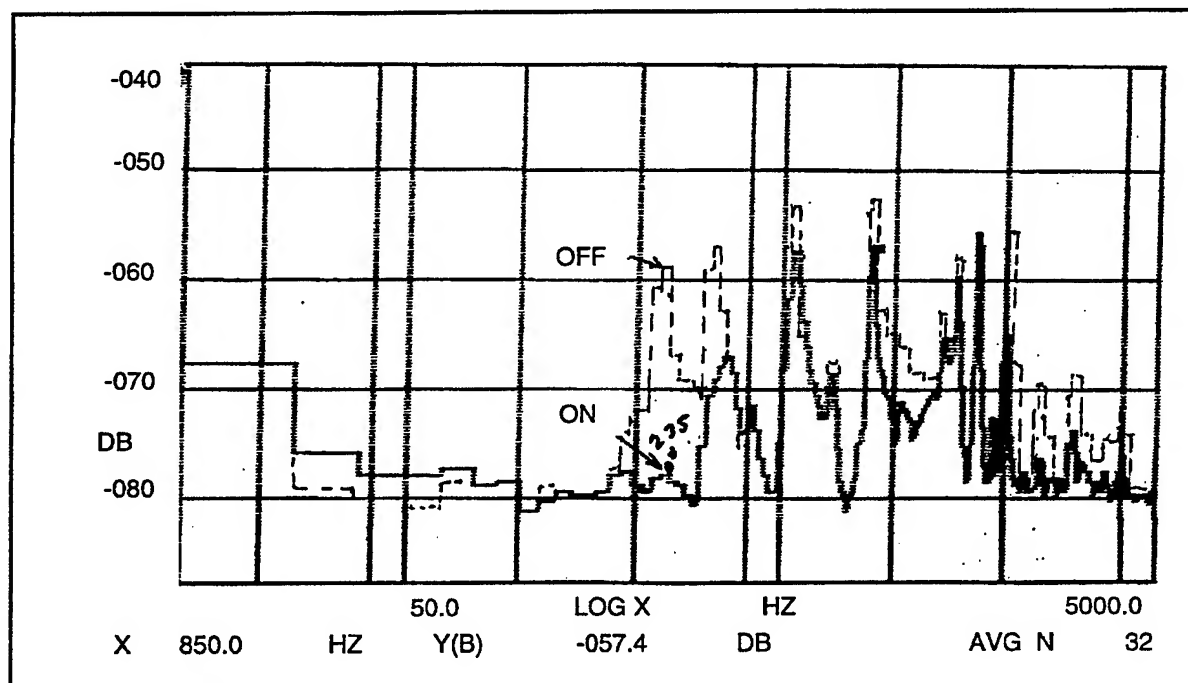


Figure 2-28. Closed- and Open-loop Response Flat Panel

The flat plate was tested on April 6, 1997 using acoustic noise inputs at overall levels of 126, 136, and 141 dB and with and without control. The acoustic spectra shapes were the same as those taken from previous measurements on the B-1B aft fuselage. Results for a noise level of 136 dB are shown in Figure 2-29.

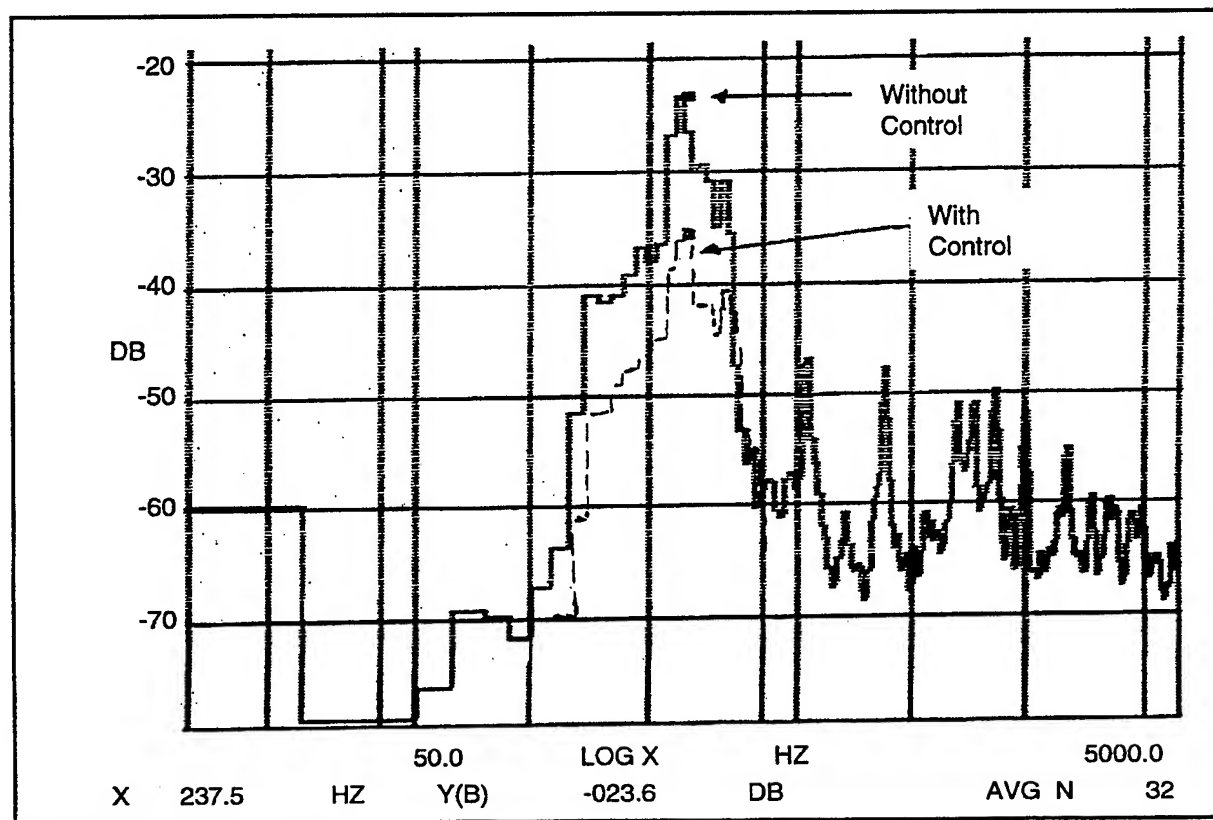


Figure 2-29. Flat Panel Response for 136 dB Input

A 12 dB attenuation was attained. This could have been improved by adding attenuation for the frequencies below 200 Hz and above 400 Hz. The flat plate closed-loop controller was never refined because the curved plate hardware was completed and available for testing. Since the B-1B test schedule had been moved up, the decision was made to start the curved plate tests without refining the flat plate controller.

2.6.2 Curved Panel

A number of tests were performed on the curved panel: PZT drive capability, linearity, mode shape measurements, tap tests, reverberation chamber tests, and temperature tests. On March 7, 1997 random and sine wave signals were sent to the symmetric controller patch. For a 140 V sine wave at the first mode natural frequency an acceleration of 100 g's was obtained. This was a significant result because the expected flight levels were possibly as high as 300 g's. Thus, this result showed that the PZTs could probably drive the panel to 150 g's at 200 V. Adequate control authority is a necessary condition for a successful control system.

Open-loop transfer functions measured on March 7th at different input voltage levels showed the system was linear, i.e., the transfer function was independent of the input amplitude. On Sat March 8th, the mode shapes were measured using sine wave inputs. These mode shapes agreed with tap test measurements and the analytical results.

Figures 2-30 and 2-31 are open loop transfer function measurements made on the curved panel on March 11, 1997. The amplifier for this open loop test was designed and built for the B-1B (Sect. 2.4.1). In the previous tests, an amplifier with a gain of 20 was used. The B-1B amplifier had a gain of 40. Figure 2-30 shows the anti-symmetric open-loop transfer function measurement using the accelerometer mounted on the top patch. Figure 2-31 is the symmetric version using the center patch accelerometer.

These open-loop transfer functions were used to design the control systems (see Sect. 2.5). This was the identical procedure used in the flat plate tests. During the design process, it was determined that a low pass filter was needed to eliminate aliasing. If the filter was used on the accelerometer output, the computer would not fold the high frequency noise back at the low frequencies. The filter was added, but on the output of the computer. This was done because it could be easily added to the amplifier unit, but not to the computer unit. The 800 Hz low pass second order filter was not optimum for eliminating aliasing in that location, but it did smooth the micro-processor ratchet signal from the D/A conversion.

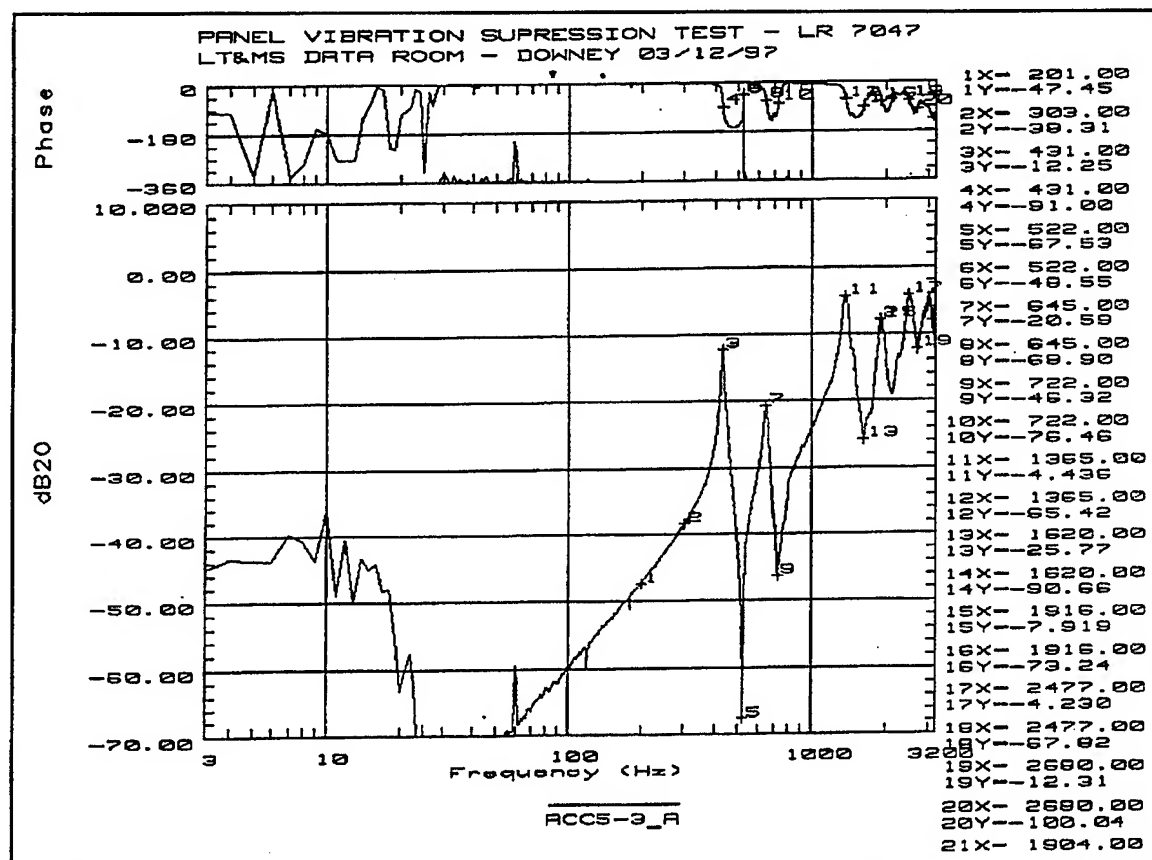


Figure 2-30. Anti-symmetric Open-loop Transfer Function

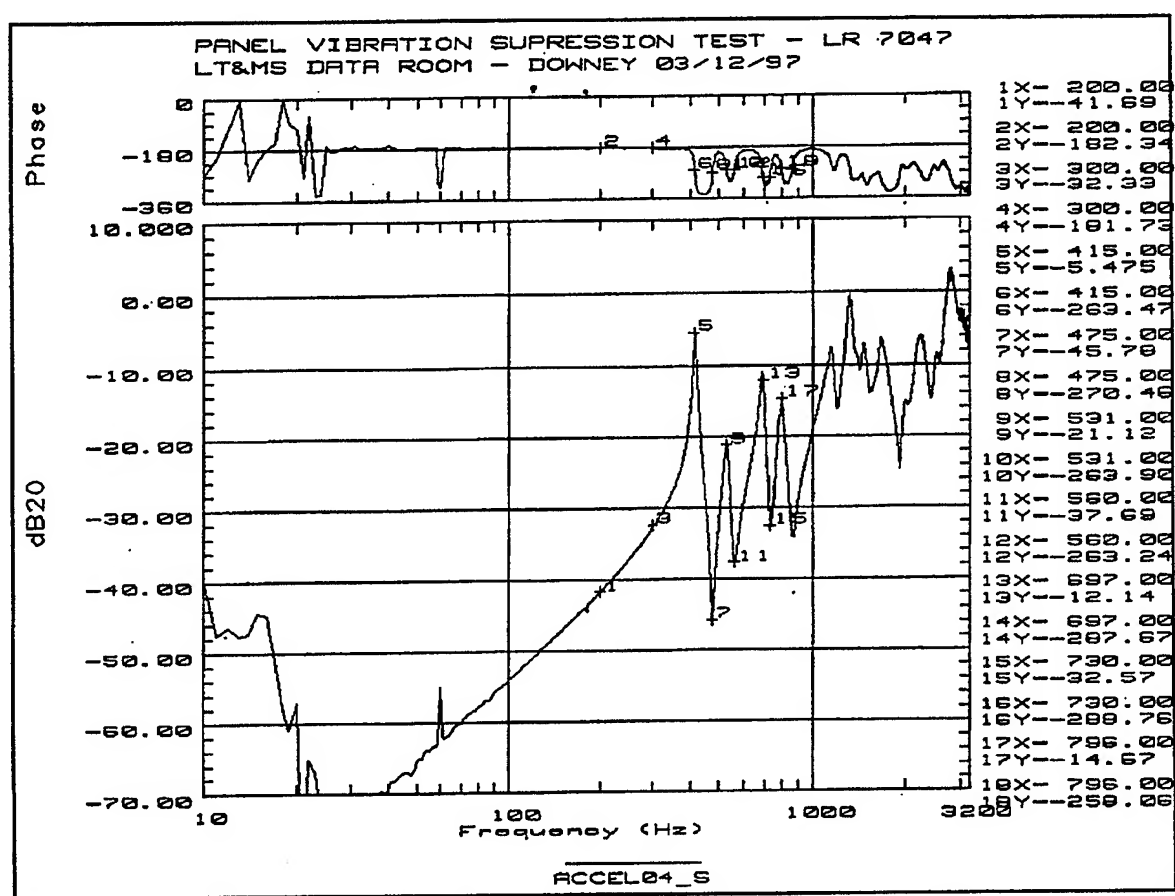


Figure 31. Symmetric Open-loop Transfer Function

The effectiveness of the control system was measured by tap tests and by tests in the acoustic reverberation chamber. The tap test data in Figure 2-32 shows the first anti-symmetric mode is attenuated by 17 dB with active control.

On April 3, 1997, the curved panel was tested in the reverberation chamber at overall acoustic levels of 127, 137, 141, 152, 157, and 160 dB. The center accelerometer which is sensitive to the symmetric modes showed that the third symmetric mode at 680 Hz had a response 10 dB higher than the first symmetric mode. This was caused by the participation of the reverberation chamber door with the first two modes. The symmetric control system was able to provide 5 dB of attenuation for the first mode at an acoustic level of 157 dB but the third mode at 680 Hz was amplified by about 7 dB. The first mode was difficult to attenuate because of the door participation. No attempt was made to damp the third mode. The higher level of vibration in the third mode was probably caused by noise created by aliasing. The participation of the door is not representative of flight and could have been avoided (with a heavier door). The anti-symmetric case did represent flight. The data with and without control at an acoustic level of 141dB is shown in Figure 2-33.

Figure 2-33 shows that active control attenuated the first anti-symmetric mode by 10 dB but amplified the second mode by about 5 dB. The 5 dB is related to the increase in the noise level floor. The over all noise level increases because of aliasing and insufficient filtering of the high frequency noise.

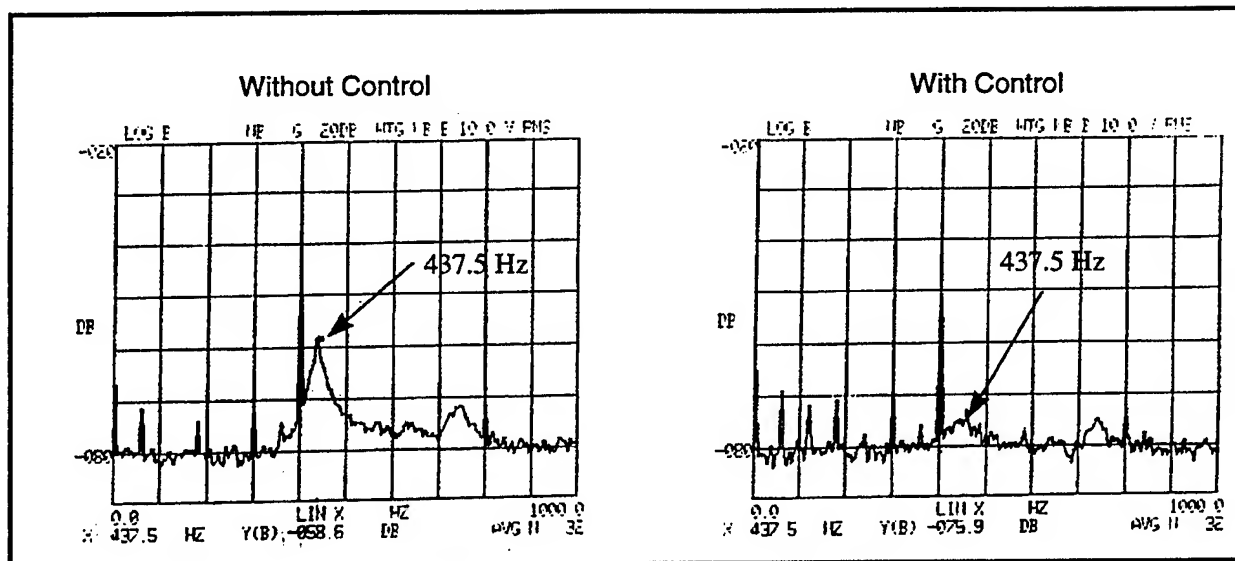


Figure 2-32. Curved Panel Tap Test Response

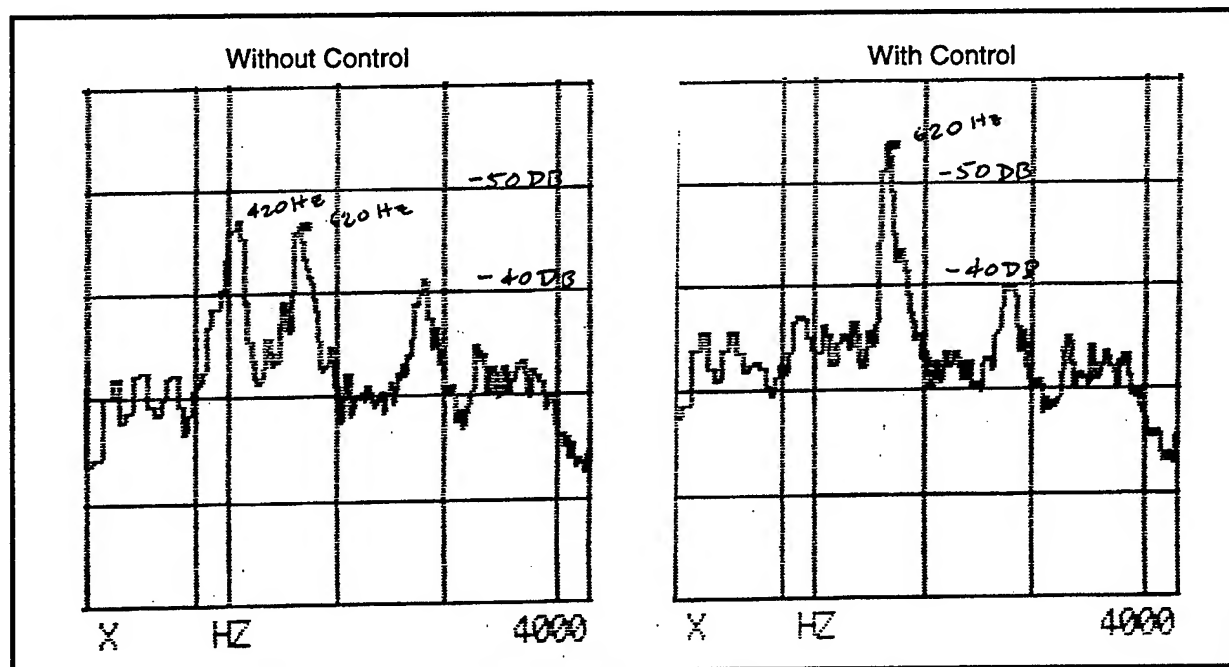


Figure 2-33. Curved Panel Anti-symmetric Response for 141 dB

On the aircraft, the skin temperatures can range between -60 and +185 degrees F. The control system was going to be designed with an adaptive controller and with temperature feedback. The effect of temperature on the frequencies was measured in the laboratory on April 13, 1997. The temperature was increased from ambient to 110, 150, 164, and 180 °F. At each level a random signal was input to the PZT actuators to determine the change in frequency caused by the increased temperature. The frequencies increased slightly (3%) with increasing temperature. Based on the modulus of elasticity of aluminum, the frequencies should have decreased slightly. At this time, a decision was made to go with a non-adapted controller design because of the accelerated B-1B testing schedule.

The laboratory tests demonstrated that the curved panel could be driven by the PZTs at g levels near the expected flight levels and that the open-loop controller was linear. It was found that the temperature shifted the natural frequencies only slightly. It was also demonstrated that the controller provided 17 dB of attenuation in the tap tests and that 10 dB of attenuation could be achieved in the reverberation chamber. Finally, it was shown that the design process for the active attenuation of the flat panel also worked for the curved panel. Thus, the same design process was expected to be successful for the B-1B.

3.0 Flight Demonstration

3.1 HARDWARE INSTALLATION

Three main items were installed in the TDS B-1B for the AVSS demonstration effort. Two of these, the control unit and the power amplifier unit, were electronic boxes, and the third was the PZT patch configuration that was bonded to the selected AEB fuselage skin panel. Figure 3-1 shows the block diagram of the AVSS installed in the aircraft. The AVSS control and power amplifier units interfaced with other boxes already in the aircraft to receive power and instrumentation signals. Operation of the AVSS was controlled from the aft crew station of the cockpit by an off/on switch; operation of the on-board analog instrumentation recording system (28 track FM/FM recorder) was controlled from the same station.

Both the control and power amplifier units were mounted in the AEB on special adapting structure that was mechanically attached to an existing equipment rack. Figure 3-2 shows the units mounted in the aircraft. The installation of the units was shock mounted to the aircraft structure because of the high vibration levels known to exist in that area during takeoff and some flight conditions. Cooling air was supplied

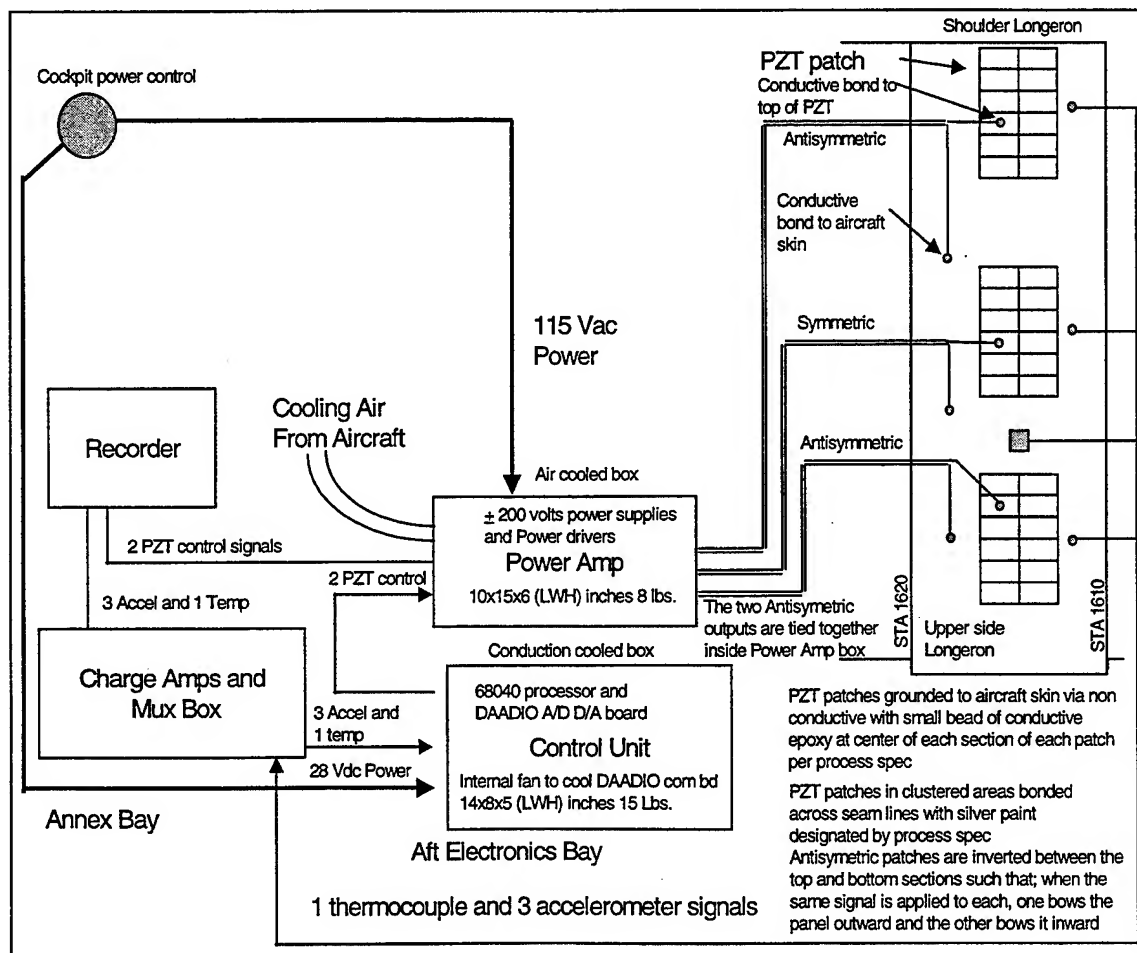


Figure 3-1. Active Vibration Suppression System (AVSS) Block Diagram

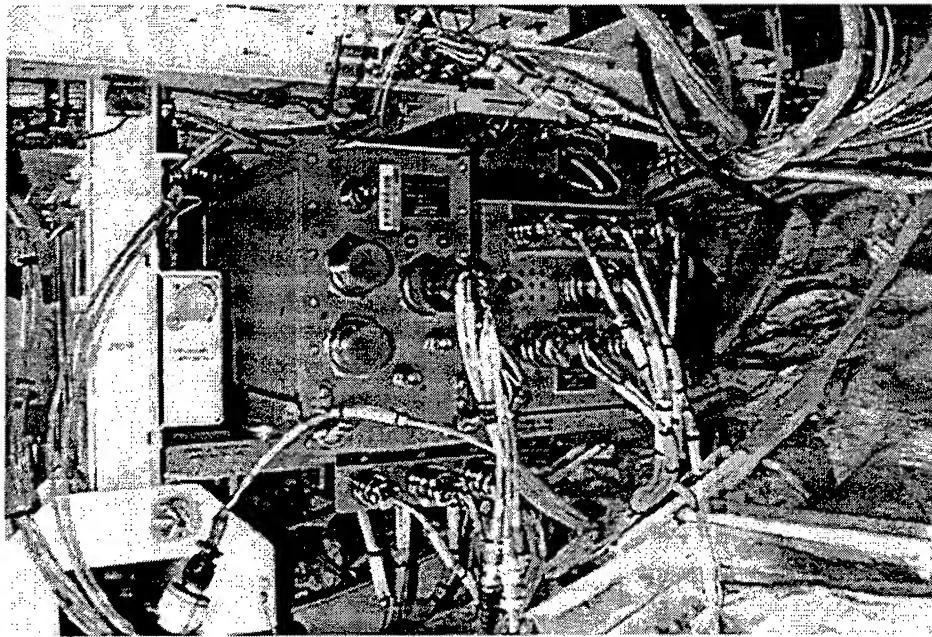


Figure 3-2. AVSS Control Unit (Left) and Supply Mounted in B-1B AEB

to the power amplifier unit and both 28 V dc and 115 V ac were supplied to the boxes from existing B-1B power sources. Figure 3-3 shows the PZT configuration mounted in the aircraft and the wiring from the power amplifier unit. An accelerometer was mounted directly on each of the PZT patches to record the level of vibration at those locations and to provide the feedback signals to the control unit for both symmetric and anti-symmetric control. The actual installation of the PZTs in the aircraft is shown by the photograph of Figure 3-4. PZTs were bonded to the aircraft using the conductive and non-conductive adhesives specified in Section 3.2 of this report. Bonding was performed by vacuum bagging the installation in order to get a uniformly thin bond line. The PZTs were bonded to the AEB skin panel in a 3-day time period with the procedure shown in Table 3-1. Figures 3-3 and -4 show the wires that provided the required electrical signal to each PZT. On the aircraft, the circuit was grounded through the aircraft skin by a wire attached to an adjacent structural frame.

3.2 INSTRUMENTATION

The aircraft contained an on-board analog instrumentation system that was used, mainly, to obtain vibration and acoustics (V&A) data for the TDS flight test program. At the time the AVSS was installed the TDS V & A testing had been completed except for a few minor requirements. Therefore, the system was available for use with the AVSS flight test demonstration. Figure 3-5 shows the instrumentation that was used and their locations. In all, the system included six accelerometers, one microphone and one temperature sensor. Output of all of these parameters were recorded on the on-board recording system. After each flight, the analog tape was down loaded and sent to the Boeing North American Dynamic Data Reduction Laboratory in Downey, California. Even though a tape was available for each flight, the amount of usable AVSS data was rather limited. This was because the crew had such a high workload with the TDS testing that the AVSS control unit was usually not cycled from the non-operating to the operating position. However, enough data were obtained to determine the performance of the AVSS for each major change to the control laws used during flight test.

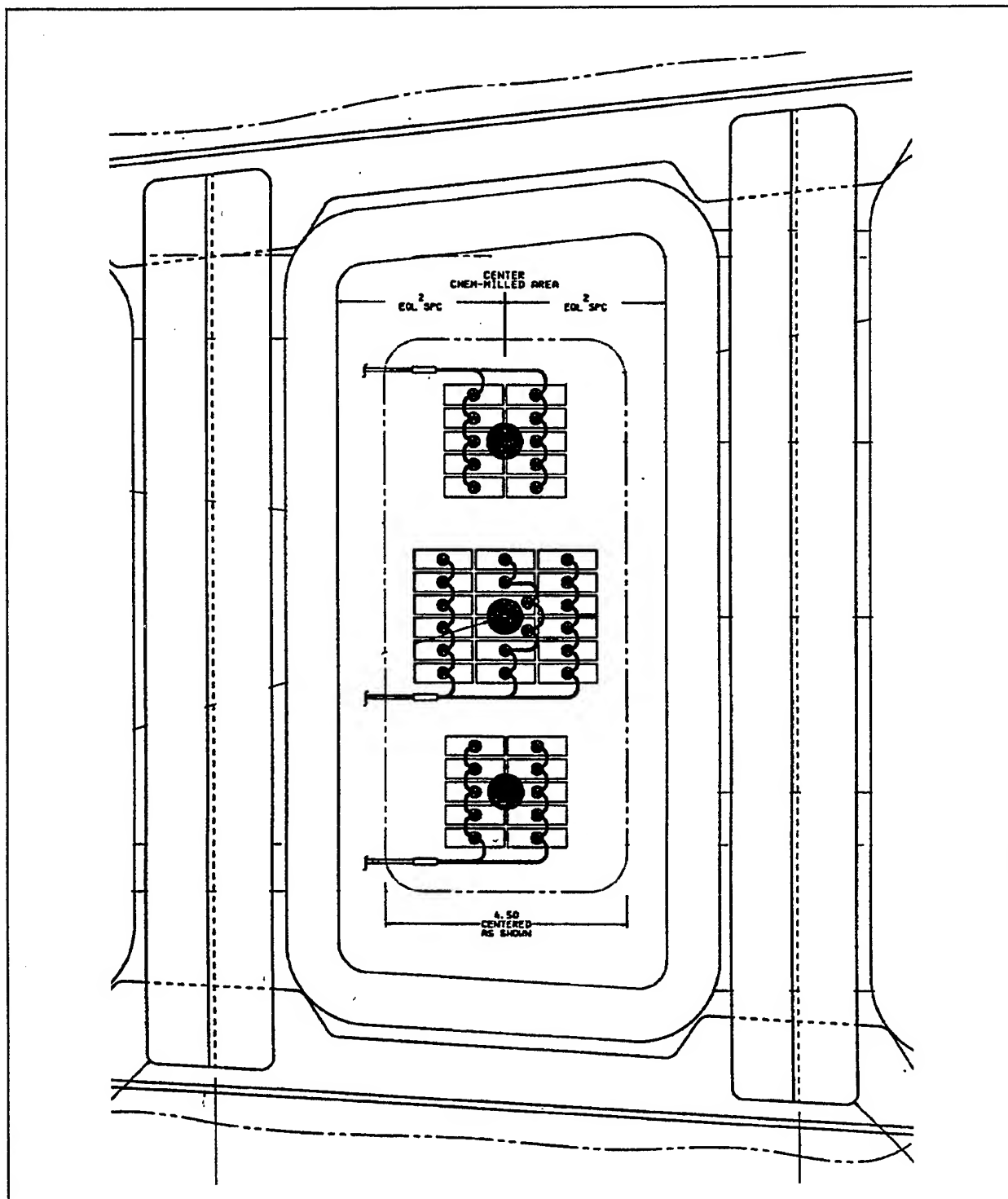


Figure 3-3. Location of the PZT Patches on the Demonstration Panel

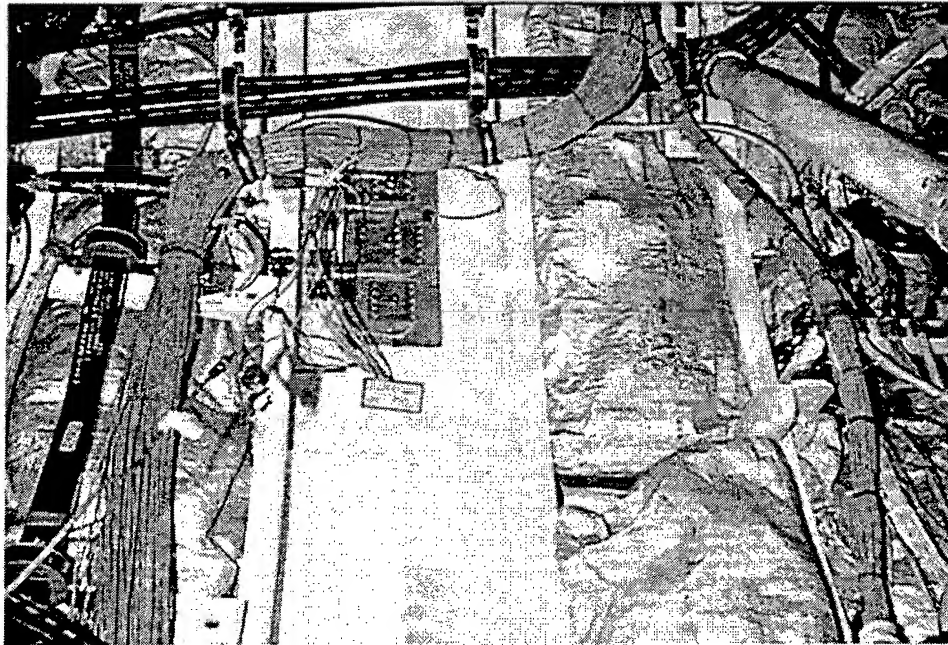


Figure 3-4. PZT Patches Located in the B-1B Aft Equipment Bay

3.3 PRELIGHT AIRCRAFT MEASUREMENTS

A nine step active control system design procedure was used: (1) measure the open loop transfer functions at EAFB with a unity gain controller board, (2) curve fit these results and input into an H_∞ analysis, (3) design the control system using H_∞ , (4) download the control design onto the Motorola computer board, (5) perform a tap test on the vehicle with and without active control (note: the difference between the two gives an indication of the amount of attenuation that is possible during flight), (6) adjust the gain 6 dB below the unstable response, (7) fly the controller and measure the attenuation, (8) adjust the controller based on the flight data, and (9) repeat the process.

3.3.1 Open-Loop Transfer Functions

Eight trips to EAFB were made for the purpose of measuring the open-loop transfer functions and for adjusting the gains. After the open-loop transfer function was measured on one trip, a time period of 3 to 4 days was needed to curve fit the data and design a control system. This control system was then loaded on a Motorola 68040 controller board with a work station. The board was taken to EAFB for the purpose of adjusting the gain. The open-loop transfer functions were measured on the first trip to Edwards on April 26, 1997. The transfer function measurement is made by inputting a random signal into the symmetric or anti-symmetric amplifier input and measuring the output of the computer.

3.3.2 Closed-Loop Gain Adjustments

On May 2, 1997, the first control system design was taken to EAFB for the purpose of adjusting the gain. The gain is changed by first installing the controller board and performing a tap test with the power on. The tap test can excite an unstable mode, and the panel will make a loud singing noise. Sometimes the panel

Table 3-1. PZT Patch Actuator Attachment Procedures for B-1B

1. Clean paint or other coating from the aircraft skin in the areas where the PZT arrays will be bonded. Include a 0.5-inch margin around all sides of the PZT array areas. Per the sketch, this means an area of 4.2 inch wide by 3.4 inch high for the middle array, and an area of 3.1 inch wide by 3.0 inch high for the top and bottom arrays.
2. Mask off the areas on which the PZT arrays are to be bonded and clean these areas of the aircraft skin using standard strain gage cleaning processes.
3. Using a pencil and a clean straight edge, draw boxes depicting the arrangement of the patches on the aircraft skin, taking care to keep proper alignment with the horizontal and vertical axes.
4. Follow the manufacturer's instructions for mixing both the conductive and non-conductive epoxies.
5. Using a clean applicator, place a dot of conductive epoxy approximately 1 mm in diameter in the center of each box.
6. Using the non-conductive epoxy, apply a thin coat over the rest of the area of the aircraft skin to be covered with PZT patches, taking care not to smear or disturb the dots of conductive epoxy.
7. Each patch will be placed in the appropriate box on the aircraft skin and pressed firmly into place.
8. Once all of the PZT patches are in place, carefully wipe away any excess epoxy with a clean cloth or applicator, taking special care to keep each patch in its proper place.
9. To keep a uniform pressure on the patches during curing, a vacuum bag shall be used. The vacuum bag pressure shall be the highest attainable, given limitations due to altitude and equipment.
10. The surface will be heated with a lamp to a temperature of 125 °F for 2 hours while the surface temperature is monitored with a thermocouple.
11. The vacuum bag can be removed at the end of 2 hours.
12. Clean the upper surfaces of the PZTs with acetone.
13. Attach wires to the upper surface of each PZT patch with conductive epoxy, taking care to completely cover the wires with epoxy and NOT to get any epoxy over the edge of the patch so that it could short to the aircraft skin.
14. Tape the wires to the aircraft skin while waiting for the conductive epoxy to cure. Follow the manufacturers instructions on epoxy curing.
15. After the conductive epoxy has cured, coat the tops and edges of the PZTs, including edges around the gaps, with M-coat-A strain gage protective coating, to prevent any electrical shorts.

would start to sing after the power was turned on without even a single tap. Other times the panel would require a series of taps to excite an instability. If the panel started to sing, the system gain would be reduced; and the tap test would be repeated.

The gain on the board was changed by removing the board from the on-board controller box and inserting it into a second controller box. A portable workstation was used to communicate with the board and the gains were changed.

On May 2nd, the anti-symmetric controller was stable at a gain of 0.01 but the response at 600 Hz was too large. One accelerometer came off during this test.

A series of problems occurred until on the fifth visit at 4:30 pm on May 13, 1997, it was determined that the symmetric control signal was driving the anti-symmetric patch. After this wiring problem was corrected, the open-loop transfer functions were regenerated. On May 16, 1997, the gains were changed to +0.03 for the anti-symmetric controller and -0.02 for the symmetric controller. These latter controllers were tested on flight 17. On May 21st, the transfer functions were re-measured and the gains were adjusted on June 2nd to -0.03 for the anti-symmetric controller and -0.03 for the symmetric controller. These control laws were tested on flight 19.

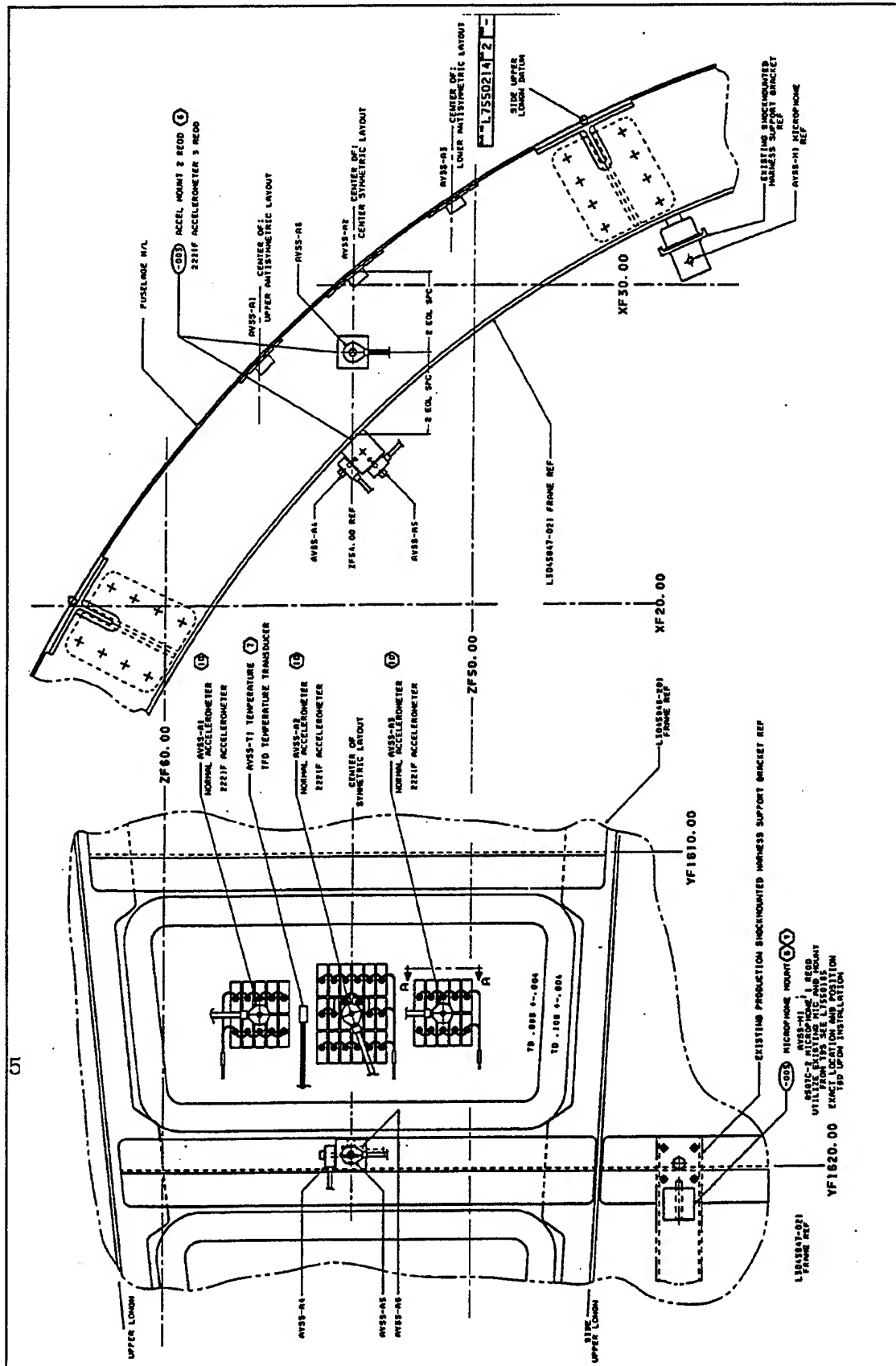


Figure3-5. AVSS Instrumentation

Table 3-2. History of AVSS on TDS Aircraft

Flight Numbers		Date	Total Time	Takeoff Power Setting	Comments
TDS Flt	86-113-00xx				
N/A	N/A	97/4/13-14	--		<u>PZT's bonded on aircraft</u> AVSS on A/C, lab control laws
10	27	4/23/97	6.5	Max. A/B	AVSS off
11	28	4/30/97	2.6	Max. A/B	AVSS off
12	29	5/3/97	5.7	Max. A/B	AVSS off
13	30	5/7/97	2.4	Max. A/B	AVSS off
14	31	5/10/97	6	Max. A/B	AVSS on
15	32	5/14/97	2.9	Mid. A/B	AVSS off
			0.2	Military	AVSS off
		5/16/97			<u>Initial control laws installed</u>
16	33	5/17/97	5.5	Mid. A/B	AVSS on
			0.2	Military	AVSS on
			0.3	?	AVSS on, PA circuit breaker found tripped
17	34	5/22/97	3.3	Max. A/B	AVSS on, In-flight data obtained
18	35	5/31/97	0.6	Mid. A/B	AVSS on, Two in-flight conditions obtained
N/A	N/A	6/2/97			<u>AVSS control laws revised</u>
19	36	6/3/97	7.7	Max. A/B	AVSS on, In-flight data all at 420 kts.
	37	6/4/97	4.7	Max. A/B	AVSS on, No takeoff on tape. Accel. 1 broke off with PZT piece In-flight data all at 420 kts.
20	38	6/6/97	4.3	Mid. A/B	AVSS on during takeoff and in-flight
21	39	6/10/97	4.9	Mid. A/B	AVSS on during takeoff and in-flight
22	40	6/11/97	4.9	Max. A/B	AVSS off, Accel 1 no good
23	41	6/13/97	5.3	Max. A/B	AVSS off
24	42	6/17/97	4.3	Max. A/B	AVSS off
	43	6/18/97	1.7	Max. A/B	AVSS off
25	44	6/20/97	5.3	Max. A/B	AVSS on, Accels bonded back on
26	45	6/25/97	8.5	Mid. A/B	AVSS on
27	46	6/27/97	5.1	Max.A/B	AVSS on
	47	7/1/97	4.9	Max.A/B	AVSS on
	48	7/3/97	5.9	Max.A/B	AVSS off, In-flight data all at 420 kts.
	49	7/8/97	5.6	Max.A/B	AVSS off
N/A	N/A	7/10/97	--		<u>Control Law gains increased</u>
	50	7/11/97	5.9	Max.A/B	AVSS on
	51	7/15/97	4.9	Max.A/B	AVSS on, In-flight ?
	52	7/16/97	7	Max.A/B	AVSS off, In-flight ? & 420 kts.
	53	7/17/97	4.3	Max.A/B	AVSS cycled off and on
	54	7/22/97	3.7	Max.A/B	AVSS on In-flight, data all at 420 kts
	55	7/23/97	4.7	Max.A/B	AVSS on
	56	7/24/97	4.5	Max.A/B	AVSS off
	57	7/29/97	2.1	Max.A/B, 2 Military	No data recorded, range problems
	58	7/31/97	8.3	Max.A/B	AVSS off, Robins to EAFB
N/A	N/A	8/13/97			AVSS demod completed

N/A = not applicable

PZT's on aircraft for a total of 154.7 flight hours during 35 flights

Twenty-six minutes of Max. A/B, 6+ minutes of Mid-A/B, 4 minutes of military power at take off.

3.4 RESULTS

3.4.1 Life Issues

One of the main goals of the AVSS flight demonstration test was to determine the reliability, maintainability, and durability of the installed system. Table 3-2 shows a history of the AVSS on the TDS aircraft. The operating system was on the aircraft for 4 months. This included testing at Edwards AFB, where the conditions included a dry desert environment and testing at Robins/ Eglin AFB where the environment was considerably more humid. In all, the AVSS was on the aircraft for 154.7 hours of flight time, which was accomplished during 35 flights. More importantly, this included a total of about 26 minutes of time at the highest acoustic and vibration environments that the aft fuselage of the aircraft is exposed to, during takeoff and climbout at four engine afterburner operation. During that time, only one anomaly was recorded associated with the AVSS control and power amplifier units. This was when a circuit breaker on the amplifier box was found tripped after one flight. Since this incident only occurred once it was not considered a system problem. Another problem that occurred during testing involved the debonding of the accelerometers that were mounted directly on top of the PZTs. Unfortunately, when this occurred it caused part of the underlying PZTs to break off. This was mainly due to the large accelerometers and the 1 inch cube aluminum blocks that were used to mount the accelerometers. Smaller accelerometers would not have produced the same effect because of the reduced mass. When smaller accelerometers were used in the laboratory tests and directly bonded to the PZTs; similar failures did not occur. For future programs it will be possible to use PZTs as sensors, thus, eliminating accelerometers altogether. Even after the accelerometers were rebonded the system continued to perform well. At the end of the flight test program all of the installed PZTs were still bonded to the aircraft skin and functioning. The reliability of the installation was excellent; the data indicated that the system worked whenever the switch in the cockpit was turned to the "on" position. Maintenance required for the system during the flight test program was minimal and only required that the installation be inspected for damage. The only damage, as stated above, was loss of the accelerometers, which were subsequently bonded back on. The fact that part of PZTs underlying the accelerometers were broken off indicated that those actuators probably lost some of their effectiveness. However, this could not be quantified since the aircraft was stationed in Georgia at the time, and no on-board AVSS testing could be performed.

3.4.2 Performance During Takeoff (Maximum engine noise)

During the TDS flight test program, AVSS testing was performed by the crew on a non-interference and piggybacked basis. This meant that the flight conditions for which data was received were those that were required for TDS testing. In many cases these conditions were too benign for obtaining AVSS performance data. Also, AVSS required that data be obtained both with the system non-operating and operating at the same condition so that a comparison could be made to determine the system effectiveness. The crew was advised of this during pre-flight briefings. However, with their heavy TDS workload, this did not always occur. Over the time that the system was installed in the aircraft, enough data was obtained to evaluate system performance for three major phases of the installed AVSS control laws. These phases

were (1) the initial control laws installed May 16, 1997; (2) the revised control laws installed June 2, 1997; and (3) increase of the system gains made July 10, 1997. The first phase comparison was performed using the data from TDS flight number 17, Ref. Table 3-1, which contained both on and off data. After phase 1, the control system was redesigned. One observation made during the phase 1 gain adjustment was, "a sizzling noise was heard." That sound indicated that high frequency noise was being folded back at low frequencies. By inserting a high pass filter, the amplification of this unwanted signal was reduced. Another adjustment was to add more high frequency roll off to reduce the magnitude of the high frequency noise. The third adjustment was to provide some attenuation (6dB) of the second anti-symmetric mode and to increase the attenuation of the first symmetric mode. For Phase 2, it was necessary to compare the "on" data from Flight 19 with the "off" data from Flight 17. Flights 51 and 52 were used to compare results for the last phase where only the gains were changed. Data for each condition is presented as "symmetric" response by plotting the response of Accelerometer A2 (Ref. Figure 3-5) and "anti-symmetric" response by plotting the outputs of Accelerometers A1 and A3. Local frame responses and noise effects for the on /off comparisons were evaluated by the plots of A4, A5 and A6 and microphone M1.

Table 3-3 is a summary of the data obtained during the takeoff event for Accelerometers A1 and A3, the anti-symmetric response parameters. Table 3-4 is a summary of the data obtained during the takeoff event for Accelerometer A2, the symmetric response parameters. Figures 3-6, -7 and -8 are comparison response plots for the AVSS "on" and "off" for the three phases of the control law development.

From the table and the figures, it can be seen that the anti-symmetric unattenuated response was composed of two modes with frequencies of 426-427 Hz and 556-558 Hz. With the initial control laws, the first mode is greatly attenuated, but the second mode is essentially unchanged. These results were very close to the curved panel lab test results. There, the first anti-symmetric mode of 420 Hz was attenuated about 10 dB (Figure 3-3). Here, a first mode of 427 Hz was attenuated about 8 dB. The important modes to reduce are the first symmetric and first anti-symmetric, since the highest stresses in the panel will be due to these. Stress will nominally decrease by the square of the frequency. A considerable decrease in acceleration spectral density level occurs when the system is operating, indicating the effectiveness of the system. However fatigue life is usually determined using a Root Mean Square (RMS) value of stress, and since RMS stress is directly proportional to RMS acceleration, the significant statistic is the percentage reduction of RMS acceleration. The initial control laws, developed from the laboratory test, show a reduction from 44.2 to 47.3 percent. Revised control laws improved this reduction by increasing the percentages to 60.4- 61.5 percent. In addition to increasing the reduction of the first anti-symmetric mode, the revision also decreased the response of the second mode a nominal amount, 9.1 - 11.9 percent. Changing the gains, Phase 3, had the effect of bringing the attenuation close to where it was for the first Table 3-3. Anti-symmetric Response Summary set of control laws. Whether this was a result of the gain changes alone, or also includes any loss of PZT effectiveness that occurred when the accelerometers debonded and took some PZT material with them, is not known. However, a decrease of RMS stress of 60 percent shows excellent performance for the AVSS.

Table 3-3, Anti-Symmetric Response Summary

Initial Control Laws, Flight 17 AVSS Off and On							
		Accel A1, Top Patch			Accel A3, Bottom Patch		
		Off	On	% Reduction*	Off	On	% Reduction*
1st anti-symm	Frequency Hz	426	422		427	427	
	Ampl. g^2/Hz	564.7	84.4	85.1	567	105.8	81.3
	(g)RMS	82.5	43.5	47.3	90.5	50.5	44.2
	Delta dB			-8			-7.3
2nd anti-symm	Frequency Hz	556	558		556	558	
	Ampl. g^2/Hz	340.4	325.7	4.3	387.4	349	9.9
	(g)RMS	88.5	83.6	5.5	89.9	87.1	3.1
	Delta dB			0			0
Revised control laws 6-2-97, AVSS Off: Flight 17, AVSS on: Flight 19							
1st anti-symm.	Frequency Hz	426	425		427	426	
	Ampl. g^2/Hz	564.7	20.7	96.3	567	34.8	93.9
	(g)RMS	82.5	32.7	60.4	90.5	40.4	61.5
	Delta dB			-14			-12
2nd anti-symm	Frequency Hz	556	551		556	549	
	Ampl. g^2/Hz	340.4	202.5	40.5	387.4	251.6	35.1
	(g)RMS	88.5	78	11.9	89.9	81.7	9.1
	Delta dB			-5.6			-2
Control Law Gains Increased 7-10-97, AVSS off: Flight 52, AVSS On: Flight 51							
1st anti symm.	Frequency Hz	426, 430	422		430	433	
	Ampl. g^2/Hz	319.2, 322.1	47.3	85.3	453.3	54.1	88.1
	(g)RMS	69.5	41	41	75.8	43.5	42.3
	Delta dB			-9.3			-11
2nd anti symm	Frequency Hz	558	555		558	555	
	Ampl. g^2/Hz	298.7	196.9	34.1	339.5	235	30.8
	(g)RMS	87.3	80.5	7.8	88.4	82.2	7
	Delta dB			-2.4			-2.2

Table 3-4. Symmetric Response Summary

Initial Control Laws, Flight 17 AVSS Off and On				
		Accel A2, Middle Patch		
		AVSS off	AVSS on	% Reduction*
1st symm.	Frequency Hz	437	432	
	Ampl. g ² /Hz	638.7	86.4	86.5
	(g)RMS	88.9	43.5	51
	Delta dB			-8.5
Revised control laws 6-2-97, AVSS off: Flight 17, AVSS on: Flt 19				
1st symm.	Frequency Hz	437	430	
	Ampl. g ² /Hz	638.7	68.9	89.2
	(g)RMS	88.9	38.2	57.0
	Delta dB			-10
Control law gains increased 7-10-97, AVSS off: Flight 52, AVSS on: Flt 51				
1st symm.	Frequency Hz	437	438	
	Ampl. g ² /Hz	405.6	65.1	83.9
	(g)RMS	86.3	53.3	38.2
	Delta dB			-8.5

Only one symmetric mode is significantly excited by the engine noise at takeoff, and it has a natural frequency of 437 Hz which, as predicted by FEM analysis and the prior aircraft tap test, is also very close to the fundamental anti-symmetric mode frequency (426 Hz).

The first symmetric mode response was attenuated by 51 percent for flight 17 and 57 percent for flight 19 with the revised control laws. Changing the gains for Phase 3 lowered the reduction. The reasons for this latter result are unknown. A reduction of 57 percent in RMS stress is still a considerable reduction and could translate into a significant increase in structural life.

3.4.3 Performance for In-Flight Conditions

Figures 3-9 and 3-10 show the anti-symmetric (Accelerometer A1) and symmetric (Accelerometer A2) performances, respectively, of the AVSS during flight. The conditions are for straight and level flight, and the control laws are the original ones loaded in the computer. Data from Flights 17 and 18 were used. Acceleration PSD levels found in-flight are much lower than those experienced by the panel during takeoff, because the in-flight turbulent pressure field is not as effective in exciting the panel as the engine noise at takeoff. Data were obtained for three different Mach numbers at approximately the same altitude. The same panel modes are excited; however, there is a slight increase in the frequencies seen in the flight data. The

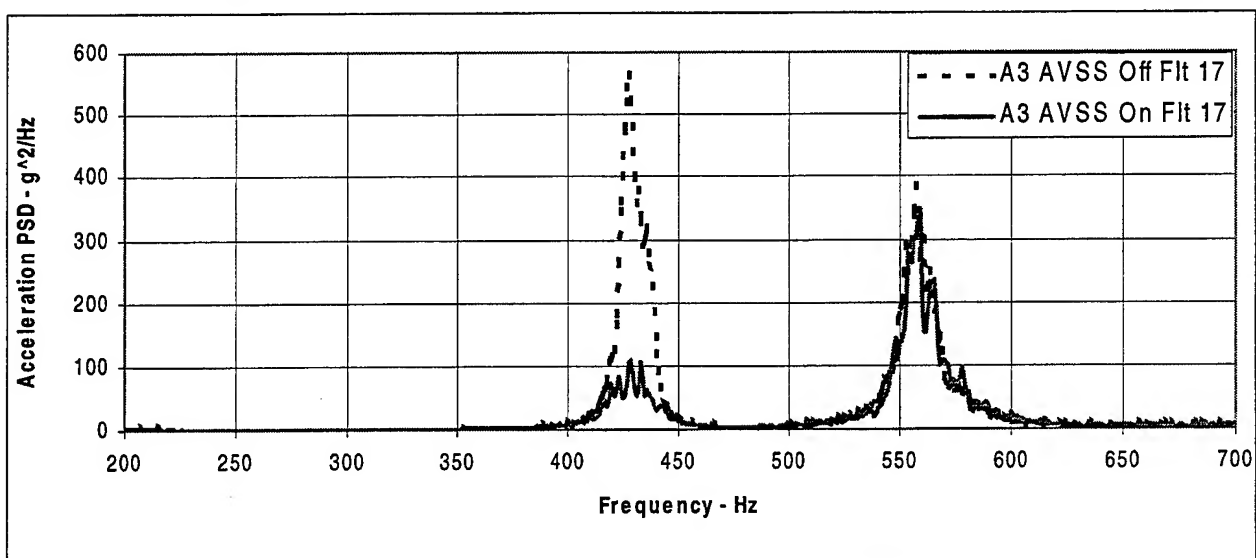
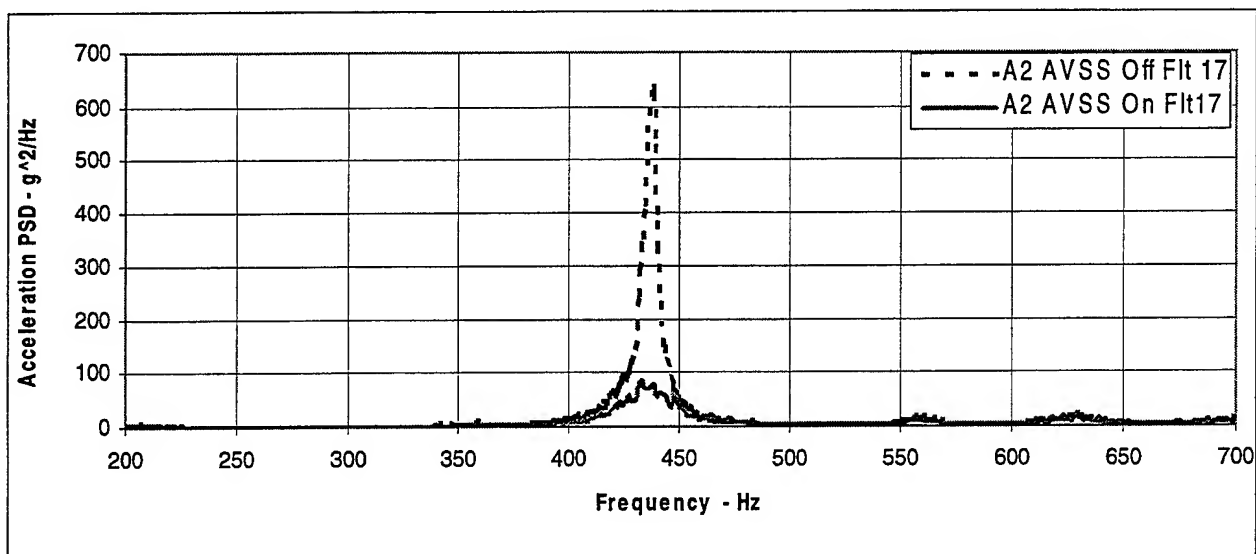
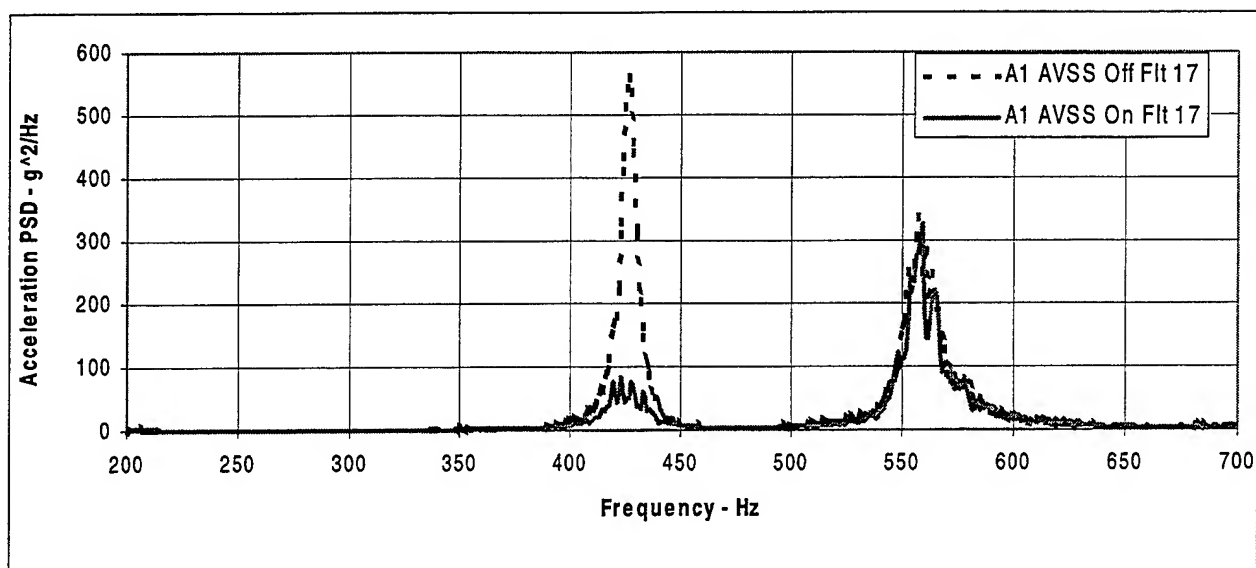


Figure 3-6. Comparison AVSS Off and On, Initial Control Laws

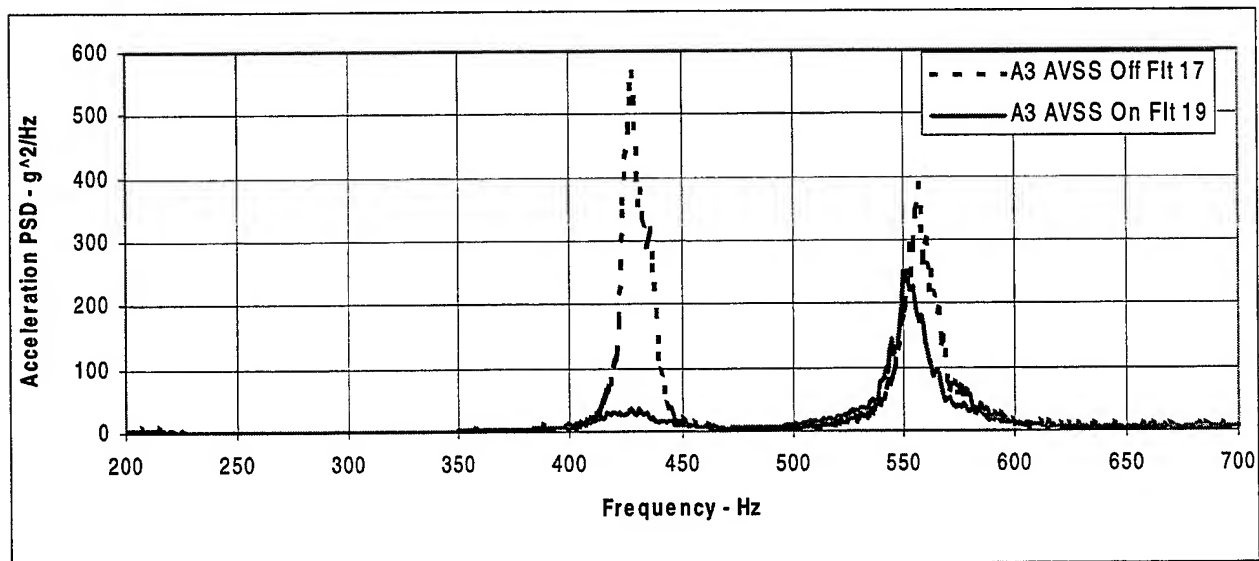
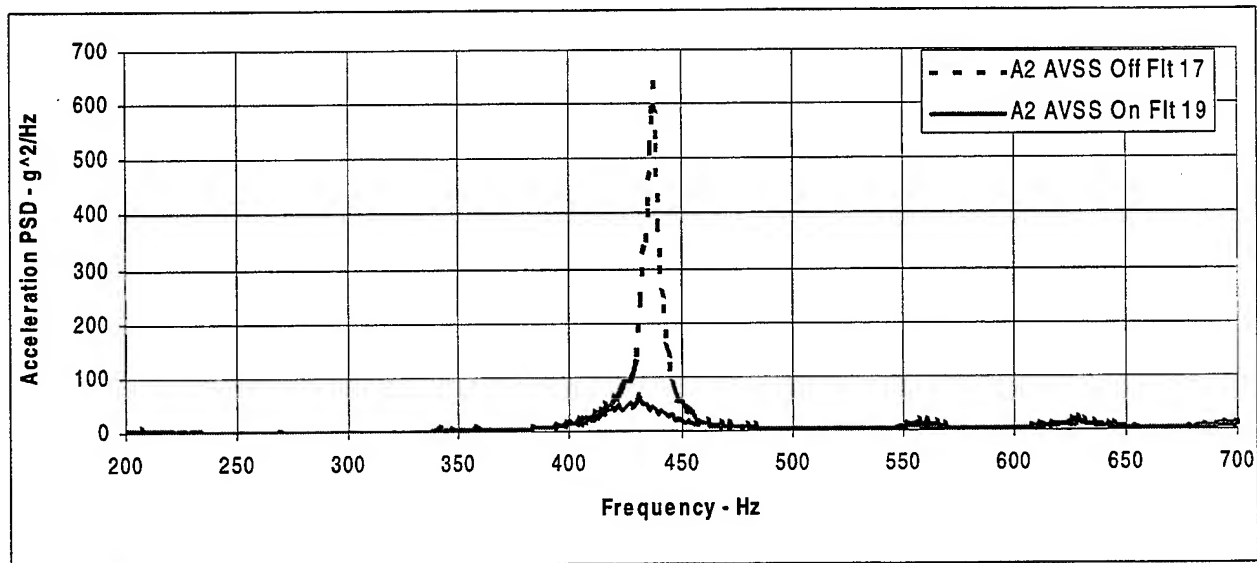
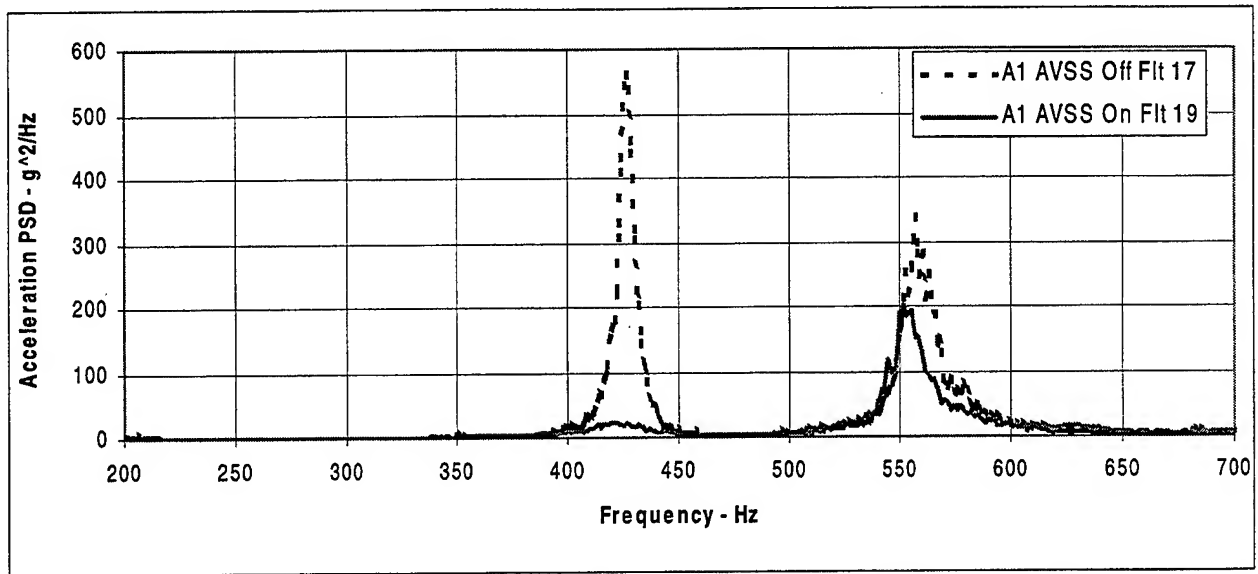


Figure 3-7. Comparison of AVSS Off and On, Revised Control Laws

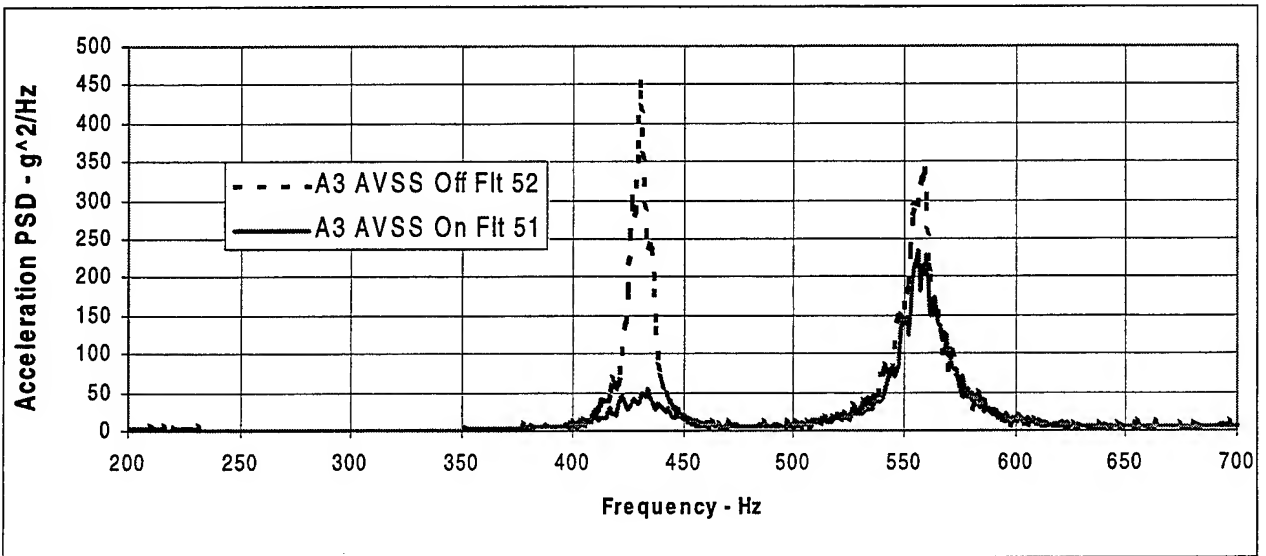
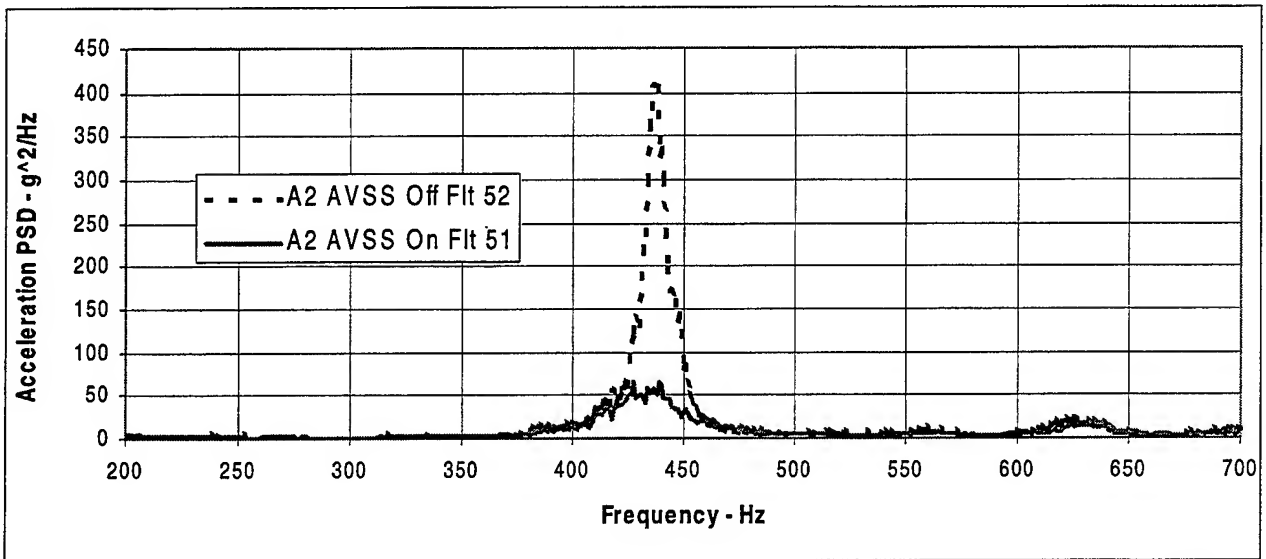
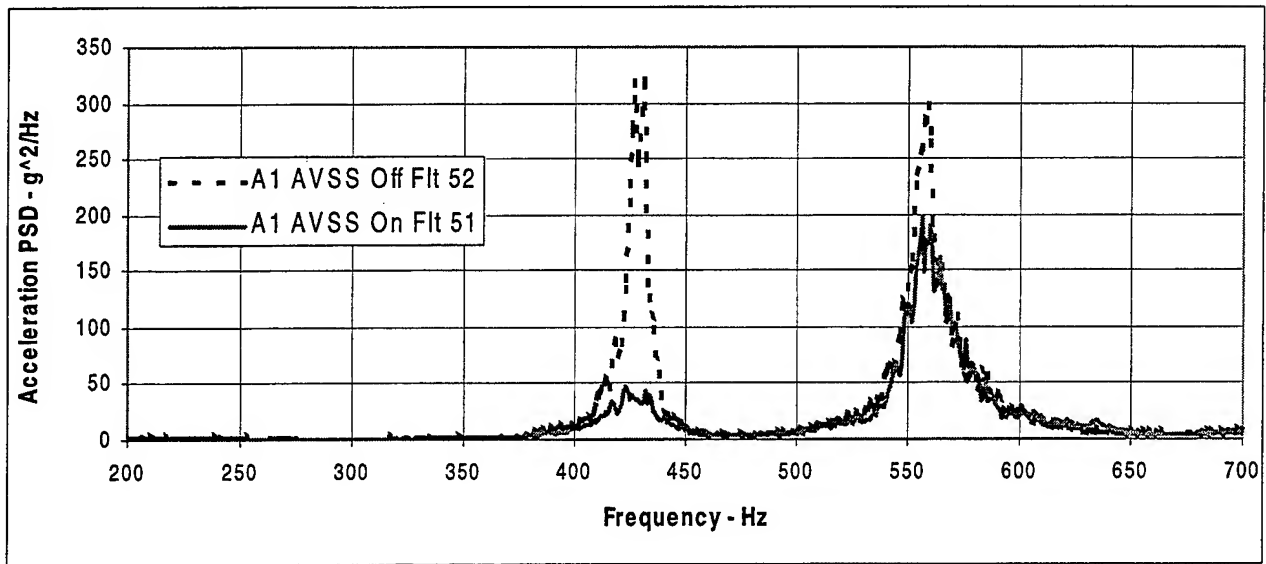


Figure 3-8. Comparison for AVSS off and On, Gain Change

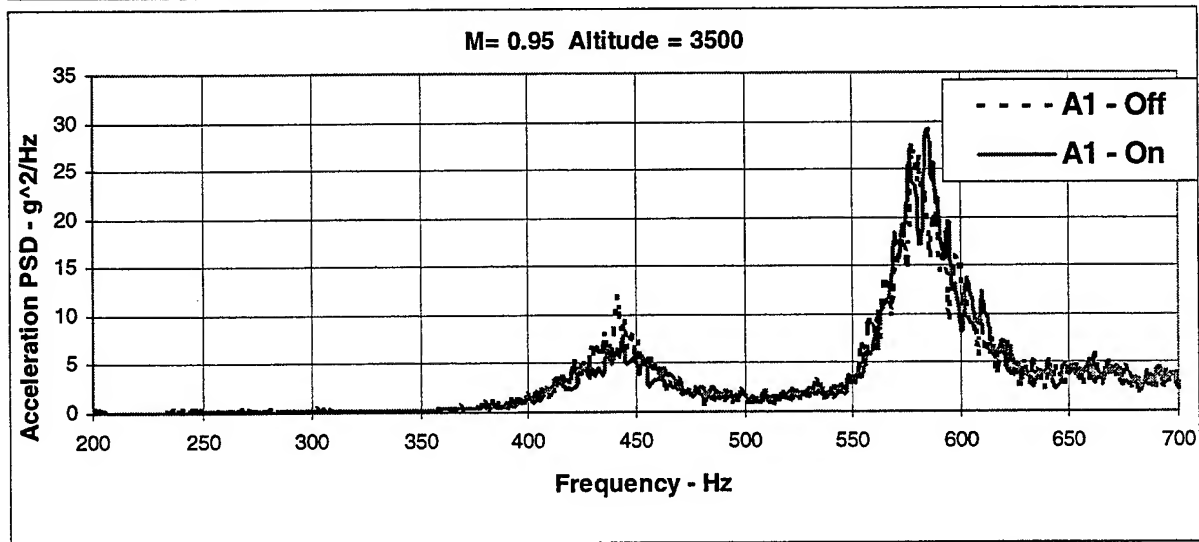
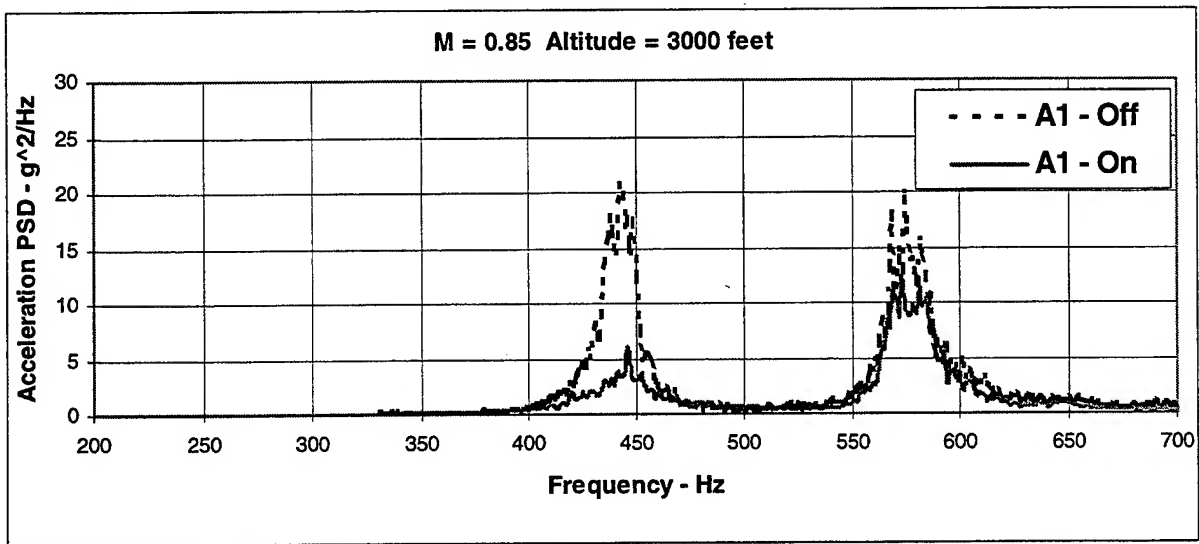
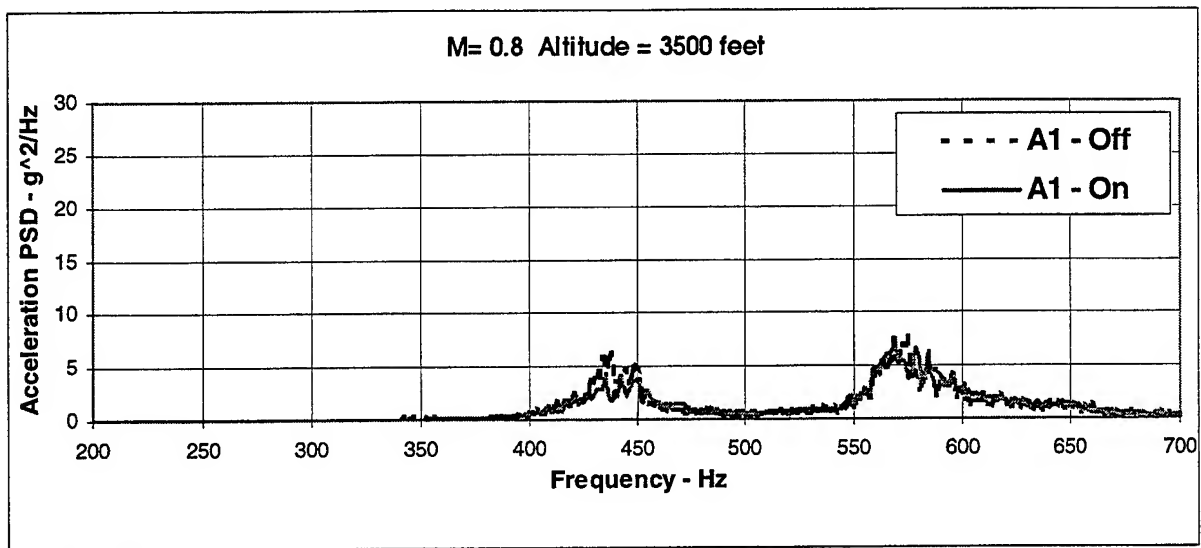


Figure 3-9. Anti-symmetric Panel Response During Flight With AVSS "Off" and "On"

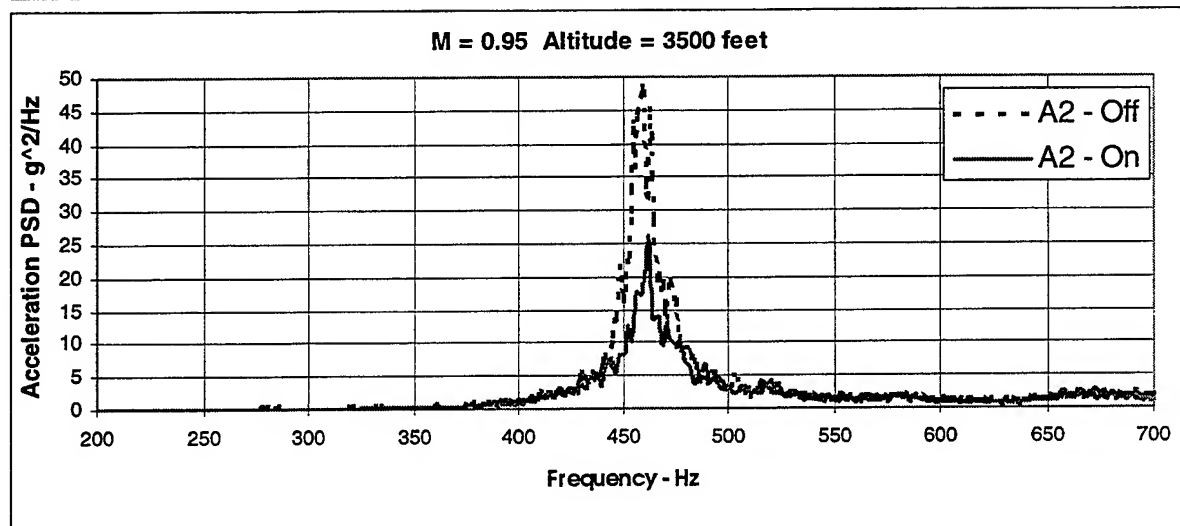
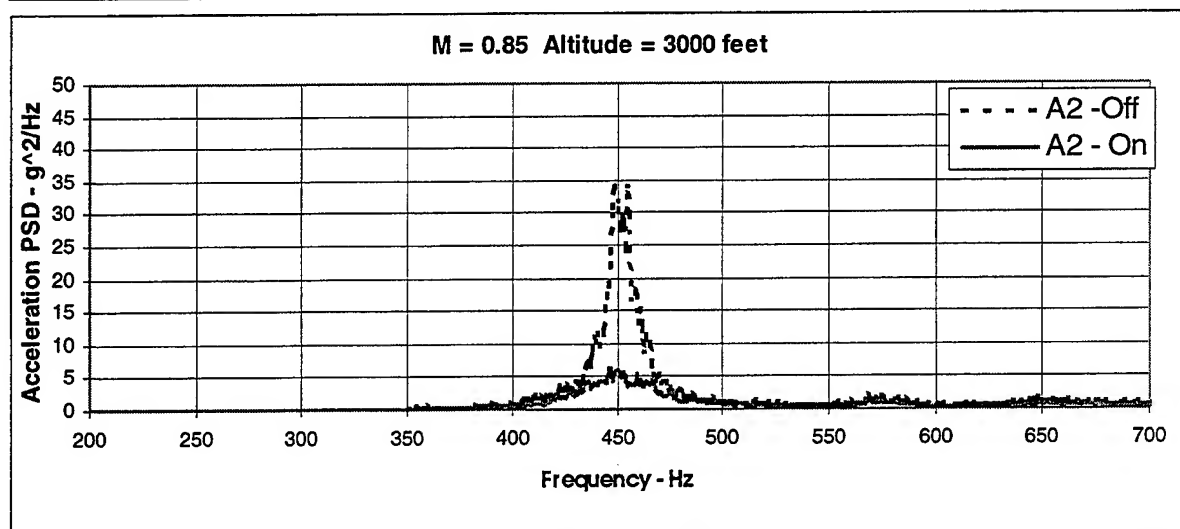
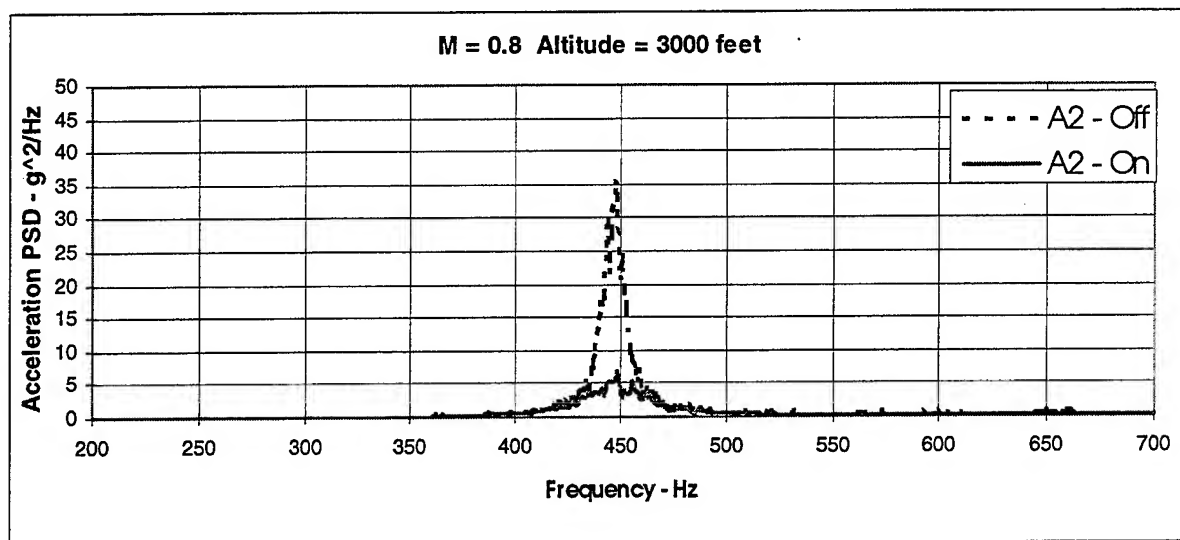


Figure 3-10. Symmetric panel Response During Flight With AVSS "Off" and "On"

modulus of elasticity of 6061-T4 aluminum increases from 9.8×10^6 to 10.2×10^6 as the temperature changes from 160 °F to -60 °F. This accounts for some of the frequency increase observed in the data. The first mode anti-symmetric response went from a frequency of 426 - 427 Hz at takeoff to about 440 Hz in flight, and the second mode went from 556 - 558 to 575 Hz. For the symmetric response (Accelerometer A2) the frequency increase of the primary mode went from 437 - 446 to 450-458 Hz. Even though the unattenuated levels were low compared to takeoff the AVSS was still able to attenuate the response, especially for the symmetric mode. Peak acceleration PSD for Mach numbers of 0.8 and 0.85 were about the same, but 0.95 Mach exhibited a somewhat higher response both with AVSS off and on. The flow region near the empannage in the transonic regime varies considerably due to local Mach number changes and the presence of shock waves and flow reattachment points. The responses for the anti-symmetric modes show considerable variation with Mach number and the effect of AVSS operating. The flight data emphasizes that the AVSS control laws should be optimized for the takeoff conditions.

3.4.4 Adjacent Structure/Acoustic Responses

Other instrumentation mounted near the selected AVSS demonstration panel is shown in Figure 3-5. It consisted of three accelerometers mounted on an adjacent frame, a microphone near the panel and a temperature sensor on the panel. No data was obtained from the temperature transducer. Accelerometers located on the adjacent frames and the microphone showed no discernable differences in levels measured, even at the frequencies where the AVSS significantly reduced the demonstration panel response. This is not too surprising since there are many other adjacent panels responding to the acoustic excitation. Their responses mask the differences from the demonstration panel with AVSS off and on. In addition, the microphone is influenced by the total noise in the AEB and not just that being transmitted through the demonstration panel. Obviously, many panels in the AEB area must have PZTs mounted to them to reduce the interior noise significantly.

4.0 Summary and Recommendations

4.1 SUMMARY

The effort documented in this report successfully demonstrated the use of PZT ceramic actuators to damp out the acoustically excited vibration of a skin panel on an operational military aircraft. A team composed of Boeing North American and Air Force personnel performed all of the required tasks within the time and budget constraints of the contract and the limitations imposed by the flight test program to which this effort was piggybacked. A skin panel on the aft end of the B-1B aircraft was chosen as the demonstration panel, because it is excited by engine noise at takeoff and by turbulence in flight. The panel is highly curved with a radius of 38 inches and has a thickness of 0.077 inch in the center.

A finite element model made up of shell elements was developed to determine the shapes and frequencies for the panel modes, whose vibration was to be attenuated. A tap test of the actual panel on the aircraft was performed to verify the model. Test results were used to update the model so that it would have dynamic characteristics similar to those exhibited by the aircraft panel. The first fundamental symmetric and anti-symmetric mode shapes were used to locate the PZT actuators at the mode anti-nodes. For the symmetric mode, this was at the center of the panel, and for the anti-symmetric modes, they were ± 3.5 inches from the center.

A series of coupon tests were performed to select the PZT patch size, thickness and the best of three adhesives for bonding the patches to the aircraft. The selected adhesive had to meet the -60 to $+185$ °F aircraft requirement with minimum loss of the applied PZT force. The final PZT configuration chosen was 0.020 inch thick and had dimensions of 0.333 by 1 inch. It was lapped in the width direction to accommodate the 38 inch radius. Fatigue testing of coupons showed that the metal coupon would fail before the actuator would de-bond from material.

Laboratory tests were performed with both flat and curved panels. The flat panel was chosen to help build on the knowledge gained from prior testing. Then the curved panel was tested to introduce curvature to the problem. Size, shape, thickness, and material of the curved panel were similar to the test panel on the aircraft. Each panel was mounted in the wall of a small acoustic chamber and testing consisted of determining the natural modes and frequencies, determining the open-loop transfer functions and exposing the panel to an acoustic excitation environment. On the curved panel, there were 14 PZTs at the center for symmetric control and 4 PZTs on each anti-symmetric anti-node. The panels were mounted in the acoustic chamber so they could be exposed to an environment that represented the actual B-1B engine noise at takeoff. Control and power amplifier units developed for the aircraft were used in the laboratory. A first symmetric mode attenuation of 20 dB was attained in the lab for the flat panel during tap testing and 12 dB during acoustic excitation of the panel. Results on the curved panel were a 17 dB reduction in the first anti-symmetric mode during tap testing and 10 dB with an acoustic excitation. The first symmetric mode was contaminated by motion of the wall support in the acoustic chamber and this essentially prevented obtaining laboratory results for that mode. Laboratory testing also showed that there would only be a small 3% increase in

frequency for the +185 degree temperature environment and that did not require an adaptable control system.

The computer board chosen for the control unit was a Motorola 68040. It was capable of achieving the required sampling rate of 10,000 Hz. At the center of the 3 PZT patch locations (panel center and ± 3.5 inches) an accelerometer was located to both feedback a signal to the control unit and also to be recorded for response information with the system operating and non-operating. Control laws were developed for the system using the H_∞ method. This method attenuates the chosen modes and helps stabilize other adjacent modes. These laws were programmed on the control board using vsWorks. Both the vsWorks software and the control law code were placed in the flash memory of the computer board. The high speed of the board allowed the accelerometer signals to be digitized (A/D conversion), the control equations processed and the digital control signals converted back to analog and sent to the power amplifier unit within the 120 μ s allowed by the board.

The PZTs were bonded onto the aircraft, and then all of the associated hardware were mounted in the aft end of a B-1B aircraft, which was undergoing flight testing for another program. Sixteen 0.333 by 1 inch PZTs were in the center of the panel for symmetric control, and 10 were at each of the two anti-nodes of the anti-symmetric mode. Open-loop transfer functions were obtained, and the aircraft control laws developed. These control laws were loaded into the computer and flight test data were obtained for three configurations of the laws. Data were obtained, both with the system operating and non-operating, so that the panel vibration attenuation could be quantified. The maximum attenuation was obtained with the second set of control laws loaded into the computer. It was determined that an 800 Hz low pass filter had to be added to both the symmetric and anti-symmetric circuits. Performance results for these control laws are summarized in the following table.

Table 4-1.

Aircraft Mode	Frequency - Hz	Avg. dB Reduction*
1 st Symmetric	437	-10
1 st Anti-symmetric	426	-13
2 nd Anti-symmetric	556	-3.8
*On acceleration PSD level (g^2/Hz)		

The system was on the aircraft for a total of 154.7 hours of flight time, which was accumulated over 35 flights of the aircraft. More importantly, the system operated successfully for a total of 26 minutes at the full after burner takeoff environment. Only minor problems occurred in the system while on the aircraft, and nothing occurred that would have prevented the system from becoming an operational part of the aircraft. Results were also obtained for a limited number of in-flight conditions of the aircraft. They showed that the unattenuated vibration levels occurring in flight are much less than those at take off. The flight attenuation varied from a negligible amount, to as much as 5.4 dB. Flight results emphasized that the control laws should be optimized for the take off condition.

4.2 CONCLUSIONS

The following can be concluded from the successful completion of the Active Vibration Suppression Program on the B-1B aircraft.

- Acoustically induced high vibration levels on a military aircraft skin panel can be successfully attenuated by the use of PZT actuators
- The PZT actuator configuration chosen, 0.020 inch thick, 0.333 inch wide and 1 inch long can be successfully bonded to an aircraft structure and survive the acoustic and thermal environments encountered.
- The chosen actuators, when grouped on the panel at the fundamental mode anti-nodes, can provide sufficient force to attenuate high vibration levels
- Hysol adhesives EA 9395 and 9360 can be used to successfully bond the PZTs to the aluminum skin and transmit sufficient force over the wide temperature range encountered by the aircraft.
- Preliminary testing of the methodology and hardware in a laboratory environment is an excellent way to develop the procedures and processes needed to add an active vibration suppression system to an aircraft
- Control and power supply units can be successfully developed to survive the aircraft environment and perform their required functions to attenuate acoustically driven panel vibration. With additional effort, they can be miniaturized to reduce their size, weight, power, and cooling requirements.
- The H_∞ method can be successfully used to develop the control laws for the system using open loop transfer functions obtained on the actual system. Selected modes can be attenuated and the adjacent modes stabilized.
- For successful utilization of the control system, accelerometer data should be sent through a low pass filter to eliminate aliasing.
- The use of a vacuum bag during bonding of the PZTs to the aircraft skin insured a strong bond that had a minimum bond line.
- There were no problems on the aircraft that indicated that maintainability or reliability of the system on an operational aircraft.
- The excellent performance of the PZTs in attenuating panel vibration indicates that vibration induced stress levels in the panel can be reduced significantly, thus, greatly extending the structural life of the structure if required.

4.3 RECOMMENDATIONS

This program has shown that PZTs can be used effectively to reduce aircraft skin panel vibration, due to acoustic excitation. Many other R&D efforts have been used to demonstrate this technology on aircraft structures to reduce interior noise during lab or ground tests. However, none of these has resulted in an actual flight test vehicle. It is recommended that a representative fuselage section of a flight vehicle be fitted with PZT patches and a control system similar to that developed for the B-1B be used to demonstrate the extension of this technology for interior noise control. Boeing North American is exploring use of the Russian TU-144 Supersonic

Transport aircraft as a demonstration vehicle. Currently, Boeing North American is involved in other testing on that aircraft.

Humans are sensitive to noise in the frequency range between 400 and 8000 Hz. If the noise can be attenuated between 400 and 1000 Hz, the interior noise level can be significantly improved. Noise attenuation requires not only vibration attenuation at the natural frequencies, but also at the forced vibration frequencies. When the noise source frequencies are known, the controller designer includes disturbance accommodation in the H_∞ analysis. The control system will then react at the forced vibration frequencies and provide attenuation.

Other obvious extensions of this technology that should be investigated are the control of vibrations at elevated temperatures on fighter aircraft structure. The Rockwell PZT patches are being upgraded to meet this need.

Another extension of this technology that requires more study are ways of making it more commercially acceptable by the use of light weight amplifiers and off-the-shelf computer chips. This technology is well known but was not used more on the B-1B demonstration program, because of the extremely short period of time that was available for developing the flight hardware. System capability could be doubled or tripled by driving at higher voltages. This may not be a solution for aircraft because of the safety considerations, but for unmanned launch vehicles this is a consideration.

5.0 References

- [1] E. T. Falangas, J. A. Dworak, S. Koshigoe, "*Methods for Controlling Plate Vibrations using PZT Actuators.*" Presented at the AIAA Guidance Navigation, and Control Conference, Aug. 93, in Monterey, California.
- [2] J. C. Doyle, K. Glover, P. P. Khargonekar, B. A. Francis, "*State-Space Solutions to Standard H_2 and H_∞ Control Problems.*" IEEE Trans. on Automatic Control, Vol 34, No 8, Aug 1989
- [3] B. C. Moore, "*Principal Components Analysis in Linear Systems: Controllability, Observability, and Model reduction.*" IEEE Trans. on Automatic Control, Vol. AC-26, No 1, Feb 81.